FLUID FLOW CHARACTERIZATION AND IN SILICO VALIDATION IN A RAPID PROTOTYPED AORTIC ARCH MODEL

A Thesis

presented to

the Faculty of California Polytechnic State University,

San Luis Obispo

In Partial Fulfillment

of the Requirements for the Degree

Master of Science in Biomedical Engineering

by

Alexandra Knauer

September 2016

COMMITTEE MEMBERSHIP

TITLE:	Fluid Flow Characterization and In Silico Validation in a Rapid Prototyped Aortic Arch Model
AUTHOR:	Alexandra Knauer
DATE SUBMITTED:	September 2016

COMMITTE CHAIR:	David Clague, Ph.D. Professor of Biomedical Engineering
COMMITTEE MEMBER:	Cameron Purcell, M.S. Senior R&D Engineer at Claret Medical
COMMITTEE MEMBER:	Lanny Griffin, Ph.D. Professor of Biomedical & General Engineering

ABSTRACT

Fluid Flow Characterization and In Silico Validation in a
Rapid Prototyped Aortic Arch Model
Alexandra Knauer

Transcatheter aortic heart valve replacement (TAVR) is a procedure to replace a failing aortic valve and is becoming the new standard of care for patients that are not candidates for open-heart surgery [2]. However, this minimally invasive technique has shown to cause ischemic brain lesions, or "silent infarcts", in 90% of TAVR patients, which can increase the patient's risk for stroke by two to four times in future years [3]. Claret Medical Inc., a medical device company, has developed a cerebral protection system that filters and captures embolic debris released during endovascular procedures, such as TAVR. This thesis utilized CT scans from Claret Medical to create a physical construct of the aortic arch to experimentally validate a theoretical computer model through flow visualization. The hypothesis was that the empirical model can accurately mimic the fluid dynamic properties of the aortic arch in order validate an in silico model using the finite elements program COMSOL MultiPhysics® Modeling Software. The physical model was created from a patient CT scan of the aortic arch using additive manufacturing (3D printing) and polymer casting, resulting in the shape of the aortic arch within a transparent, silicone material. Fluid was pumped through the model to visualize and quantify the velocity of the fluid within the aortic arch. COMSOL MultiPhysics® was used to model the aortic arch and obtain velocity measurements, which were statistically compared to the velocity measurements from the physical model. There was no significant difference between the values of the physical model and the computer model, confirming the hypothesis. Overall, this study successfully used CT scans to create an anatomically accurate physical model that was validated by a computer model using a novel technique of flow visualization. As TAVR and similar procedures continue to develop, the need for experimental evaluation and visualization of devices will continue to grow, making this project relevant to many companies in the medical device industry.

Keywords: Computer model validation, 3D printing, aortic arch, TAVR, transcatheter aortic valve replacement, additive manufacturing, rapid prototyping, COMSOL MultiPhysics®

ACKNOWLEDGMENTS

Thank you to:

i) My advisor Dr. Clague for introducing me to the project, providing project support, and always sharing great photos of his dog.

ii) Claret Medical, specifically my industry contact Cameron, for providing project feedback, CT scans, and the context that made this project possible.

iii) Brandon Cohen for improving the STL file and contributions to the original experimental set-up. Additionally, his knowledge of pumps from previous projects was very valuable in the success of this project.

iv) David Baik for iterating on the original COMSOL MultiPhysics® model and providing input during brainstorming.

v) Andrew Janicki for providing clarifications of his model and allowing access to his project files

vi) Daniel Greinke and Rachel Willis for allowing me to further develop their flow visualization concept and for providing further elaboration of their methods.

vii) Dylan Sigley for 3D printing this project at a very reasonable cost as well as contributing time to the development of the mold concept. The project would not have been possible without his contributions and I greatly appreciate his help.

viii) Brooke Wheeler from Reynold's Advanced Materials who provided consultation on the materials and samples for testing.

ix) My parents and brothers. Thank you for always being there for me.

TABLE OF CONTENTS

Page

APPENDICES

LIST OF TABLES

LIST OF FIGURES

LIST OF EQUATIONS

Equation 1: $Re = \frac{Inertial\ Forces}{Viscous\ Forces} = \frac{\rho v D}{\mu}$

Equation 2: $CO = SV \times HR$

Equation 3: $1\ mL/min = 0.0158503\ Gallons/min$

Equation 4: $\rho\left(\frac{d\bar{V}}{dt} + \bar{v} \cdot \overline{\nabla v}\right) = \overline{\nabla} \cdot \bar{T} + \rho\bar{\bar{g}}$

Equation 5: $Q = \frac{\pi R^4 (P_i - P_o)}{8\mu L}$

Equation 6: $x_{rot} = [\left((x - C_x) * cos\theta\right) - \left(\left(y - C_y\right) * sin\theta\right)] + C_x$

Equation 7: $y_{rot} = [\left((x - C_x) * sin\theta\right) + \left(\left(y - C_y\right) * cos\theta\right)] + C_y$

CHAPTER 1: INTRODUCTION

1.1 Purpose and Background

Every year, more than five million Americans are diagnosed with heart valve disease, the most common affecting the aortic valves [1]. Transcatheter aortic heart valve replacement (TAVR) is a procedure to replace a failing aortic valve and is becoming the new standard of care for patients that are not candidates for open-heart surgery [2]. However, this minimally invasive technique has shown to cause ischemic brain lesions, or "silent infarcts", in 90% of TAVR patients. This can increase the patient's risk for stroke by two to four times in future years [3].

While TAVR is a minimally invasive procedure, the high risk of silent cerebral lesions and the risk of stroke can be life threatening for a patient. Claret Medical Inc., a medical device company, has developed a cerebral protection system that filters and captures embolic debris released during endovascular procedures, such as TAVR. The device is used globally, though is not yet commercially available in the United States [4]. Previous studies by Andrew Janicki (2015) used CT scans from Claret Medical to track particulates within the aortic arch using COMSOL MultiPhysics®, a finite element analysis computer-modeling program.

This project will utilize the same CT scans from Claret Medical to create a physical construct. The goal is to create a construct that can be used to experimentally validate the theoretical computer model through flow visualization. As TAVR and similar procedures continue to develop, the need for experimental evaluation and visualization of

devices will continue to grow, making this project relevant to many companies in the medical device industry.

1.2 General Approach

This study has three aspects: a physical model, a computer simulation, and flow visualization experiments. The physical model of the aortic arch will be created from a patient CT scan of the aortic arch. The CT scan will be converted to an STL file, 3D printed, and cast with an optically clear rubber. This will create the shape of the aortic arch within an enclosed, transparent material that can be used to visualize and characterize the flow of fluid within the aortic arch.

The COMSOL MultiPhysics® model of the aortic arch, first evaluated by Janicki (2015), will be modified to improve the model's accuracy. Current modifications defined by Janicki are improvement of the STL file and a change in the fluid viscosity within the model. Additional modifications of the model will be defined through evaluation of the previous work and further development of the project.

The final aspect of this thesis is flow visualization within a physical aortic arch model. Fluid will be pumped in the physical model and dye will be injected and evaluated to quantify the flow within the arch. The output of the flow within the physical model will be compared to the output of the COMSOL MultiPhysics® model for statistical significance.

1.3 Study Aims

The specific aims of this study are as follows:

i) To create a three-dimensional, physiologically accurate construct of the aortic arch using additive manufacturing techniques for the purpose of clinical testing.

ii) To improve a predictive COMSOL MultiPhysics® model of blood flow conditions within the aortic arch.

iii) To validate a model in COMSOL MultiPhysics® model through comparison to the fluid dynamics in an empirical model.

The hypothesis of this study is that the empirical model can accurately mimic the fluid dynamic properties of the aortic arch found in the human body as well as validate an in silico model using the finite elements program COMSOL MultiPhysics® Modeling Software.

CHAPTER 2: BACKGROUND & RELATED STUDIES

2.1 Anatomy and Clinical Relevance

The aortic arch carries blood from the heart to the rest of the body, first branching from the top of the arch. The most common anatomy of the aortic arch (Figure 1) has, from left to right, the first branch of the innominate (or brachiocephalic) artery, the second branch of the left carotid artery, and the third branch of the left subclavian artery. With respect to Figure 1, blood travels from the heart on the left to the descending aorta on the right or to the branching vessels [5].

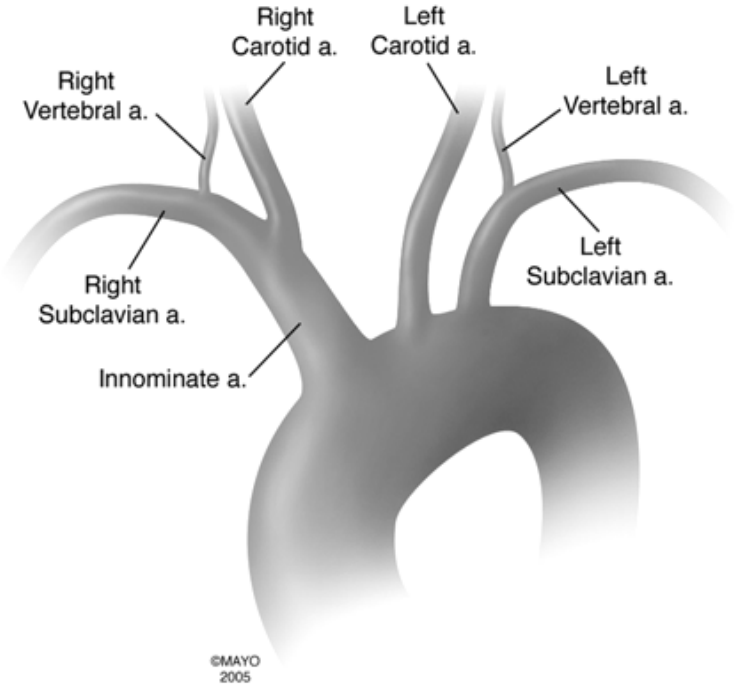

Figure 1. Typical aortic arch anatomy with branching arteries.

In this anatomy, blood that travels into the brachiocephalic artery bifurcates into the right common carotid and the right subclavian arteries. The right subclavian flows into the arm and the right common carotid flows into the cerebral circulatory system. Blood that travels into the left common carotid artery flows into the cerebral circulatory system.

Finally, the left subclavian artery bifurcates into the vertebral artery, leading to the cerebral circulatory system, and the left subclavian artery [J].

The second most common pattern of human aortic arch anatomy is the “bovine arch”, as shown in Figure 2. This arch anatomy has a common origin for the brachiocephalic artery and the left common carotid artery.

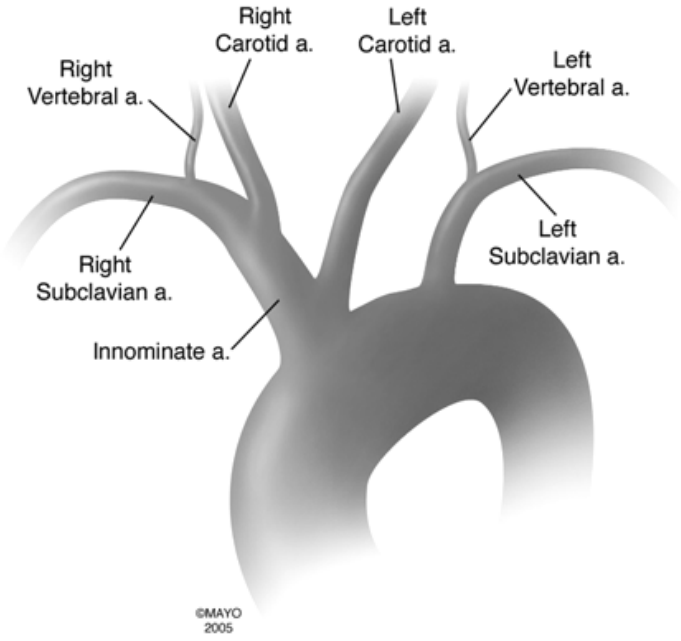

Figure 2. The "bovine arch" anatomy with innominate and left common carotid arteries with the same origin.

Other variations of the aortic arch occur with different branching patterns and distances between artery origins [5]. While there is no “standard arch”, the anatomy of the aortic arch with three, distinct branching vessels is seen in about 70% of individuals [5, 6].

The aortic valve controls blood flow to the aortic arch; blood is pumped from the lungs, to the left atria, to the left ventricle, through the aortic valve and into the aortic arch. The valve, as seen in Figure 3, separates the heart from the aortic arch, and

subsequently the rest of the body. The purpose is to maintain one-way blood flow out of the heart and into the aortic arch. The aortic valve opens when the left ventricle contracts and closes when the left ventricle relaxes, obstructing blood from flowing back into the heart [13].

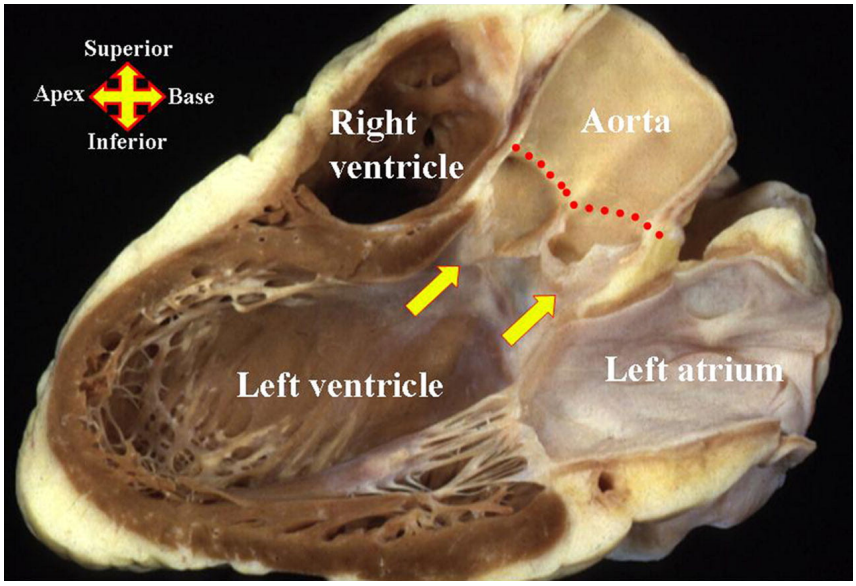

Figure 3. Anatomy of the heart with the aortic valve leading to the aortic arch.[7]

There are two main types of aortic valve disease that can affect blood flow through the aortic valve: stenosis and regurgitation [8]. Stenosis is when the valve does not open entirely and the blood is obstructed from leaving the heart [9]. Regurgitation is when the valve does not close completely after blood is pumped out of the heart, allowing blood to leak backwards. Both abnormalities can be congenital or acquired; patients are either born with a valve abnormality, for instance with only two cusps instead of the normal three, or the patient's valve leaflets become calcified and develop scar tissue that limits the opening and closing of the valve [9].

Patients with aortic valve disease show symptoms such as shortness of breath, chest pain, dizziness, or loss of consciousness. The symptoms are due to the narrowed or leaky valve causing improper blood flow. Left untreated, aortic valve disease can lead to hypertrophy of the left ventricle and potentially sudden death [8, 9]. Symptomatic aortic stenosis, if left untreated, has an annual mortality of 25% and an average survival rate of 2 to 3 years [10]. Currently, there is no medication that can cure aortic valve disease and it is most often treated with surgery.

The three most common surgeries are aortic valve repair, surgical aortic valve replacement, and transcatheter aortic valve replacement [8,10]. The risk factors affecting a doctor's surgical decision include the severity of the valve disease, age, general health, and whether other heart surgery procedures are required for the patient at that time [11]. Repair of the aortic valve can be done by adding tissue to support the valve, removing or reshaping tissue, or separating fused valves [11]. While valve repair is preferred, as it preserves the function of the heart muscle, not all valves can be repaired, as is often the case with the aortic valve [11]. Valve replacement requires replacing the aortic valve with a man-made or biological valve through surgical aortic valve replacement or transcatheter aortic valve replacement surgery.

Surgical aortic valve replacement (SAVR) is the most common treatment for aortic valve disease and is an open-heart procedure. During the procedure, the surgeon creates a 6- to 8- inch incision down the center of the sternum to remove and replace the diseased valve [12,18]. The procedure typically takes a few hours and involves using a heart-lung (bypass) machine through an incision in the chest.

Transcatheter aortic valve replacement (TAVR) is an alternative to SAVR and currently indicated for patients that have high surgical risk and are not candidates for open-heart surgery. Specifically, TAVR was developed for patients with severe symptomatic aortic stenosis who have an unacceptably high estimated surgical risk [15]. The indication could expand to lower surgical risk patients in near future, although SAVR is still the standard treatment of care for low risk patients [14]. Transcatheter aortic valve replacement is less invasive and allows a new valve to be inserted within the native, diseased aortic valve. It does not require a bypass machine and the surgery is performed using a catheter through a small incision. The most common type of TAVR is through transfemoral approach, using a small incision in the patient's leg to access the heart. The delivery system carries the valve to the heart and the aortic valve; when the valve is expanded, typically through a balloon delivery system, the new valve is placed over the diseased valve [16]. The valve is secured and immediately replaces the diseased valve, as shown in the procedure outline in Figure 4.

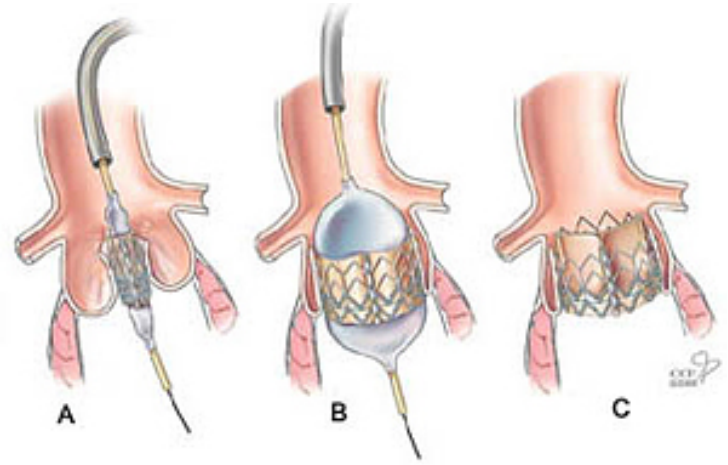

Figure 4. The TAVR procedure outlined. A) The valve is inserted into the aortic valve through a catheter. B) The balloon is expanded over the diseased valve. C) The new valve is expanded and placed over the diseased valve.

2.2 Complications of TAVR

In recent studies, TAVR has shown safety, efficacy, and non-inferiority to conventional surgical aortic valve replacement (SAVR). In a study published in 2012, TAVR was shown to reduce the rates of death and hospitalization for patients that were not candidates for surgery. Data from 2-year outcomes showed patients had a 25 percent decrease in death from any cause, a 50 percent decrease in heart related death, and a significant improvement in symptoms [18]. Currently, TAVR is approved in the United States for extreme risk or inoperable patients. Trials are being conducted in Europe for intermediate risk patients and initial results have shown equivalency to SAVR [19]. A study published in 2016 compared TAVR to SAVR in a randomized study in lower-risk patients with severe aortic valve stenosis. The reported two-year outcome showed TAVR to be safe and effective for lower risk patients [20].

Though TAVR has shown to be beneficial for patients that are at high risk, complications such as paravalvular leak and stroke risk have been associated with TAVR in comparison to SAVR [20]. Specifically concerning stroke risk, randomized studies have shown a significantly higher stroke rate after TAVR procedures as opposed to SAVR [21]. For both procedures, strokes are considered to be embolic (as opposed to ischaemic or haemorrhagic); the mechanism and risk occurs during the insertion of a new valve. When the new valve is replacing the diseased or calcified valve, there is a risk of material being dislodged and traveling to other parts of the body. This can include the branching brachiocephalic and left carotid arteries on the aortic arch, leading to the cerebral system and potentially causing stroke complications [22]. In the case of TAVR,

the calcified or diseased valve remains in the body and mechanism of the atheroemboli or calcified material is thought to be during balloon predilation, valve positioning, or valve implantation, mechanisms which are not present during SAVR [21,22].

While stroke rate is declining for TAVR as technology continues to improve, in recent studies decreasing from 7 to 1.7-4.8%, the embolization of debris is still a concern for TAVR procedures [21]. Silent cerebral lesions were detected in 68-93% after TAVR and 38-54% after SAVR [21]. Silent cerebral lesions, or silent ischaemic infarctions, are defined as brain lesions that are a result of a vascular occlusion and are often only detected through magnetic resonance imaging (MRI) [23]. Unlike strokes, patients with silent cerebral lesions do not show immediate symptoms. While data is varying regarding the correlation between silent cerebral lesions and neurocognitive function [21], silent cerebral lesions have been linked to progressive brain damage and as a precursor to symptomatic strokes [23]. Due to the significantly high rate of silent cerebral lesions complicating TAVR procedures, medical device companies have recognized these risks and have developed cerebral protection systems. The purpose of these devices, such as Claret Medical's Sentinel Cerebral Protection System (CPS) is to reduce brain embolism by filtering or deflecting debris [23].

2.3 Claret Medical's Sentinel Cerebral Protection System

Claret Medical is a medical device company founded in 2009 and located in Santa Rosa, California. The company has developed the Sentinel ™ Cerebral Protection System (CPS) with the purpose of reducing stroke risk during interventional cardiology and cardiovascular procedures. The device is indicated for TAVR procedures as well as in

thoracic endovascular aneurysm repair (TEVAR), left atrial appendage occlusion (LAAO), and transcatheter mitral valve replacement [24]. The Sentinel CPS is "the only device designed to protect the brain from the risk of stroke by filtering, capturing, and removing debris dislodged during certain interventional and surgical cardiovascular." [24] The Sentinel CPS is currently an investigational device in the United States and is undergoing clinical trials.

The Sentinel CPS is comprised of two embolic filters made of polyurethane film with laser-drilled holes, mounted on self-expanding nitinol loops, and delivered through a catheter. The device is inserted through the radial artery in the right arm and the filters are placed within the brachiocephalic artery and the left common carotid artery during procedures, as shown in Figure 5.

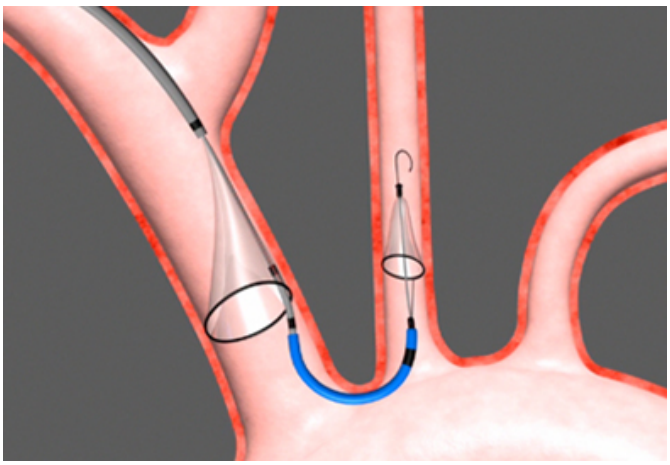

Figure 5. Claret Medical Sentinel Cerebral Protection System is placed within the brachiocephalic artery and the left common carotid artery. [25]

The filters collect any debris released during a procedure and prevent debris from traveling through the brachiocephalic artery and the left common carotid, and consequently the head and neck. The debris can include valve tissue, calcification, or

thrombus that is dislodged at any point during the procedure. In the example of TAVR, once the valve is placed and the procedure is completed, the filters and collected debris are recaptured into the catheter and removed from the patient [26]. In initial clinical trials, Claret has shown a 65% reduction in the total volume of new brain lesions and a 57% reduction in the number of new brain lesions 7 days after the procedure [27].

2.4 CT Scans for Device Testing

A significant difference between procedures for the surgical aortic valve replacement (SAVR) and transcatheter aortic valve replacement (TAVR) is in the visualization of the patient's anatomy. In SAVR, there is direct, open access to the anatomy that allows for visual evaluation of the aortic arch and aortic valve. TAVR lacks open access and requires different methods of visualization during the procedure. Techniques such as echocardiography, computed tomography, and fluoroscopy are used to understand the aortic geometry for device selection and placement [28].

Prior to TAVR, patients undergo assessment of the aortic root anatomy and the coronary and iliofemoral arteries to evaluate the feasibility of the procedure [29]. The diagnostics include echocardiography, cardiac catheterization, aortioilliac angiography, transcatheter heart valve sizing, and computed tomography (CT) scans [29]. Of those methods, CT scans have been increasingly recognized as an optimal method to address the evaluation of the surgical geometries and image for TAVR.

Due to varying anatomies, TAVR must be individualized for a patient [29]. For example, the sizing of the catheter for transfemoral access is key to the success of the procedure. As shown in Figure 6 of a CT angiographic image, the image reveals an area

in the right external iliac artery that would inhibit endovascular access, as indicated by the arrow.

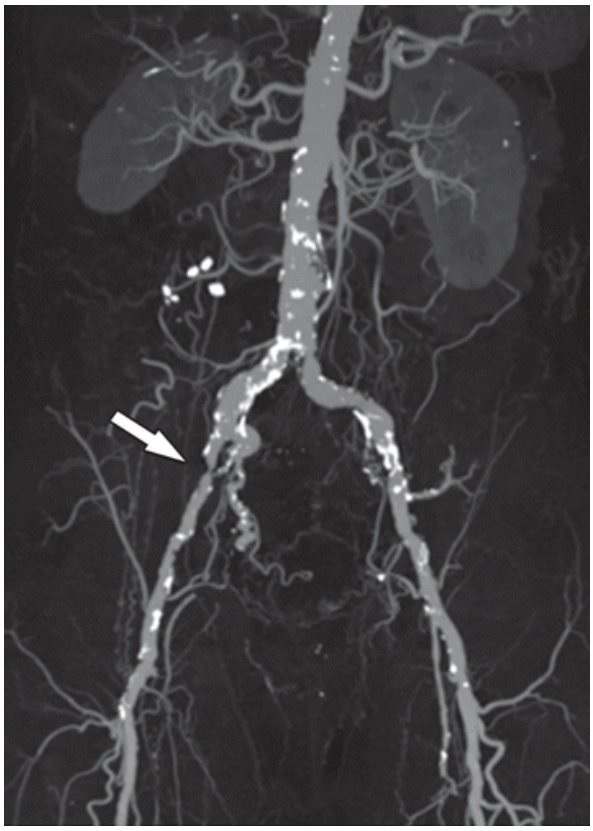

Figure 6. CT angiographic image showing the right external iliac artery (arrow) that would inhibit endovascular access. [30]

In this example, the patient would not be a likely candidate for transfemoral TAVR as the patient's femoral artery could be incompatible with a femoral catheter. This does not necessarily disqualify a patient from TAVR, but is a risk factor that needs to be taken into consideration.

Conventional angiography allows for basic assessment of the luminal size, though it is not suitable for morphologic features. CT is considered a valuable tool to determine

the presence and amount of anomalies such as atherosclerotic calcifications and can determine patient eligibility, access strategy, and prosthetic valve selection [29].

While CT scans are useful for initial analysis, this method of imaging can be further applied to three-dimensional analysis by converting the file. Programs such as Mimics and OsiriX, can convert the CT scan into a different file format that is compatible with computer-aided design (CAD) programs. A common application is the conversion of a CT scan to a stereolithography (STL) file, which is a triangulated representation of a three-dimensional object's surface [31]. The file format is widely compatible with programs related to CAD, rapid prototyping, and 3D printing. By converting a CT scan into an STL file, or similar file format, the patient's anatomy can be analyzed in a variety of programs and is available for more applications, such as 3D printing and creating models for physicians to visualize patient anatomy.

2.5 Existing Vascular Constructs and 3D Printing in Clinical Applications

Physical models are widely used in the biomedical field for applications from physician training to marketing, to device testing. Vendors such as Elastrat, United Biologic Silicone Vasculature, and DialAct Corporation manufacture anatomical models based on engineering approximation, CAD files, or patient specific data [32,33,34]. While these models are widely used, rapid prototyping is a popular as a method of prototyping models and visualizing patient anatomy.

The fundamental purpose of 3D printing is to create a rapid prototype of a model through additive manufacturing. Fused Deposition Modeling (FDM) was originally developed by Statasys and has become one of the most popular rapid prototyping

techniques [35]. FDM works by horizontally depositing molten thermoplastic material, extruded from a nozzle. The material is deposited layer-by-layer based on a 3D CAD data file, filling each layer of the object (Figure 7).

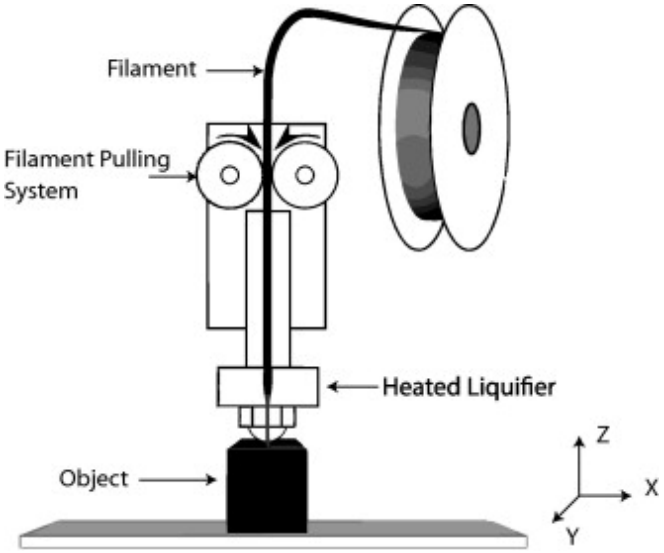

Figure 7. Diagram of FDM rapid prototyping.

The liquefied filament cools after being laid down prior to the nozzle depositing the following layer of filament. The nozzle also contains a second filament that provides support material for the cooling filament, for features such as overhangs, which is removed after printing. A limitation of FDM is that it has a rough finish and often the ridges between layers of plastic are visible on the part. Additionally, in a medical application the material is rigid does not mimic the properties of biological tissue [36]. However, a significant benefit of FDM is the ability to quickly print models at a reasonable price from CAD software without additional manufacturing techniques. For that reasons, among others, 3D printing has been applied within the medical field.

At the Texas Cardiac Arrhythmia Institute, 3D printing was used to recreate models of patient's hearts before performing surgery [37]. The Institute acquired CT scans of the patient's heart and used 3D printing to create transparent models that allowed doctors and patients to view internal structures when preparing for a procedure. The models were prepared within hours and produced unique patient models to "provide customized solutions for improving outcomes [37]."

Another example was in a study that created personalized brain models. Using 3D printing, molding, and casting, the study created a physiologically, anatomically, and tactilely realistic model based on magnetic resonance images (MRIs) [38]. The models were used to improve surgical training and preoperative planning with the goal of providing accurate, customized, high-precision treatment.

Similar examples exist within the hepatic system, gastrointestinal system, musculoskeletal surgeries, and the vascular system [36]. Many hospitals are purchasing in-house 3D printers for the purpose of planning complicated procedures, clinical training, patient education, and creating customized prosthesis [36]. The prevalence and growing popularity of additive manufacturing is applicable to minimally invasive procedures, such as TAVR, as the models provide visualization of the anatomy. Within biomedical engineering, 3D printing has been used to manufacture products as well as test existing products. Models based on patient anatomy have been used in bench top testing to develop medical devices and provide safety and efficacy data when applying for approval from the FDA. Specifically, the models are used to optimize product design, simulate various clinical anatomies, verify the utility of the technology, and perform wear testing [39].

2.6 Previous COMSOL MultiPhysics® Modeling Studies

COMSOL MultiPhysics® is finite element analysis (FEA) software suite that can simulate fluid flow, particle tracking, and mechanical stresses. The COMSOL MultiPhysics® model of the aortic arch was first evaluated by Andrew Janicki (2015), using CT scans and project input from Claret Medical. As this thesis project builds on Janicki's previous work, this section will summarize the past study. Janicki's study additionally built off of thesis studies performed by Ian A. Carr and Shawn Shadden, who analyzed the effect of particle size and the path of travel in the aortic arch using computational fluid models.

The purpose of Janicki's study was to track particles within the aortic arch and determine what parameters cause the particles to enter the different branching vessels on the aortic arch. The parameters evaluated were particle diameter, particle density, blood pressure, and the diameter of the catheter used during TAVR procedures. By using finite element analysis in COMSOL MultiPhysics®, Janicki determined that the diameter of the catheter was not statistically significant. Additionally, larger particles have a higher probability of entering the brachiocephalic artery, the left common carotid artery, and the left subclavian artery, while smaller particles would continue in the descending aorta. Averaging all particle diameters, densities, and blood pressure outcomes, Janicki determined that 54.95 $\pm$ 13.66% of the 1,000 particles released would travel into the cerebral circulatory system within his model.

Janicki's COMSOL MultiPhysics® model used the Creeping Flow module and had nine simulations run for 13 seconds with 0.5-second time steps. The results were

analyzed using multivariate analysis of variance in JMP Pro 11 statistical software. The study used the same CT scan, provided as a stereolithography (STL) file. The original file with truncated daughter vessels, as seen in Figure 8, had 61,543 faces within the mesh file.

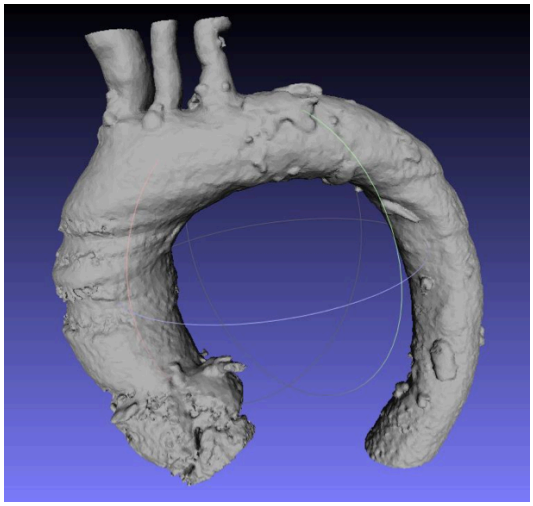

Figure 8. Original STL file of the aortic arch with 61,543 faces.

Janicki used MeshMixer to simplify the model to 251 faces, as seen in Figure 9. The geometry, while usable in SolidWorks, was an oversimplification of the original CT scan.

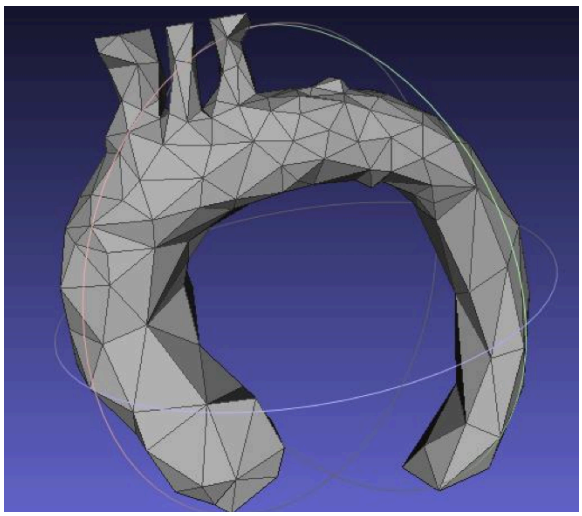

Figure 9. The STL file modified on MeshMixer to 251 faces.

While the general shape of the arch remained intact and it reduced computational time, the significant reduction of faces caused the model to have sharp sections that are not anatomically accurate. This study will re-process the original STL file to have it be more anatomically accurate as well as compatible with COMSOL MultiPhysics® and SolidWorks.

David Baik, an undergraduate in the Cal Poly BioFluidics Lab, evaluated creep flow and laminar flow within the aortic arch as a part of this thesis study. Creep flow versus laminar flow is determined by a fluid's Reynolds's number. The Reynold's number describes the ratio of inertial to viscous forces with Equation 1 [40].

Equation 1: $$\mathrm{Re} = \frac{\rho U d}{\mu}$$

Where ρ is the density, U is the characteristic velocity, d is the vessel diameter, and μ is the dynamic viscosity. At higher Reynold's numbers both inertial forces and the Laminar Flow module should be used on COMSOL MultiPhysics®; however, Janicki's (2015) model utilized the Creeping Flow interface, assuming a low Reynold's number

accounting only for viscous forces. In contrast, in Baik's studies it was determined that both inertial and viscous forces were present and that laminar flow is optimal for future studies.

In relation to the current study, Baik and Janicki's findings are relevant as the results use the same original CT scan and concern the development of test methods for procedures such as TAVR. Therefore, this study will improve the mesh size and use laminar flow.

CHAPTER 3: MODEL DESIGN AND METHODS

3.1 Model Geometry

The geometry of this model is based on a CT scan obtained from Claret Medical. The scan is from a patient that underwent TAVR surgery with Claret's Sentinel CPS device. Therefore, the file used to create this model (physical and COMSOL MultiPhysics® models) is from a real patient anatomy. This file was chosen for it's anatomical simplicity and since it has the most common anatomy of the aortic arch. The CT scan from the patient was converted to a stereolithography (STL) file by an external company for Claret Medical.

3.1.1 STL Processing

The file was processed using MeshMixer to reduce the number of faces on the model and reduce anomalies along the arch. When opened in MeshMixer, the original CT scan had 54,190 triangles within the mesh, as shown in Figure 10.

Figure 10. Original CT scan opened in MeshMixer with 54,190 triangles.

While the high number of faces allows the computer to accurately represent the biological model, it creates a complexity to that increases computational time and can be incompatible with computer programs. Additionally, the high number of faces in the original model was not necessary to represent the critical features of the model. By simplifying the geometry, it reduced the computational time and made it possible to import the model into SolidWorks and COMSOL MultiPhysics®.

The file was imported into MeshMixer and processed to reduce the number of faces, as seen in Appendix A written by Brandon Cohen. The processing focused on removing extraneous aspects of the arch that were not pertinent to fluid flow within the arch. The number of faces was reduced to 9,488 faces, as seen in Figure 11, and the file type was converted to be compatible with SolidWorks.

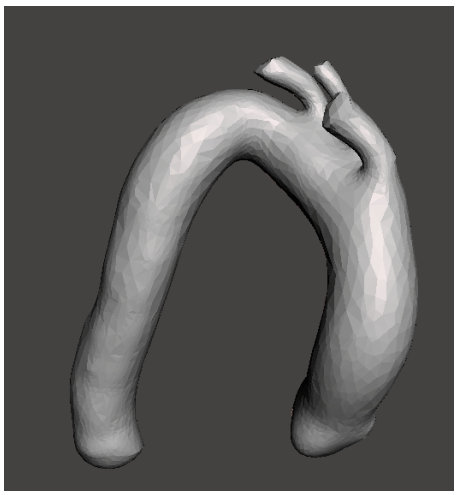

Figure 11. Modified STL file of the aortic arch with 9,488 faces.

3.2 Physical Model Design Concept

The physical model utilized the modified STL file with 9,488 faces. The goal was to create a transparent model of the aortic arch in order to visualize fluid flow. The

material selected for the model was polydimethylsiloxane (PDMS), since it is translucent and has the ability to capture features at the microscopic level. The material is commonly used in the manufacturing of microfluidic chips. As seen in Figure 12, models are typically made with PDMS by having a master mold, pouring PDMS over the mold, and then removing the PDMS containing a negative of the master mold.

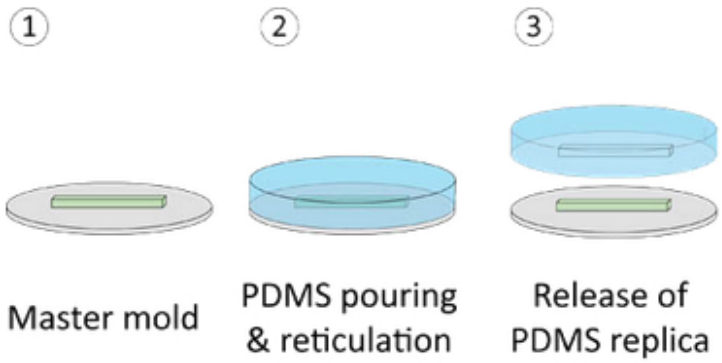

Figure 12. An overview of microfluidics manufacturing methods. 1) A master mold exisits with the shape. 2) PDMS is poured over the master mold. 3) The PDMS is removed from the master mold, leaving a cavity in the shape of the master mold. [41]

The physical model of the aortic arch utilizes a similar molding process. However, unlike microfabrication, the aortic arch geometry contains daughter vessels and is non-symmetrical, making the release of the PDMS negative a challenge. In order to create a negative of the aortic arch, a process was developed that allowed the master mold to be removed without damaging the PDMS or altering the shape of the vasculature.

In a previous thesis project by Daniel Greinke, a dissolvable polymer was cast within PDMS to evaluate an iliac aneurysm. The study 3D printed the entire aneurysm using water-soluble polyvinyl alcohol (PVA) filament. The full aneurysm model involved the following steps (as seen in Figure 13): a triangular box was created using acrylic, blue painter's tape, and caulk to encase the aneurysm. One kilogram of PDMS was poured

into the box and the 3D printed part of PLA was floated on top. The PDMS was allowed to set before the remainder of the 3D printed part was covered in 1 kg of PDMS and the entire model was set. Excess material was cut away from the outlets and the model was submerged in hot water with the intention of dissolving the PLA.

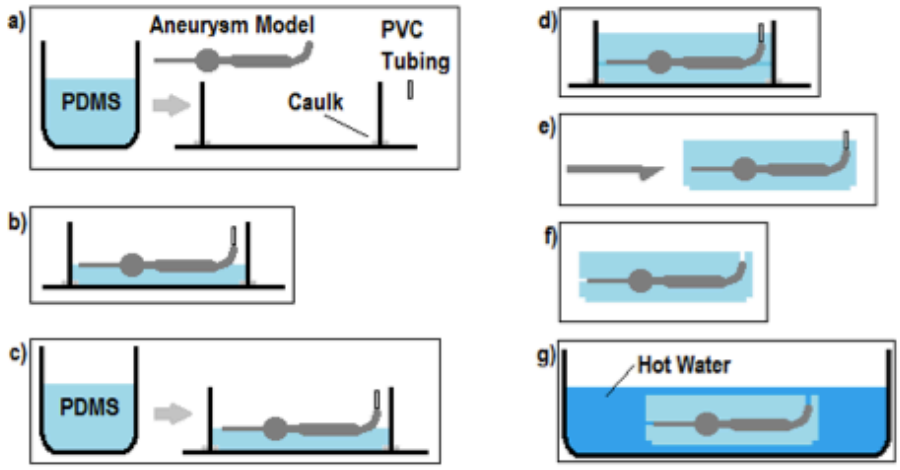

Figure 13. An overview of Greinke's PDMS full mold process. A) the mold is assembled. B) Half of the PDMS is poured into the mold and the aneurysm is allowed to "float" on top. C) The remainder of the PDMS is poured over the aneurysm. D) The PDMS is allowed to set. E) Excess material is removed. F) The aneurysm is submerged in water. G) The water is heated to dissolve the PVA. Source: Greinke

Although the model was submerged in hot water for 6 to 8 hours, it was ineffective to completely dissolve the PLA. The model was also submerged for 14 days in water that was periodically reheated to 120°F. However, regardless of the water temperature and the amount of time the model was submerged, the PLA did not dissolve. As seen in Figure 14, the study was unable to obtain a cavity in the shape of the vasculature. The study ceased using the full aneurysm model for their experiments.

Figure 14. Greinke's full vessel construct of an iliac aneurysm after being submerged in hot water. The PVA did not dissolve from the PDMS and material remained in the construct.

Despite the previous study not achieving a full vascular model, the study showed that PDMS is an optimal material for its ease of use and the clarity for flow visualization. For this study, the material needed to be transparent and semi-flexible, yet durable enough to withstand the flow visualization tests. Other silicone-based materials were considered, including Reynold's Materials SORTA CLEAR series, SmoothOn Clear Flex 30 or 50, and SmoothOn Ecoflex. While these materials were feasible, PDMS (Sylgard 184 Silicone Elastomer Kit) was chosen for the model due to Greinke's success in having a transparent model, the ease of use, and material cost. However, a different method of creating a 3D printed model will be used in this study.

The construction concept is based on having two half constructs bonded together to create a cavity of the arch within a transparent material. The construction had the following process (see the following sections for additional detail):

1) The CT/STL file was simplified in Mesh Mixer and saved as an STL
2) The arch was imported into SolidWorks and split into two halves
3) Each half was used to create a box mold within SolidWorks with alignment pins

4) The two box halves were 3D printed
5) Each half was coated with Reynold's Advanced Materials XTC-3D
6) PDMS was mixed and poured into each box
7) The PDMS castings were removed from the 3D printed boxes
8) A thin layer of PDMS was used to bond the two halves of PDMS
9) PDMS was removed from the inlets and outlets of the bonded PDMS halves
10) Tubing and adaptors were press fit into the inlets and outlets of the arch

3.2.1 Proof of Concept Prototyping

The concept was to create two half vessels and bond the halves together to create a full model of the aortic arch. This method eliminates the need to dissolve PLA and build an acrylic box as a mold. Also, this concept allows for the addition of alignment pins and guarantee that the dimensions of each mold half are equivalent.

Proof of concept prototyping was done using a 3D printed 1-inch cube filled with PDMS and with a cylinder through the middle, as seen in Figure 15.

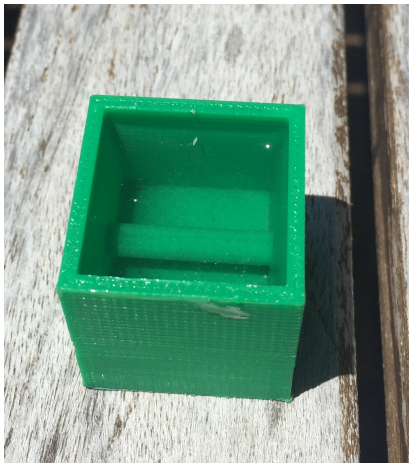

Figure 15. Proof of concept prototyping of the 3D printed mold.

The cylinder was created to test the ability to demold the vessels when using PDMS when it is poured directly into the mold. The cube also tested the Reynold's Advanced Materials XTC-3D coating; the coating was applied to the cube's surface and allowed to dry for 24 hours. The purpose of the coating was to smooth the step sizes between the 3D printed layers. (Refer to section 3.2.2 for more detailed descriptions of PDMS mixing and coating application.)

The casting of the cube was removed from the mold using a chisel and hammer to break the mold open. The cylinder was cut at one end of the cube and slid out through the opposite end. As seen in Figure 16, the proof of concept was successful.

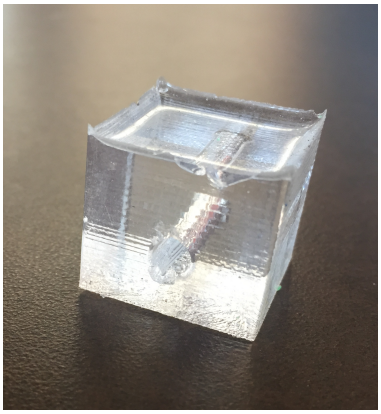

Figure 16. Proof of concept PDMS cube with cylindrical cavity.

The cube was transparent, maintained the cylindrical and cube shape without apparent damage, and the layer lines were reduced without residue from the XTC-3D coating. For these reasons, the 3D printed box concept was applied to the STL file of the aortic arch.

The proof of concept cube was also used to assess different bonding techniques for PDMS to PDMS. In microfabrication, plasma bonding is used to bond PDMS to glass. While the author tested this concept, a study by Eddings et al also showed that

using uncured PDMS adhesive demonstrated an improvement in bond strength and consistency when compared to oxygen plasma bonding for PDMS to PDMS bonding [42]. Based on this study and prototype testing, uncured PDMS was determined to be the optimal method to bond the PDMS halves.

3.2.2 SolidWorks Design and 3D Printing

The arch was imported into SolidWorks and split lengthwise into Part A and Part B by inserting a plane and using the Split function. As seen in Figure 17, the green Part A and the blue Part B split created two pieces without any detached segments. Each arch half was designated as a separate part within SolidWorks.

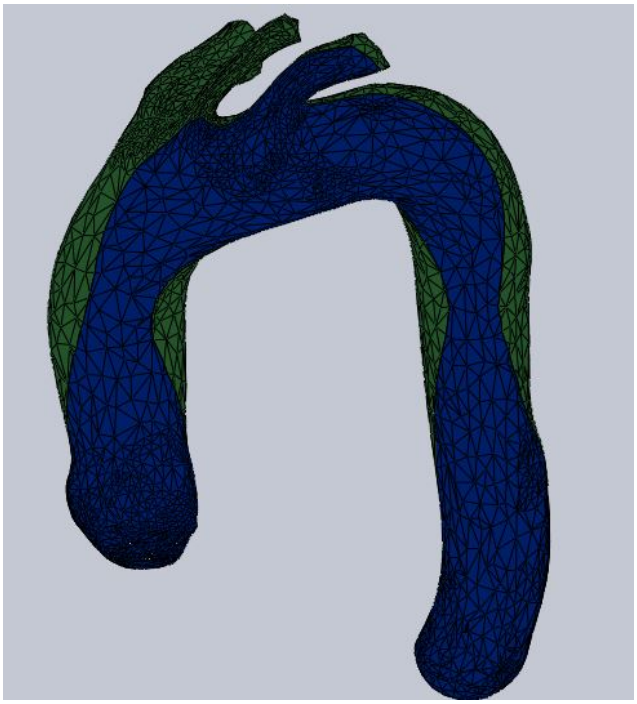

Figure 17. The aortic arch file split lengthwise into Part A (green) and Part B (blue).

The split plane was used to create a 1/4 inch base plane under each part. A box was drawn from that plane and alignment pins with alternating directions were drawn for Part A and Part B. The alignment markers for Part A and Part B were created to be complimentary, making it possible for the halves to interact and align correctly. As seen in the sequence of Figure 18, Part A was drawn to have outward pegs on the 3D printed part.

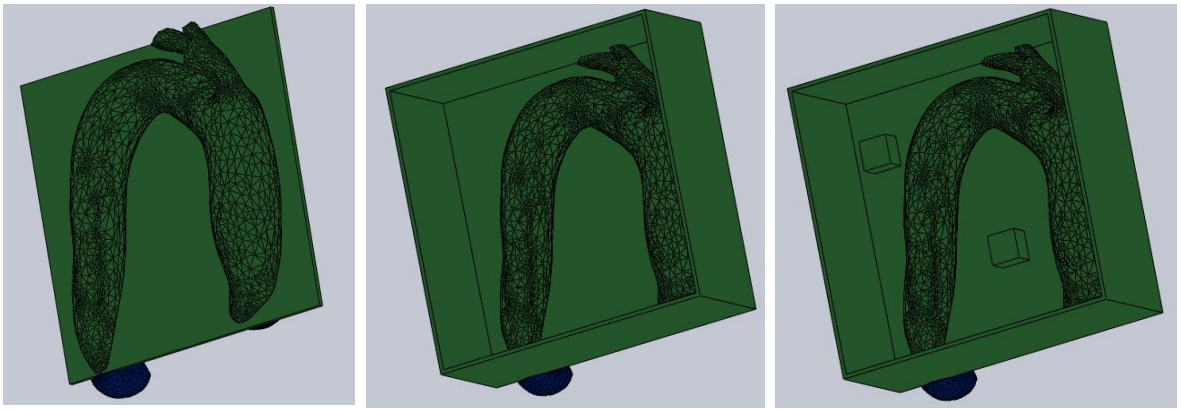

Figure 18. The sequence of creating the 3D printed box with alignment pins for Part A in SolidWorks.

The box was created to maximize the build space of the 6” by 6” 3D printer as well and fully enclose the arch halved. Part B, as seen in Figure 19, was created with the same method but with inward alignment pins. The alignment pin was created with a slight detent for mold removal purposes.

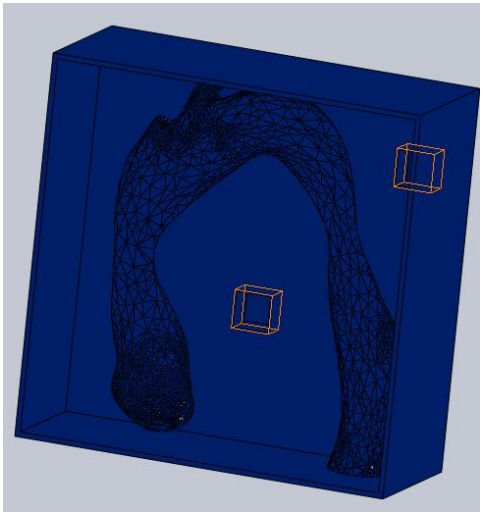

Figure 19. Part B of the aortic arch with inward alignment pins.

For Part A, the brachiocephalic artery did not reach the edge of the box. Since the box is being used as a mold, the vessel was extended with an added cylinder in SolidWorks so the future cavity would have an outlet, as seen in Figure 20.

Figure 20. The added cylinder to Part A to allow the brachiocephalic artery to extend to the edge of the 3D printed box.

As previously mentioned, the two halves were drawn to interact. As shown in Figure 21, Part A and Part B are complimentary and have the same dimensions for the box and the alignment pins.

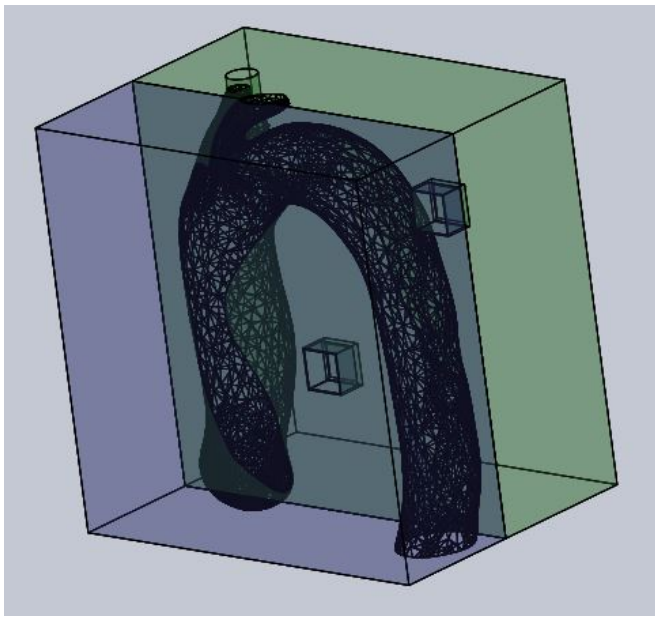

Figure 21. The interaction of Part A and Part B in SolidWorks.

Dylan Sigley, a Cal Poly student that privately owns a 3D printer, printed the parts. The printer is a Printrbot Simple Metal with a 6 inch by 6 inch build space that prints using an additive manufacturing technique with PLA. The program Cura 15.04.6 was used to slide the models and generate the code to print the model. Figure 17 shows Part A (left) and Part B (right), unaltered after being 3D printed. Part A took 17 hours and 9 minutes to print, taking 75.98 meters of filament (or 226 grams). Part A had a build failure towards the end of the build, causing the box to be a 1/2-inch shorter than intended. However, it did not affect the structure of the aortic arch. Part B took 15 hours and 33 minutes to print and took 70.99 meters of PLA filament (or 212 grams). Refer to Appendix B for specific printer basic and advanced settings.

Figure 22. 3D printed boxes of Part A and B.

The inner portion of both parts (the area within the box containing the aortic arch) was coated with two layers of Reynold's Advanced Materials XTC-3D with a paintbrush. The coating is intended to be a protective coating for smoothing and finishing 3D parts. The coating was mixed by volume with a 2A:1B ratio with 20 milliliters of A and 1 milliliter of B. The first layer was allowed to dry 24 hours before applying the second. As seen in

Figure 23, the coating made the 3D printed parts appear shiny and filled space between the different layers of material.

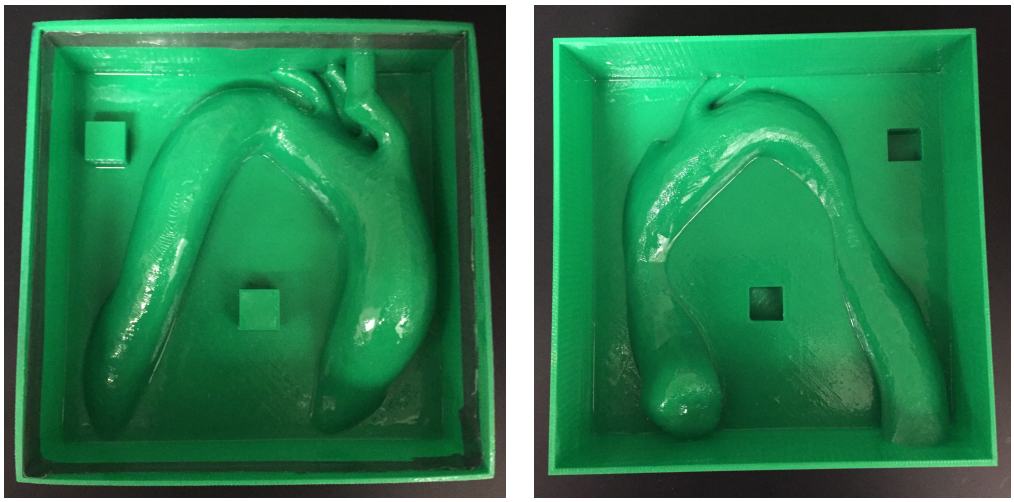

Figure 23. 3D printed boxes of Part A (left) and Part B (right) with Reynold's Advanced Materials XTC-3D coating. Part A has an extension piece taped to the top of the box.

Since Part A had a build failure that caused the box to be shorter than intended, a 1/2" extension piece was printed and taped to the top of Part A. The piece had the same width, length, and thickness as the Part A box, but was only a 1/2" in height. It was superglued and then duct taped to extend the height of the Part A box to original height created in SolidWorks. The extension piece was necessary for the mold to have the correct volume to contain the PDMS.

3.2.3 PDMS and Demolding

The polydimethysiloxane (PDMS) used was the Sylgard 184 Silicone Elastomer Kit from Dow Corning. The volume of PDMS needed for Part A and Part B was calculated using the inner dimensions of the boxes in SolidWorks. The calculated volume

was then used to determine the volume needed for a 10A:1B ratio for the PDMS, using 10 parts of the base material and 1 part of the curing agent material. While the calculated volume proved to be a larger volume than needed, as shown in Table 1, it served as an initial baseline to predict how much material to purchase.

Table 1. PDMS Volumes Calculated and PDMS Volumes Used

	Part A	Part B
Total PDMS Volume (ml)	1208.94	1051.25
PDMS Base (ml)	1090	955
PDMS Curing Agent (ml)	110	95
Total Base Used (ml)	885	675
Total Curing Agent Used (ml)	89	68

The discrepancy between the calculated volume and the volume used for the model is due to the volume of the aortic arch. The volume of the arch was not taken into account during these calculations since the author intended to acquire and mix extra PDMS. This proved to be necessary as 900 milliliters of PDMS were lost when a cracked beaker shattered during degassing of the PDMS and the material was not usable. Therefore, calculating and purchasing extra PDMS was necessary in creating this model.

With the exception of material volumes, the process of mixing and pouring for Part A and Part B were identical. The PDMS was measured in glass beakers and mixed for 10 minutes with a paint stick. A vacuum (Figure 24) was using to de-gas the PDMS for 2 hours. (Due to the high volume of PDMS, the de-gassing took longer than expected. Additionally, after the process the author discovered a valve that had not been closed that

would have decreased the degassing time.) Meanwhile, Part A and Part B were prepared by pressing Scotch tape on all parts to remove dust and debris from the molds.

Figure 24. The vacuum used to degas PDMS and remove bubbles.

The purpose of degassing was to remove all oxygen bubbles from the PDMS prior to pouring to ensure the material cures translucent. Once the bubbles were no longer visible, the PDMS was slowly poured into Part A and Part B. The parts were allowed to cure for 72 hours at room temperature (Figure 25).

Figure 25. Part A (left) and Part B (right) with curing PDMS.

After the PDMS had cured, the models were demolded. Unfortunately, demolding was a destructive process; a hammer and chisel were used to break the mold surrounding the PDMS and remove the arch halves (Figure 26).

Figure 26. The removal of the PDMS from the 3D printed molds.

The removal of the PDMS from the molds took about two hours. A segment of the arch on Part A ripped while it was being demolded (Figure 27) and was mended with PDMS between the segments and allowed to dry 24 hours.

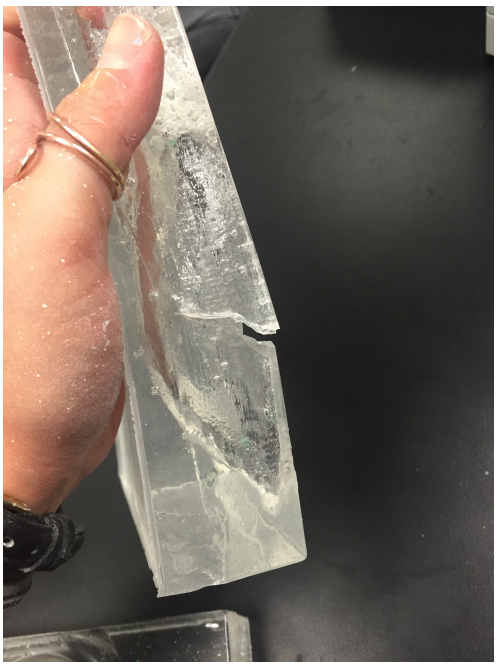

Figure 27. The ripped section of Part A.

After the halves had been demolded and the rip was repaired, the alignment pins were tested and proved to be successful. The two halves of the arch had the same outer dimensions, allowing the two halves of the arch to align correctly. The two halves of the PDMS casting can be seen in Figure 28.

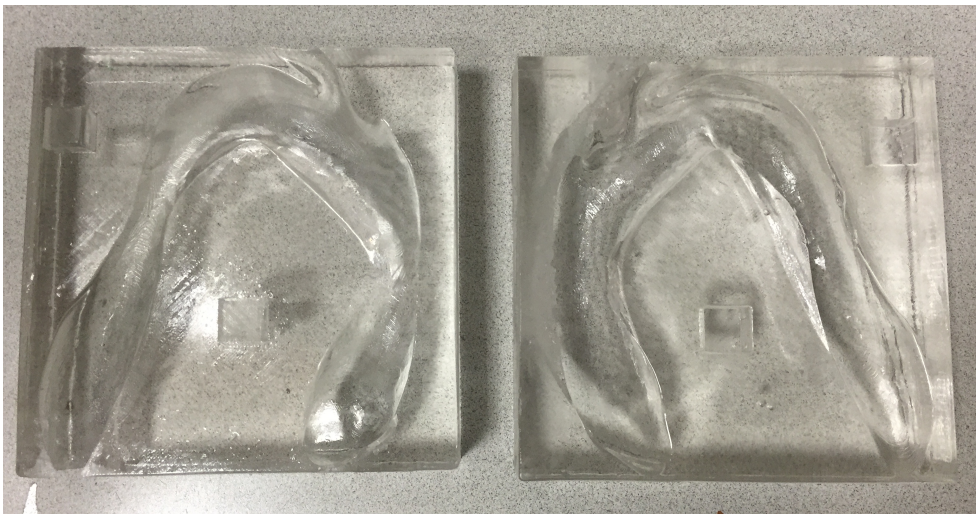

Figure 28. The PDMS casting of the 3D printed parts with Part A (left) and Part B (right).

The halves were bonded together using 10 milliliters of base and 1 milliliter of curing agent. The materials were mixed for five minutes, degassed for five minutes, and applied to the surfaces of both halves in a thin film. The halves were pressed together and aligned, using force distributed evenly on the top surface, as seen in Figure 29. The weight applied was approximately 10 lbs.

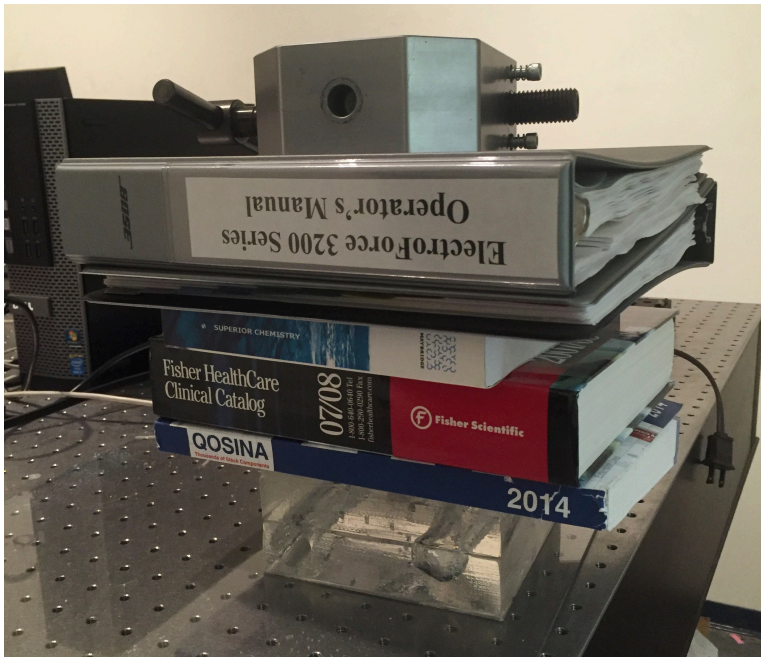

Figure 29. The halves were bonded by PDMS with applied weight.

Once weight was applied, the model was visually inspected for PDMS leaking into the aortic arch cavity. The bonding PDMS was allowed to dry for 48 hours before the weight was removed.

3.3 Flow Visualization Set-Up

For this study, steady-state flow was used to simulate the pumping of blood from the heart. While the heart is pulsatile, pulsatile flow was beyond the scope of this study.

From a study by Spodick et al, the average resting heart rate of a person is between 50 and 90 beats per minute, via [44]. The normal stroke volume in the human heart is 70 mL/beat. Therefore, the cardiac output through the aortic arch can be found for this range of normal beats per minute (Equation 3). Cardiac output is given in mL/min, so this is converted into US Gallons/min in order to find the correct pump to be used (as seen in the conversion in Equation 3).

Equation 2: $CO = SV \times HR$

Equation 3: $1\ mL/min = 0.0158503\ Gallons/min$

From these calculations, the suitable rate for a pump to be used to simulate the heart is between 55 to 100 Gallons/hour. A TotalPond Submersible Fountain Pump was chosen as it can reach a rate of 102 Gallons/hour when run through 5 feet of tubing and was within the project's budget. The pump has a ½" outlet, therefore tubing with a ½" inner diameter was used for the model.

To connect the pump to the arch construct, a razor blade was used to remove PDMS from the model to create a ½ inch inlet of the model. A ½ inch male adapter with barbed tubing was then twisted and screwed into the inlet of the aorta. Once placed into the arch, the fitting was then adhered to the PDMS with clear silicone caulking. In addition to a barbed fitting placed at the inlet, a section of tubing was placed into the outlet of the arch to help direct flow at the outlet of the arch. The construct with the inlet adaptor and outlet tubing is shown in Figure 30.

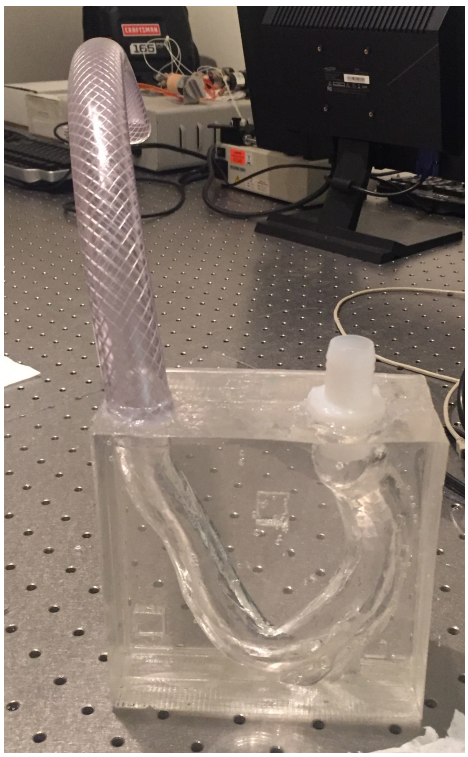

Figure 30. Physical model with an inlet adaptor and outlet tubing.

The daughter vessels had 3/8” and ½” tubing press fit into each, according to size, to drain the aortic arch at the outlets. The entire PDMS construct was placed on a piece of acrylic.

The insertion of the ½” adaptor showed to be detrimental to the model, as the space in the PDMS was not large enough for the adaptor and caused the two halves to begin to peal apart. Applying pressure with a C-Clamp, as seen in Figure 31, mitigated this problem.

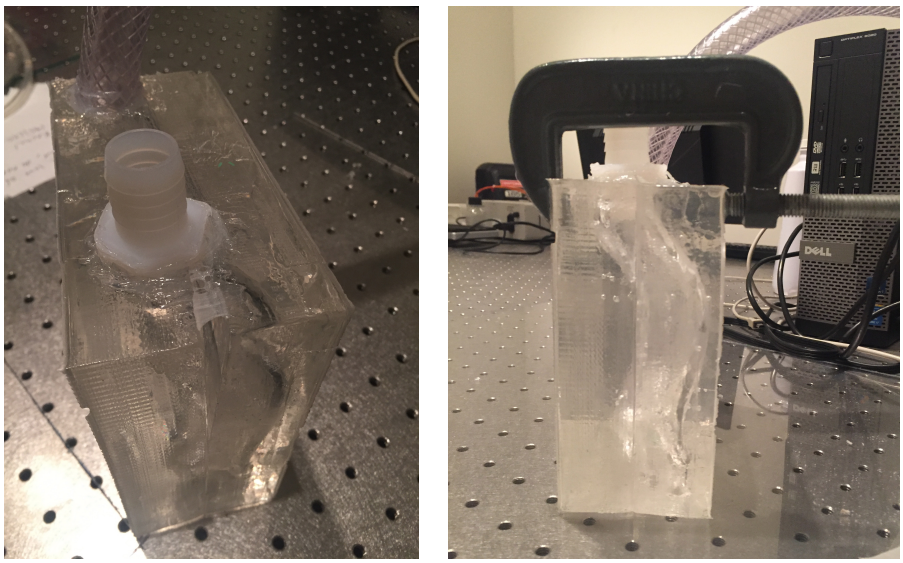

Figure 31. The halves of the construct became unattached with the addition of adaptor (left) and were fixed by applying pressure with a C-Clamp (right).

The model was placed on clear acrylic and elevated (using two 2 foot tall buckets) over a light source. The light was placed underneath to properly illuminate the arch for imaging. All imaging was done using an iPhone 6, placed over the set-up with a metal stand and another piece of clear acrylic. The pump was submerged at the bottom of a bucket filled with water. A side view and top view of the set-up are shown in Figure 32.

Figure 32. The flow visualization set-up side view (left) and top view (right).

However, when the pump was plugged in and water was run through the arch, the flow was extremely turbulent. Air bubbles were present throughout the arch and could not be removed regardless of tube length or pump settings. Red food coloring were injected at the inlet of the pump to better visualize the flow within the arch, as seen in Figure 33.

Figure 33. Turbulent flow with physiologic conditions within the aortic arch. Red food coloring was used to better visualize the fluid flow.

Two methods were used to improve the fluid flow. First, a second pump was purchased for slower fluid flow. The X-Small TotalPond Submersible Fountain Pump pumps 70 gallons per hour at 1.5 feet of tubing. This slower flow rate is still within the range of the average adult stroke rate of the heart. Second, the arch had an inlet and maximum diameter of 1 inch; therefore, the ½" male inlet was removed and 1 inch tubing was press fit into the model. Additional adaptors and tubing were purchased to attach the 1 inch inlet of the arch to the ½ inch outlet of the pump. However, while these modifications eliminated the turbulent flow, an air bubble was still present to the right of the branching vessels (Figure 34).

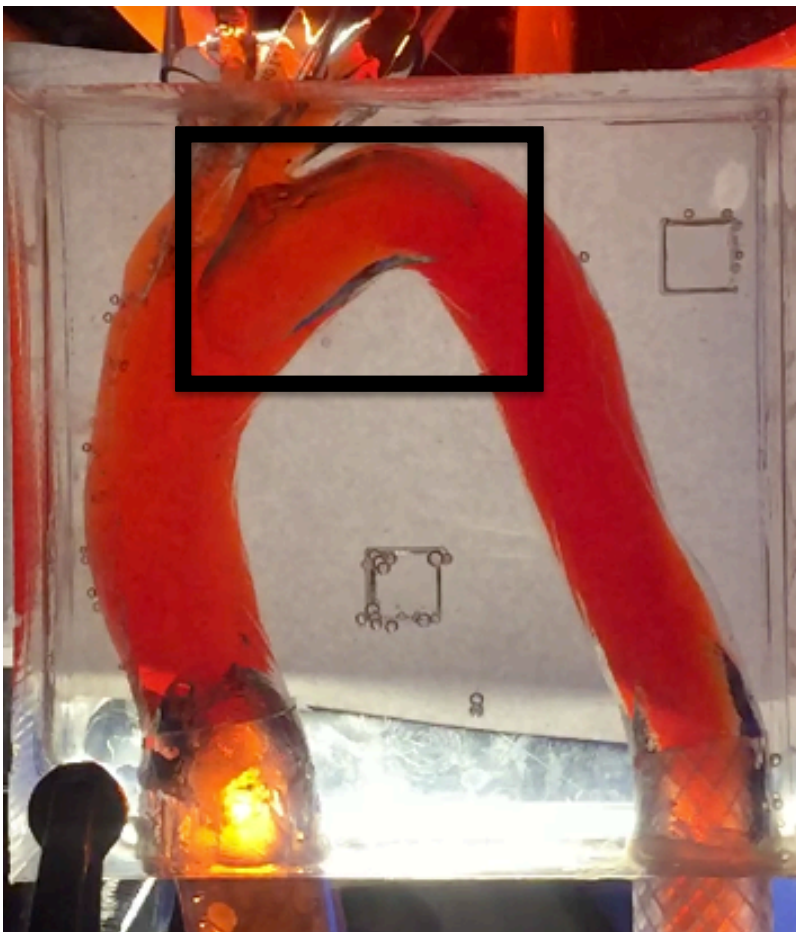

Figure 34. Fluid flow within the arch with red food coloring. A bubble is present to the right of the branching vessels with the slower fluid flow, as indicated by the black box.

The larger inlet eliminated the majority of the air within the cavity of the arch, however the loss of fluid from the outlet of the daughter vessels caused a bubble. At a stationary and horizontal orientation, the fluid within the arch was not sufficient to fill the entire diameter.

The bubble was removed by allowing the fluid to fill the arch, plugging the outlets of the branching vessels, and inverted the model with the branches plugged. This allowed the bubble to flow up the tubing and stay at the connection between the 1" and ¾" tubing. This method made it impossible to use outlet tubing and the set-up of the experiment had to be altered. The arch was placed on plastic sheeting and placed over a

bucket. This allowed the author to tilt the arch and still contain the liquid to a small area. The arch was illuminated using headlamps, sealed in Ziplock bags, within the bucket. The altered, finalized set-up is shown in Figure 35.

Figure 35. The finalized flow visualization set-up side view (left) and top view (right).

This method was not consistent, as sometimes the bubble would dislodge itself and travel back into the arch. In these instances, the arch was inverted again before injecting dye.

The two set-ups were qualitatively compared for lighting within the arch, as seen in Figure 36.

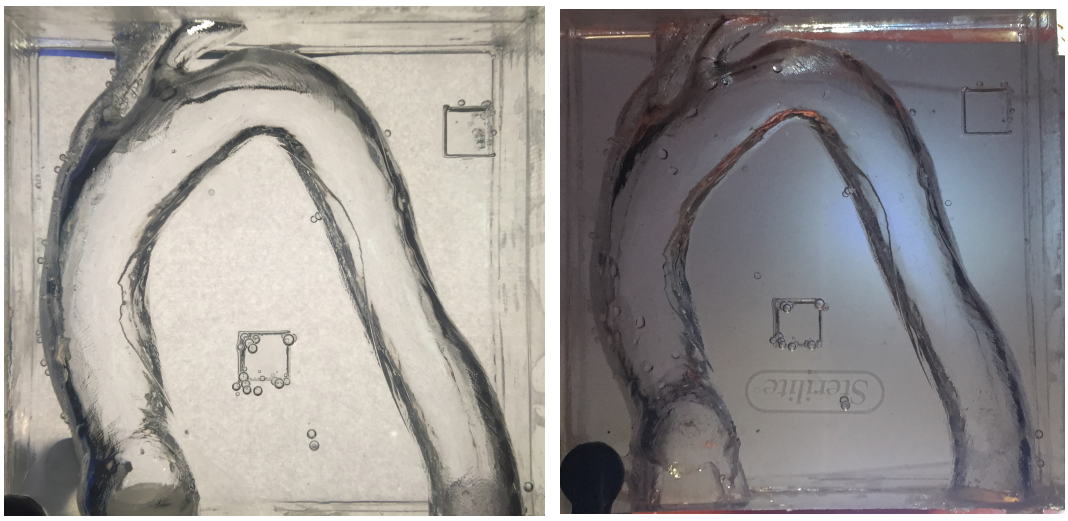

Figure 36. The original arch set-up (left) and the finalized arch set-up (right).

There was not an improvement in lighting and arch visualization between the original set-up (left) and the finalized set-up (right). However, the modified set-up allowed the bubble to be removed and was adequate for image analysis. Lighting should be improved in future studies.

3.3.1 Flow Visualization Trial Methods

For each trial, the pump was submerged in a gallon of water and water was flowed through the arch. Once flow was established in the model, the bubble was removed by plugging and inverting the arch model over the bucket. The arch model was returned to a horizontal position and checked for bubbles. An iPhone 6 on "SLO-MO" mode was used to record a video of the fluid flow. After the bubble was removed and steady flow was established within the model, the iPhone was set to record and 3 milliliters of red food dye (Liquid Color Cherry Red Shade, Esco Foods Inc.) was

injected towards the inlet of the pump. The general flow of dye can be seen in screenshots of the video in Figure 36.

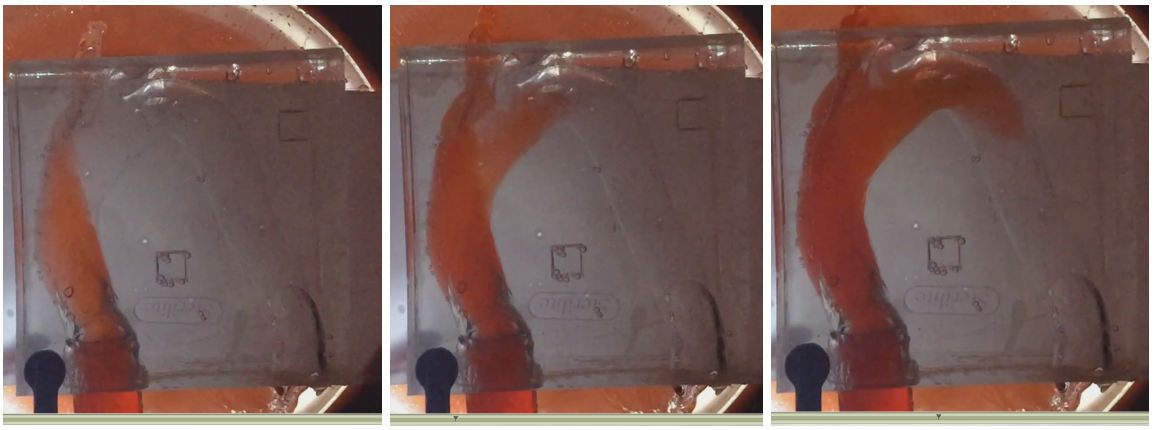

Figure 37. An example of the flow of dye through the aortic arch model.

The flow rate of the pump was measured at the same height and the same tube length as used within the arch. It was assumed that the inlet of the vessel has the same flow rate as the outlet of the tubing. Ten trials were conducted to measure how much time it takes to fill 1 Liter using the pump, with an average of 13.74 seconds per liter. The inlet velocity was calculated using the 1 inch cross section of the inlet, as seen in Appendix C. The outlet velocity of the pump and inlet velocity of the model is 0.1436 meters per second.

3.3.2 Flow Visualization ImageJ Methods

The videos from the flow visualization trials were opened in QuickTime 7.2 at half size. The video was converted from seconds to frames, each frame representing an average of 0.034 seconds per frame. (This value was calculated by taking the average of

seconds per video divided by frames per video.) Screenshots were taken from the videos every 10 frames (every 0.03 seconds) from the instance of the dye initially entering the arch to when the dye filled the arch.

Each trial was individually imported into ImageJ, an open source image processing and analysis software. As shown in Appendix D, the images were converted into stacks and a color threshold was set at 130 saturation. Setting a color threshold added consistent contrast to the image to determine how far the dye had traveled within the arch. The author chose a saturation of 130 as the value selected the majority of the dye within the arch and was then applied across all trials for consistency. Some erroneous red pixels outside of the arch are visible in some images, as seen in Figure 37, and are due to the orange bucket used to catch the water and dye. An example of a trial that had the threshold applied can be seen in Appendix E.

Figure 38. The dye within the arch that was set with a color threshold in ImageJ. The threshold was also applied to the bucket due to the orange color.

The red threshold that was not within the arch is not considered dye movement for this study and is assumed to be the orange bucket or orange reflection. After the color threshold, the images were converted from a stack into individual images and saved for analysis.

3.3.3 Flow Visualization Analysis Methods

The still images, processed in ImageJ, were used to determine the coordinates of the dye front. The coordinates were determined with the following method, which was applied to every image of each trial:

1) Determine an origin (common feature) in COMSOL MultiPhysics® and ImageJ
2) Find the absolute distance from the origin in x and y coordinates
3) Convert the distance from pixels to meters
4) Find the coordinates of the common feature in COMSOL MultiPhysics®
5) Calculate the velocity between dye front locations
6) Measure the angle of rotation within ImageJ
7) Apply the coordinate transformation equations to find COMSOL MultiPhysics® equivalent coordinates

The method was adapted from a procedure developed by Daniel Greinke (2015) and Rachel Willis (2016); the velocity and position of the dye front was determined by comparing the furthest downstream pixel value to the furthest downstream pixel value on the proceeding frame.

The origin was identified as the intersection of the left subclavian artery and the aortic arch, as this location could be easily identified in both the physical and computer models. The coordinates of that location were identified in COMSOL MultiPhysics® as x, y, and z coordinates. This origin point was used to align the coordinate systems and as point of reference for the physical model.

The flow visualization images were imported from each trial into ImageJ stack. A scale was applied to convert pixel distances to meters. (Refer to Appendix D for more detail.) The origin point was identified within the physical model for each trial and the Line Tool was used to measure the distance between the origin point and the pixel that had travelled the farthest within the arch model. The x and y coordinates were recorded for each image, as the images are a 2-dimensional representation and did not have a z coordinate. The absolute coordinates were calculated by subtracting the pixel coordinates from the origin coordinates to determine the distance between the two coordinates. From the absolute coordinates, the change of position of the dye front was calculated by comparing the absolute distance traveled between consecutive frames; the absolute distance of the preceding point was subtracted from the absolute distance of the point of interest. The change in position was used to calculate the velocity by dividing the change in position by the amount of seconds equivalent to ten frames (approximately 0.03 seconds). The outcome of this sequence were values of x and y for the experimental model in terms of absolute coordinates and velocity.

The angle of rotation of the experimental model was measured in ImageJ for each trial. The angle of rotation was defined as the shift in the physical model in relation to the frame of the image. The physical model was compared to the frame of the image to check

whether it was parallel. If the model was not parallel to the image frame, the Angle Tool was used to measure the degree of rotation of the physical model in relation to the image frame. The value was converted to radians and used to relate the experimental model to the COMSOL MultiPhysics® model.

The pixel coordinates were transformed to COMSOL MultiPhysics® coordinates using the coordinate transformation equations, Equations 6 and 7, adapted from studies by Greinke and Willis, as shown below:

$$\text{Equation 6: } x_{rot} = [((x - C_x) * cos\theta) - ((y - C_y) * sin\theta)] + C_x$$

$$\text{Equation 7: } y_{rot} = [((x - C_x) * sin\theta) + ((y - C_y) * cos\theta)] + C_y$$

Where x_{rot} and y_{rot} represent the coordinates in the COMSOL MultiPhysics® model, x and y represent the coordinates of a point of interest in the image (after conversion to meters and calculations), C_x and C_y represent the COMSOL MultiPhysics® origin coordinates, and θ represents the angle of rotation measured from the experimental model. The origin point made it possible to relate the two coordinate systems, as COMSOL MultiPhysics® does not have a clear method of establishing a customized coordinate system.

The output from the overall sequence were x and y coordinates within COMSOL MultiPhysics® that represented the farthest moving pixel within the model as well as the associated velocities. These coordinates were input into the COMSOL MultiPhysics® model to compare velocity measurements.

3.4 COMSOL MultiPhysics® Model Validation Methods

The computer model was created using a student license of COMSOL MultiPhysics® 4.4, which is a finite element analysis (FEA) multiphysics software suite

that can simulate fluid flow, particle tracking, and mechanical stresses. The geometry was simplified in MeshMixer and opened in SolidWorks 2011 as a solid part. Prior to being imported to COMSOL MultiPhysics®, SolidWorks was used to create inlet and outlet planes on the arch using the "Cut with Surface" function within Solidworks (Figure 38).

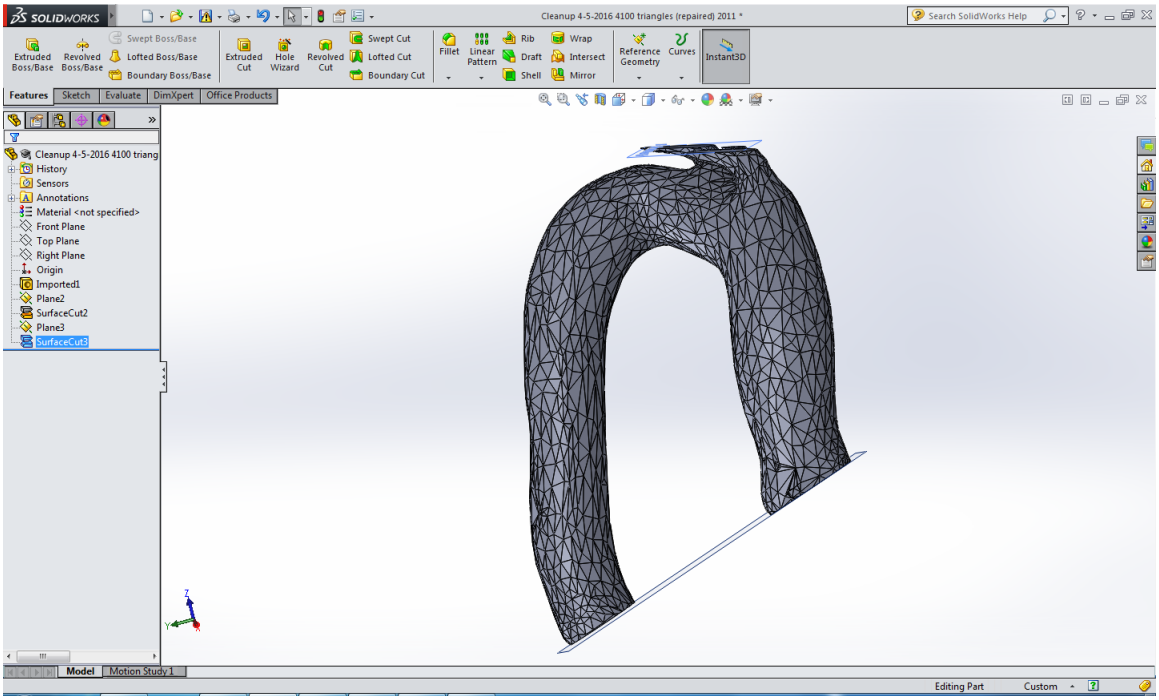

Figure 39. SolidWorks was used to create flat, planar inlets and outlets of the arch.

The plane slice created single surfaces at each of the inlets and outlets of the arch, as opposed to multiple faces. The sliced arch was saved as an IGES and imported into COMSOL MultiPhysics® as the model geometry. The imported geometry was scaled (as dimensions were lost in the resaving of the file) and moved to have positively scaled axis.

Within the imported geometry, the coordinates of the empirical model were plotted as point geometries in the COMSOL MultiPhysics® model; for every physical model coordinate, a point geometry was inserted into the model. Due to the planar cutting in SolidWorks, some points were beyond the inlets and outlets of the COMSOL

MultiPhysics® model and were omitted in the study. As the coordinates from the physical model were 2-dimensional, having been acquired from still images, an array was created for each point in the z-direction. Using x and y coordinates from the physical model, the array spanned the width of the vessel in the z-direction with a point every 1 mm. An example of three point arrays can be seen in Figure 39.

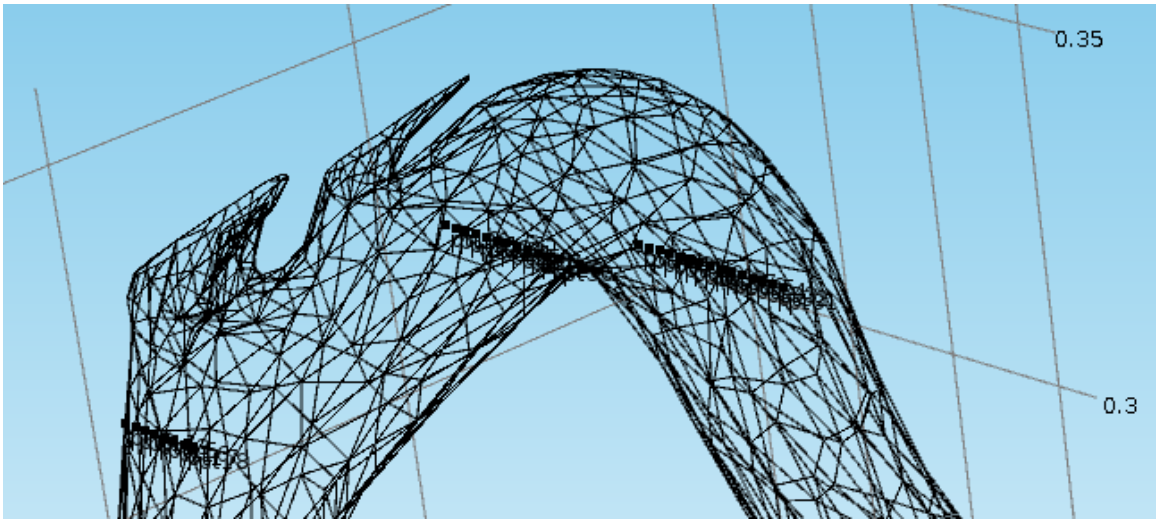

Figure 40. An example of a point array in the COMSOL MultiPhysics® model.

The point arrays were used to acquire point evaluations of the velocity within the arch. The data was exported to Microsoft Excel and the average velocity was determined across the array, based on the assumption that the velocity from the physical model also describes the average velocity across a path length. This allowed for a direct comparison of a single value of the velocity within the COMSOL MultiPhysics® model and the velocity in the physical model.

As this study is validating the physical model, fluid properties of water were used within COMSOL MultiPhysics® with a Newtonian viscosity of 0.89 cP and a density of 1000 kg/m^3. The model assumes a solid conduit with a no-slip condition at the conduit

surface as well as a shear rate of zero at the centerline, where the fluid is at maximum velocity. Laminar flow was selected for the study based on a Reynold's number of 3647, as calculated with Equation 1 and indicated by Table 2. The equation of laminar flow is as seen in Equation 4, accounting for both inertial and viscous forces in the model.

Equation 1: $Re = \frac{Inertial\ Forces}{Viscous\ Forces} = \frac{\rho v D}{\mu}$

Equation 4: $\rho\left(\frac{d\bar{V}}{dt} + \bar{v} \cdot \overline{\nabla v}\right) = \overline{\nabla} \cdot \bar{T} + \rho\bar{\bar{g}}$

Table 2. Flow Regime According to Reynold's Number

Re << 1	**Re < 2100**	**Re > 4000**
Stoke's Flow [N]	Laminar Flow [N]	Turbulent Flow [N]

The inlet was identified as the area shown in Figure 40 and the outlets were identified as the three branching vessels and the section of the arch leading towards the thoracic aorta.

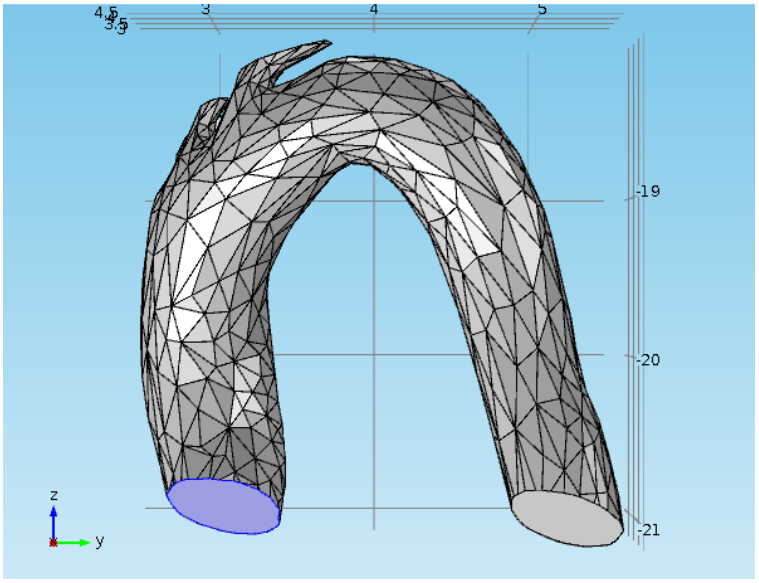

Figure 41. The arch inlet in COMSOL MultiPhysics®, as seen in the purple selection.

The initial conditions matched that of the physical model with an inlet velocity of 0.1436 m/s, as was measured during the empirical trials, and a viscosity of 0.89 cP (μ). The pressure change within the model was calculated using the Hagen-Poiseuille equation (Equation 5) to be approximately 1.388 Pascal.

Equation 5: $$Q = \frac{\pi R^4 (P_i - P_o)}{8 \mu L}$$

The calculated pressure change assumed gauge pressure, in which the outlet equivalent to 0 Pascal to account for atmospheric pressure within the pressure change. Additionally, the inlet (R) is assumed to be 1 inch in diameter and the arch length (L) is assumed to be in center of the arch at approximately 8.62 inches.

A "Fine Mesh" was used in the model, as it was the highest number of elements that could be used without crashing COMSOL MultiPhysics®. The mesh statistics are seen in Figure 41.

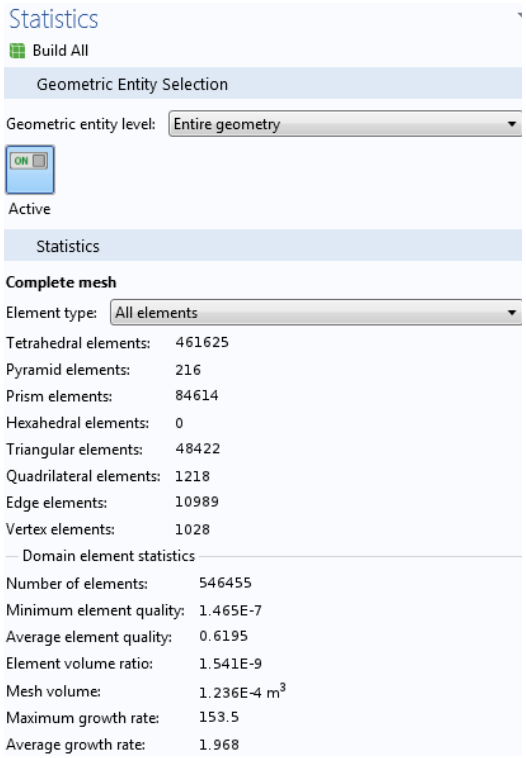

Figure 42. COMSOL MultiPhysics® mesh statistics.

The study was run using a Stationary Study to output velocity and shear stress values as well as qualitative graphs to describe the fluid properties.

CHAPTER 4: DATA COLLECTION AND RESULTS

4.1 Flow Visualization Results

The physical model yielded both qualitative and quantitative results. Qualitatively, the model was successful as an anatomically accurate cavity was created within the model and there was no lateral leakage of fluid within the model. Additionally, the model was transparent and allowed for quantitative analysis.

Five trials dye trials were conducted, three of which were analyzed in this study. Two trials were not analyzed; Trial 4 had poor lighting (which did not allow for thresholding of the image) and Trial 5 had a very large bubble and the frame was shifted as the dye ran through the vessel. From those trials, 24 coordinates were determined and 21 path-length velocities were calculated.

4.2 COMSOL MultiPhysics® Data Collection

The COMSOL MultiPhysics® model used 15 of the coordinates calculated from the physical model. Due to the planar slicing of the model needed to create inlets and outlets, 9 of the coordinates were outside of the geometry of the COMSOL MultiPhysics® model. (In future models choosing a different location to initialize and end the dye front can mitigate this discrepancy. As consistent initial locations were used between the trials, a few points were unusable from every trial.) As previously mentioned, an array was created in COMSOL MultiPhysics® and used to find the average velocity at the coordinate points.

A qualitative velocity graph of the arch cross-section, as seen in Figure 42, shows a streamline within the center of the arch of the maximum velocity. The color gradient depicts the velocities within the arch.

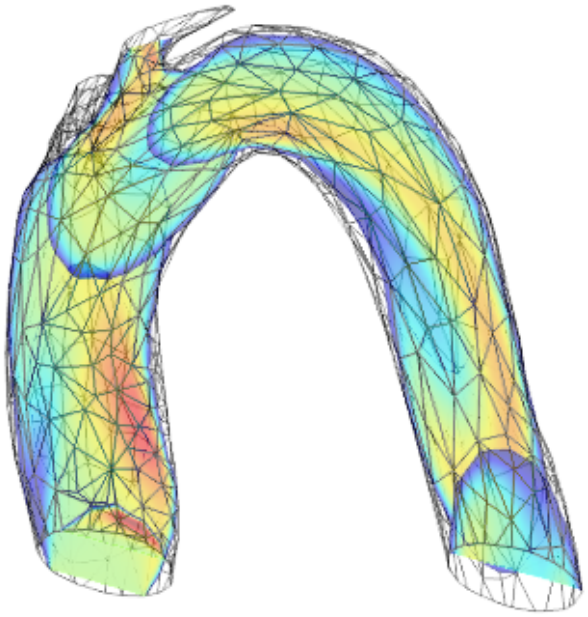

Figure 43. Cross-sectional plot of the arch velocity.

The interior of the arch has the highest velocity with lower velocities towards the walls and the thoracic aorta outlet of the arch. Another qualitative result is seen in Figure 43, showing an arrow plot of the velocities within the arch.

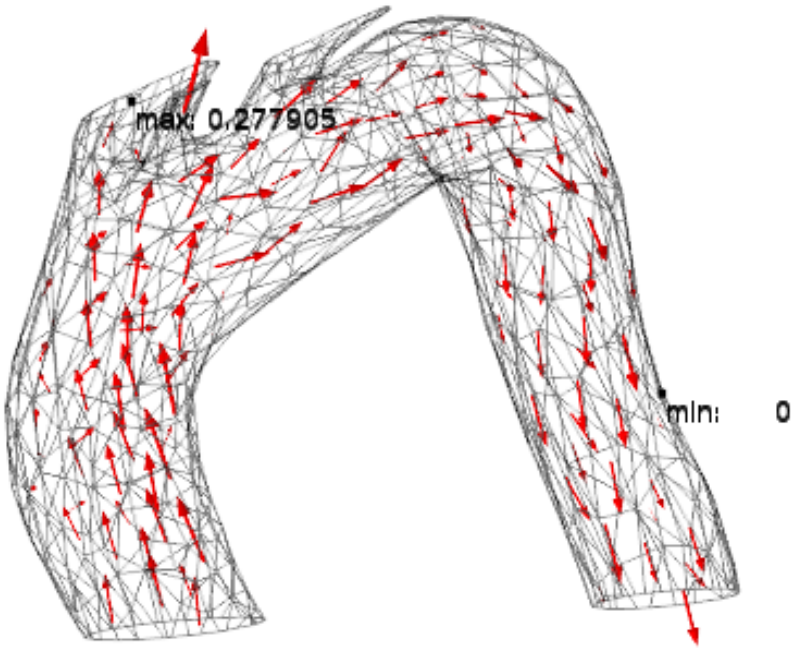

Figure 44. Arrow plot depicting velocities within the arch.

The arrow plot depicts the direction and magnitude of the fluid within the arch and notes the maximum and minimum velocities within the arch. As expected, the maximum velocity is at the centerline of the vessel and the minimum velocity is at the vessel wall.

4.3 Comparative Results

The following graphs show the three experimental trials plotted in comparison to the equivalent COMSOL MultiPhysics® coordinates. As previously mentioned, the experimental velocities were calculated by measuring the distance between the furthest downstream point of dye in one frame to the furthest downstream point of dye in the preceding frame. The distance was divided by the time between frames and represents the

average velocity at the furthest point. The velocities from the COMSOL MultiPhysics® model were calculated using the average velocity from an array of point evaluations at the same coordinates as the dye point in the physical model. The point positions used in the graphs were assigned as an integer based on the sequence of occurrence within the trial.

As seen in Figure 44, Trial 1 differed the most in velocity at the first point position with a higher experimental velocity, but was otherwise consistent.

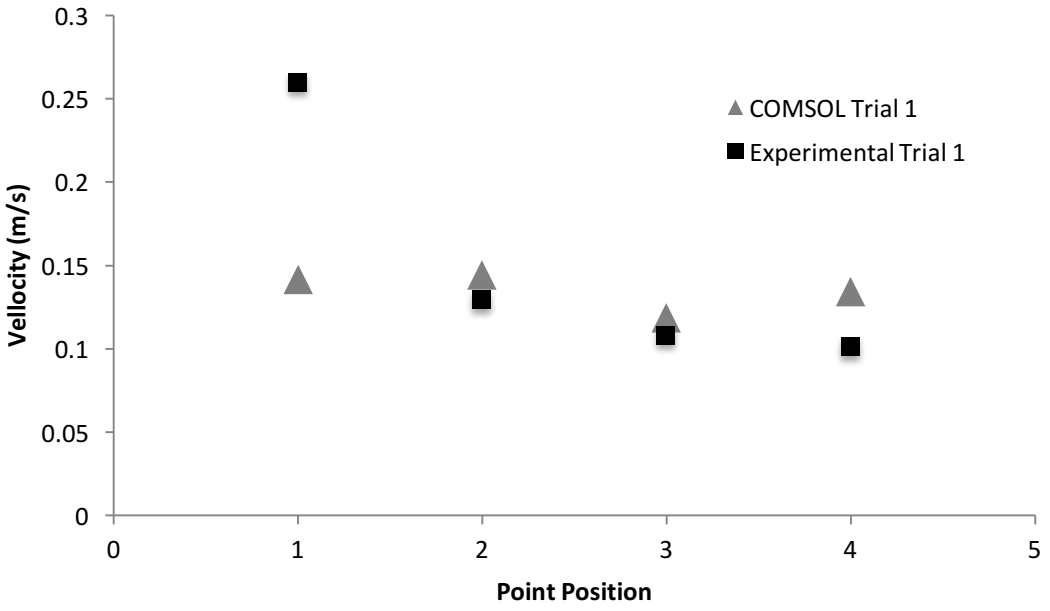

Figure 45. Scatter plot of Trial 1 comparing the COMSOL MultiPhysics® and experimental velocities.

As seen in Figure 45, Trial 2 differed at the first coordinate point with a higher experimental velocity. Otherwise, the experimental velocities were less than the COMSOL MultiPhysics® velocities.

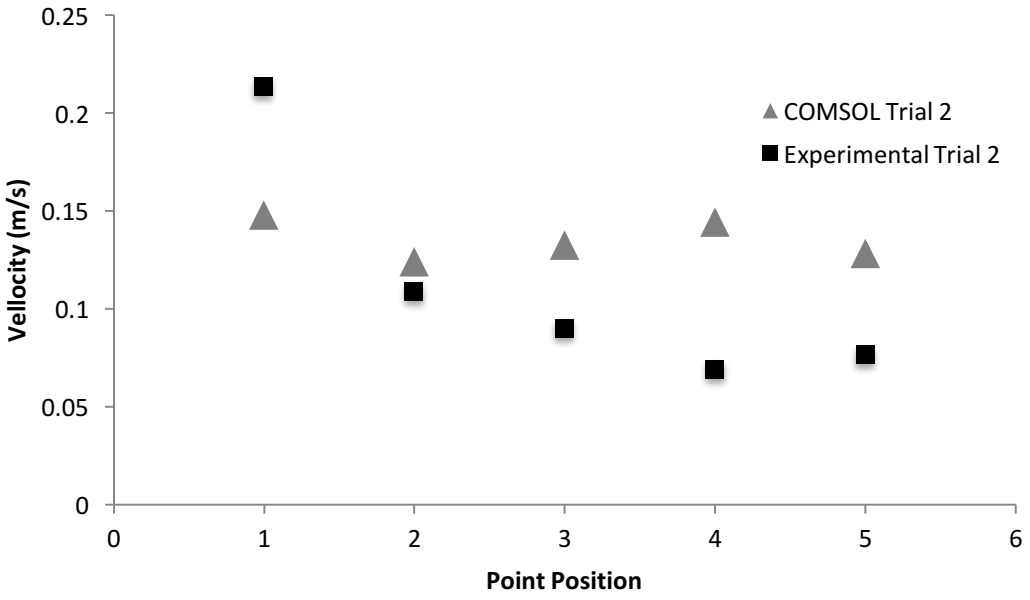

Figure 46. Scatter plot of Trial 2 comparing the COMSOL MultiPhysics® and experimental velocities.

As seen in Figure 46, in Trial 3 the first dye point was very similar. As the dye front moved through the vessel, the experimental velocities were less than the COMSOL MultiPhysics® velocities.

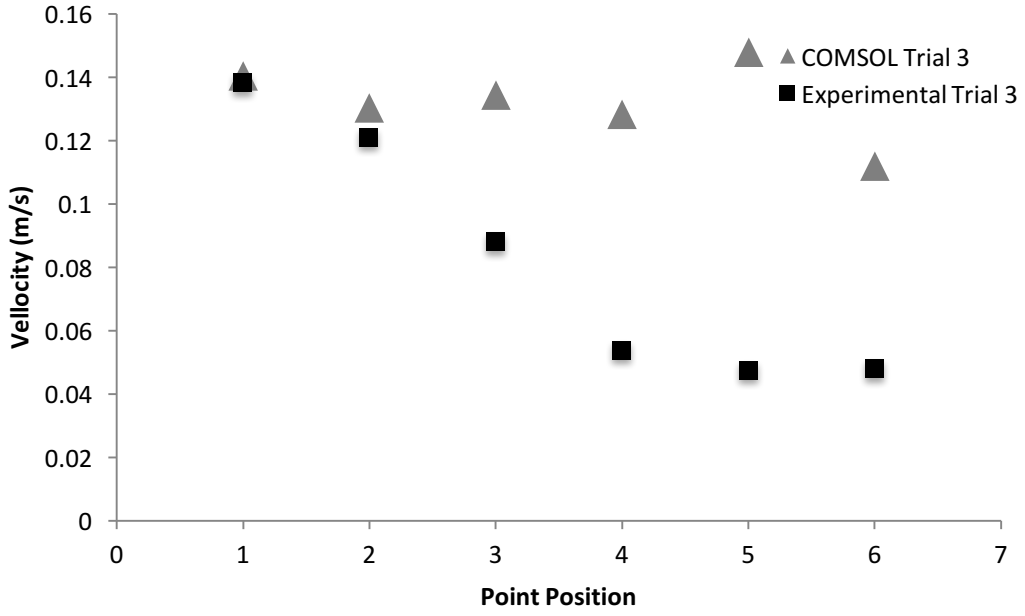

Figure 47. Scatter plot of Trial 3 comparing the COMSOL MultiPhysics® and experimental velocities.

4.4 Statistical Comparison

The statistical analysis comparing the physical model results and the COMSOL MultiPhysics® results was calculated using a Paired 2-Sample T-Test in JMP. For this study, alpha was set to 0.05, the confidence interval was set to 95%, and the alternative hypothesis denotes a significant difference in the samples. The output, as seen in Figure 47, has a p-value of 0.1058 which is greater than 0.05; therefore, we fail to reject the null hypothesis as there is not significant statistical evidence to conclude a difference between the physical model velocities and the COMSOL MultiPhysics® model velocities.

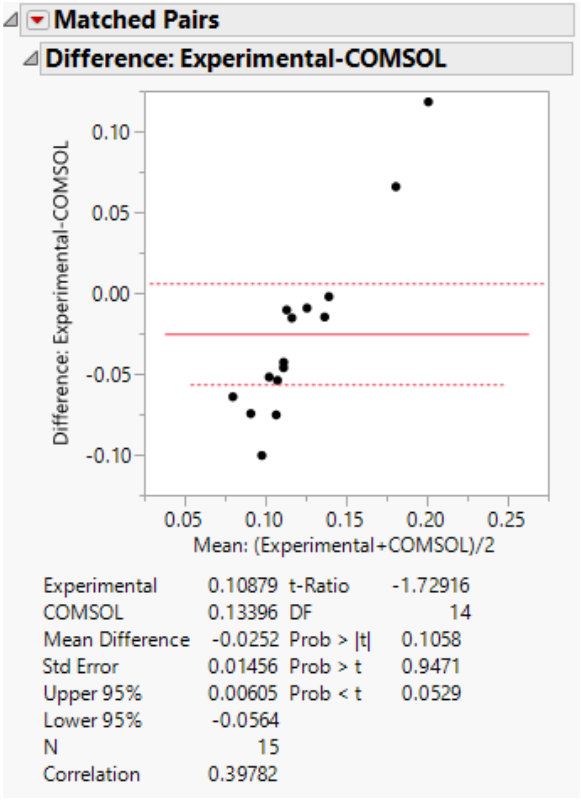

Figure 48. The JMP statistical analysis showing no significant difference between the experimental and COMSOL MultiPhysics® values.

CHAPTER 5: DISCUSSION

5.1 Interpretation of the Experimental Model

One aspect of this study was to create a three-dimensional, physiologically accurate construct of the aortic arch using additive manufacturing techniques for the purpose of clinical testing. The methods developed in this study used to create a physical model were effective and met the purpose of the study. The construction of the model utilized widely available 3D printing to maintain a physiologically accurate representation of a patient anatomy. All support material was removed in the process and the cavity within the model was an accurate representation of the intended STL file. The selected material for the model was transparent and did not become damaged during experimentation.

This model could be used in a clinical setting or in a research and development setting. One application would be to use CT scans from difficult patient anatomy to create new models; the subsequent model could be used as a training tool for surgeons to practice the use and deployment of medical devices within the aortic arch. The purpose would be to reduce surgical error and improve the adoption of new medical devices. Another application would be to use the model to test a medical device while in the development or validation stage. The model can be used to help visualize the sequence of use of the device and be incorporated into quantitative evaluation, as will be further elaborated on in Section 5.2.

5.2 Interpretation of the COMSOL MultiPhysics® Model and Comparison Study

The COMSOL MultiPhysics® model had two purposes: to iterate on the work by Andrew Janicki and to serve as a comparator to the physical model. The primary improvements on Janicki's model were the increased STL file mesh size and the accuracy of flow conditions within the arch. The studies by David Baik and Brandon Cohen, as undergraduates contributing to this study, utilized MeshMixer and SolidWorks to increase the number of faces on the model. Additionally, in COMSOL MultiPhysics® studies, a significant difference was shown between Janicki's model and Baik's model when using laminar flow. The findings from these studies were incorporated into the comparator study that was used to validate the experimental model. (Refer to external reports for more detail on Baik and Cohen's studies.)

The qualitative COMSOL MultiPhysics® outputs, specifically the velocity and arrow plots, showed higher velocity towards the center of the vessel and lower velocities towards the edges of the vessel. This result is accurate in accordance with the Hagen-Pouiselle equation and is as expected to have a maximum velocity in the center streamline of the vessel [N]. The qualitative graphs also demonstrated a lower velocity in the fluid after the outlets of the three branching vessels. This is likely due to the loss of fluid from those outlets, resulting in lower fluid flow in the remainder of the vessel and therefore a lower flow rate and velocity.

The scatter plot graphs depicting the experimental velocities in comparison to the COMSOL MultiPhysics® velocities had a few qualitative inconsistencies. At the first data point for all three trials, the experimental value was equivalent or lower to the COMSOL MultiPhysics® value. This discrepancy could be due to the lack of uniform

flow at the entrance of the vessel. While the diameter of the tubing from the pump matched the diameter of the inlet, uniform flow and velocity within the arch could not be guaranteed at the inlet. The fluid flow may have been faster in certain aspects of the inlet of the model, causing the higher velocity in the experimental model. The remainder of the data points, across all three trials, had lower experimental velocities than the COMSOL MultiPhysics® velocities. This could be due to a discrepancy of the inlet velocity location; while the measured velocity was equivalent to the initial COMSOL MultiPhysics® condition, the planar slicing in SolidWorks removed a portion of the bottom of the arch in the COMSOL MultiPhysics® model and moved the fluid inlet further up the arch. While not much of the arch was removed, the change could have increased the velocity throughout the COMSOL MultiPhysics® simulation.

While the results differed slightly, the statistical analysis of the COMSOL MultiPhysics® simulation velocities in comparison to the physical model velocities confirmed the accuracy of the in silico study. As there was no statistically significant difference between the empirical and in silico models, the study showed that the conditions created within a physical, anatomically accurate model can be emulated using a computer model. While a physical model is useful for various reasons, a computer model uses fewer resources to create, reduces computational steps, and can output more values from a single study. For instance, the COMSOL MultiPhysics® model could also be used to visualize the magnitude and direction of the velocity, as seen in the arrow plot, or output the shear stress in an area of the vessel.

This validation of the accuracy of the COMSOL MultiPhysics® model makes it applicable to medical device testing. The Food and Drug Administration (FDA) is the

regulatory body within the United States responsible for the approval and clearance of medical devices and procedures [43]. The FDA recognizes computational models, such as finite element analysis, as a tool to evaluate the safety and effectiveness of medical devices. An FDA guidance document is publicly available for the submission of "Computational Fluid Dynamics and Mass Transport", outlining the requirements for the submission of a computational model. Those requirements include and are not limited to descriptions of the system geometry, governing equations, system properties, boundary and initial conditions, and validation [45], aspects that were all met within this study. There are a variety of methods available to validate computational models, with no specific protocol yet defined within the medical community. Within computer modeling, validation is the "substantiation that a computerized model within its domain of applicability possesses a satisfactory range of accuracy consistent with the intended application of the model." (Schlesinger et al. 1979) [47]. The validation method within this study used a real world system to statistically validate a finite element analysis model and could hypothetically meet FDA requirements for submission.

An example of the value of FEA analysis is with a device for intervertebral body-fusion devices (IBFDs). The FDA required the company to test all of the products for different areas of the spine, despite having very similar designs and variations to match patient anatomy. The physical testing would have cost the company $1.2 million, making the project uneconomical. The company was able to show that the weakest IBFD, in terms of FDA testing criteria, could still pass FDA standards using FEA modeling. With computer modeling, the company was able to reduce the time, cost, and risk associated

with full-scale testing of the product and bring the product to market within the United States [46].

In the example of Claret's Sentinel CPS, the use of FEA and the validation of the computer model could be applicable in using COMSOL MultiPhysics® for particle tracking. As the company is developing the device and submitting for FDA approval, there is a need for quantitative evidence that the device removes particles from the vessels branching to the cerebral system. As shown in Janicki's study, COMSOL MultiPhysics® has the functionality to track particles within geometries. By combining the validation of this study and the improved parameters of Janicki's study, particle tracking could be performed in COMSOL MultiPhysics® to show the effectiveness of the device while reducing the cost and time associated with physical models.

CHAPTER 6: SUMMARY & CONCLUSIONS

6.1 Contributions to Biomedical Engineering

The results of this study contributed to the field of biomedical engineering by creating a method of application for CT scans, further establishing a novel technique of flow visualization, and successfully performing in silico validation. The creation of a full vessel model is useful for both engineers and clinicians. While there are vendors that make vessel models, this technique was done with limited equipment and a budget of approximately $350. It could very easily be applied to different geometries and be used as an in house method of creating new models, for reasons previously mentioned. This study also utilized a method of flow visualization recently developed in two previous studies; by further developing the method, two of the three studies have now successfully used this method of flow visualization to validate a computational model. Finally, the validation of the in silico model contributed to the field of biomedical engineering by establishing a protocol and potentially contributing to the test methods of Claret Medical.

6.2 Study Limitations

While the study was successful, there were limitations associated with the physical model and computer model. Limitations of the physical model include the seam between the two halves and the step sizes from 3D printing. While efforts were taken to mitigate this issues, including using a resin to fill in the step-sizes and bonding with the optimal technique, ridges were still present in the model that were not present in the COMSOL MultiPhysics® model and may have altered the fluid flow within the arch. During experimentation the model was interchanged with multiple inlet and outlet press-

fit tubes, which caused a slight separation of the two halves. Further damage was stopped by using a C-clamp to hold the halves together. In the future, this can be mitigated by measuring the inlet and outlets of the model to not exceed the size while press-fitting attachments. For the experimental set-up, additional lighting should be used to better visualize the arch. A significant limitation was that a uniform velocity could not be achieved at the inlet and the presence of bubbles in the model. While efforts were taken to limit these factors, further methods should be developed to improve the uniformity of inlet velocity and decrease frequency of bubbles.

Within the COMSOL MultiPhysics® model, as with all finite element simulations, there were limitations of the accuracy of the simulation. The program required a simplification of the original geometry to be able to process the file size. The mesh size that was used had the highest number of elements possible with the file size, as finer mesh sizes caused the program and simulation to crash. Another limitation was that the version of COMSOL MultiPhysics® used, COMSOL MultiPhysics® 4.4, lacked the ability to define distinct coordinates. The coordinates of the origin point were obtained through a study run with the same geometry and parameters. The study was equivalent, but had to be run prior to the comparison study, as the program version did not have the capability of displaying coordinates. Finally, the discrepancy of the COMSOL MultiPhysics® inlet location in comparison to the physical model inlet location may have caused a change in velocity throughout the model. In future studies, the planar cuts should be included in both models to eliminate the change of inlet position.

For the overall study, the significant limitations were associated with simulating in vivo conditions. The pressure was not controlled at the inlet and outlet and was

atmospheric in this study; this would not be the case in vivo as there are different pressures within the body. A second aspect is that pulsatile flow would better mimic blood flow within the body, but was outside the scope of this study. Similarly, water was used to simulate fluid in this model for budget and scope reasons. Blood, or a fluid with similar properties, would better emulate physiologic conditions for testing. Finally, the geometry used in this study was a simplified model of real patient anatomy. An assumption of this study is that the simplification of the model maintained the significant characteristics of the anatomical features.

6.3 Future Work and Conclusions

Transcatheter aortic valve replacement is a developing minimally invasive procedure and is very relevant in the medical field. As TAVR and similar procedures continue to develop, the need for experimental evaluation and visualization of devices will continue to grow, making this project relevant to many companies in the medical device industry. In future iterations of this study, fluid with physiologically accurate properties should be incorporated. Blood is a non-Newtonian fluid, which could change the results of the model. Incorporating a fluid similar to blood would better mimic conditions in the body for device testing. Additionally, different patient scans could be used to emulate difficult anatomies. Within the computer model, different anatomies could be compared to determine if fluid flow differs and in what way. Within the physical model, the model could be extended to include inlets for medical devices and the model could be used as a training device for physicians in difficult anatomies. Finally, all the studies of Janicki should be repeated with the improvements indicated in this study and in

the reports of Baik and Cohen. Additionally, the limitations of this study should be taken into consideration and mitigated.

In conclusion, this study used CT scans from Claret Medical to create an anatomically accurate physical model and improve an existing computational model. The computational model was successfully validated using a novel technique of flow visualization. The validation of the computational model is applicable to TAVR procedures and the method could be applicable for different anatomies and other procedures within the aortic arch.

REFERENCES

[1] M. Donald Lloyd-Jones, "Heart Disease and Stroke Statistics—2010 Update,"

[2] Webb JG, Wood DA. Current Status of Transcatheter Aortic Valve Replacement. *J Am Coll Cardiol.* 2012;60(6):483-492. doi:10.1016/j.jacc.2012.01.071.

[3] Sacco RL, Kasner SE et al. AHA/ASA Expert Consensus Document: An Updated Definition of Stroke for the 21st Century. Stroke. 2013;44:2064-2089.

[4] "Clinical Evidence for Sentinel CPS." *Claret Medical*. N.p., n.d. Web.

[5] American Journal of Neuroradiology." *Bovine Aortic Arch Variant in Humans: Clarification of a Common Misnomer*. N.p., n.d. Web. 14 Aug. 2016.

[6] Kau, Thomas et al. "Aortic Development and Anomalies." *Seminars in Interventional Radiology* 24.2 (2007): 141–152. *PMC*. Web. 6 July 2016.

[7] Anderson, R. H. "The Surgical Anatomy of the Aortic Root." *Multimedia Manual of Cardio-Thoracic Surgery* 2007.0102 (2007): 2527-0. Web.

[8] "Aortic Valve Disease." *The Patient Guide to Heart, Lung, and Esophageal Surgery*. The Society of Thoracic Surgeons, 27 May 2015. Web. 14 Aug. 2016.

[9] Nishimura, R. A. "Aortic Valve Disease." *Circulation* 106.7 (2002): 770-72. Web.

[10] Bates, E. R. "Treatment Options in Severe Aortic Stenosis." *Circulation* 124.3 (2011): 355-59. Web.

[11] "How Is Heart Valve Disease Treated?" *National Heart, Lung, and Blood Institute*. US Department of Health and Human Services, 22 June 2015. Web. 14 Aug. 2016.

[12] Eggebrecht, Holger, Axel Schmermund, Thomas Voigtländer, Philipp Kahlert, Raimund Erbel, and Rajendra H. Mehta. "Risk of Stroke after Transcatheter Aortic Valve Implantation (TAVI): A Meta-analysis of 10,037 Published Patients." *EuroIntervention* 8.1 (2012): 129-38. Web.

[13] Nishimura, R. A. "Aortic Valve Disease." *Circulation* 106.7 (2002): 770-72. Web.

[14] Mishra, Sundeep. "Will Percutaneous Valves Replace the Surgical Valves: Another One Bites the Dust?" *Indian Heart Journal* 68.3 (2016): 249-51. Web.

[15] Gaasch, William H., MD, Stephen JD Brecker, MD, and Gabriel S. Aldea, MD. "Transcatheter Aortic Valve Replacement: Indications." *Transcatheter Aortic Valve Replacement: Indications*. UpToDate, 30 June 2016. Web. 14 Aug. 2016.

[16] Edward's Lifesciences. "TAVR by Edwards." Edward's Lifesciences, n.d. Web.

[17] "Valve Disease Treatments." *Cleveland Clinic*. Cleveland Clinic, n.d. Web. 14 Aug. 2016.

[18] Al-Attar, Nawwar. "Faculty of 1000 Evaluation for Transcatheter Aortic-Valve Replacement for Inoperable Severe Aortic Stenosis." *F1000 - Post-publication Peer Review of the Biomedical Literature* (n.d.): n. pag. Web.

[19] Kleiman, Neal S., and Michael J. Reardon. "Advances in Transcatheter Aortic Valve Replacement." *Methodist DeBakey Cardiovascular Journal* 12.1 (2016): 33–36. *PMC*. Web. 15 Aug. 2016.

[20] Søndergaard, Lars, Daniel Andreas Steinbrüchel, Nikolaj Ihlemann, Henrik Nissen, Bo Juel Kjeldsen, Petur Petursson, Anh Thuc Ngo, Niels Thue Olsen, Yanping Chang, Olaf Walter Franzen, Thomas Engstrøm, Peter Clemmensen, Peter Skov Olsen, and Hans Gustav Hørsted Thyregod. "Two-Year Outcomes in Patients With Severe Aortic Valve Stenosis Randomized to Transcatheter Versus Surgical Aortic Valve Replacement." *Circulation: Cardiovascular Interventions Circ Cardiovasc Interv* 9.6 (2016): n. pag. Web.

[21] Grabert, Stephanie, Rüdiger Lange, and Sabine Bleiziffer. "Incidence and Causes of Silent and Symptomatic Stroke following Surgical and Transcatheter Aortic Valve Replacement: A Comprehensive Review." *Interact CardioVasc Thorac Surg Interactive CardioVascular and Thoracic Surgery* (2016): n. pag. Web.

[22] Wimmer, N. J., and D. O. Williams. "Transcatheter Aortic Valve Replacement and Stroke." *Circulation: Cardiovascular Interventions* 8.6 (2015): n. pag. Web.

[23] Lee, S.-C., S.-J. Park, H.-K. Ki, H.-C. Gwon, C.-S. Chung, H. S. Byun, K.-J. Shin, M.-H. Shin, and W. R. Lee. "Prevalence and Risk Factors of Silent Cerebral Infarction in Apparently Normal Adults." *Hypertension* 36.1 (2000): 73-77. Web.

[24] *Claret Medical*. N.p., n.d. Web.

[25] "The Sentinel CPS Procedure." *Claret Medical*. Claret Medical, n.d. Web. 14 Aug. 2016.

[26] "Sentinel Cerebral Protection Device International." *Claret Medical*. Claret Medical, n.d. Web. 14 Aug. 2016.

[27] "Randomized TAVR Clinical Trials." *Claret Medical*. Claret Medical, n.d. Web. 14 Aug. 2016.

[28] Buellesfeld, Lutz. "Optimizing Outcome of Transcatheter Aortic Valve Replacement." *JACC: Cardiovascular Interventions* 6.5 (2013): 469-71. Web.

[29] Blanke, Philipp, U. Joseph Schoepf, and Jonathon A. Leipsic. "CT in Transcatheter Aortic Valve Replacement." *Radiology* 269.3 (2013): 650-69. Web.

[30] Salgado, Rodrigo A., Jonathon A. Leipsic, Bharati Shivalkar, Lenz Ardies, Paul L. Van Herck, Bart J. Op De Beeck, Christiaan Vrints, Inez Rodrigus, Paul M. Parizel, and Johan Bosmans. "Preprocedural CT Evaluation of Transcatheter Aortic Valve Replacement: What the Radiologist Needs to Know." *RadioGraphics* 34.6 (2014): 1491-514. Web.

[31] Stratasys. "How to Prepare STL Files." Stratasys, n.d. Web.

[32] Elastrat. "Elastrat's Anatomical Vascular Models for Education Training, Research and Development." *Elastrat*. N.p., n.d. Web. 14 Aug. 2016.

[33] "United Biologics Inc. Silicone Vascular Models." *United Biologics*. N.p., n.d. Web. 14 Aug. 2016.

[34] "DialAct Corporation." *General Vascular Models*. N.p., n.d. Web. 14 Aug. 2016.

[35] O. S. Carneiro, A. F. Silva, and R. Gomes, “Fused deposition modeling with polypropylene," Materials and Design, vol. 83, pp. 768-776, 2015.

[36] Marro, Alessandro, Taha Bandukwala, and Walter Mak. "Three-Dimensional Printing and Medical Imaging: A Review of the Methods and Applications." *Current Problems in Diagnostic Radiology* 45.1 (2016): 2-9. Web

[37] Stratasys. "Printing Hearts." *Stratasys Direct Manufacturing*. Texas Cardiac Arrhythmia Institute, n.d. Web. 14 Aug. 2016.

[38] Ploch, Caitlin C., Chris S.s.a. Mansi, Jayaratnam Jayamohan, and Ellen Kuhl. "Using 3D Printing to Create Personalized Brain Models for Neurosurgical Training and Preoperative Planning." *World Neurosurgery* 90 (2016): 668-74. Web.

[39] Iaizzo, Paul A. "Bench Tests, Animal Tests, Clinical Trials and Regulatory Issues." *University of Minnesota* (n.d.): n. pag. Web.

[40] R. L. Fournier, Basic Transport Phenomena in Biomedical Engineering. CRC Press.

[41] Elveflow. "PDMS: A Review." *Elveflow: Plug and Play Microfluidics*. N.p., n.d. Web. 14 Aug. 2016.

[42] Eddings, Mark A., Michael A. Johnson, and Bruce K. Gale. "Determining the Optimal PDMS–PDMS Bonding Technique for Microfluidic Devices." *J. Micromech. Microeng. Journal of Micromechanics and Microengineering* 18.6 (2008): 067001. Web.

[43] "Products and Medical Procedures." *U.S. Food and Drug Administration*. N.p., n.d. Web. 14 Aug. 2016.

[44] Spodick DH, Raju P, Bishop RL, Rifkin RD. Operational definition of normal sinus heart rate. Am J Cardiol. 1992;69:1245–6

[45] Reporting of Computational Modeling Studies in Medical Device Submissions." *U.S. Food and Drug Administration*. N.p., n.d. Web. 14 Aug. 2016.

[46] Mraz, Stephen J. "FEA on New and Redesigned Medical Components Can save Time and Money during FDA Approval." *Machine Design*. N.p., n.d. Web. 14 Aug. 2016

[47] Sargent, Robert G. "Verification and Validation of Simulation Models." *2008 Winter Simulation Conference* (2008): n. pag. Web.

.

APPENDICES

Appendix A: MeshMixer Processing of the STL File

Written by Brandon Cohen

This is a protocol on how to transform a CT scanned part into a part that can be opened and manipulated in SolidWorks. This is important when 3D printing of the part is necessary, for if the part is too large of a mesh, it can not be opened in SolidWorks and many other 3D programs. This protocol uses Autodesk MeshMixer, SourceForge Meshlab, and Netfabb Basic to accurately cleanup the part, minimize the mesh size, and prepare it for exporting into SolidWorks. All three of these programs are freeware, and download links are supplied below.

Autodesk MeshMixer

Autodesk MeshMixer is free software used for altering STL files. Download MeshMixer at http://www.meshmixer.com/download.html.

NOTE: Since MeshMixer is a free tool, it is prone to crashing. Save early and often. Get into the habit of saving after every change is made.

Import .STL file into Autodesk MeshMixer:

1. **File → Import →** Select file
    a. You can also import by clicking Import in the top left panel (giant "+")
2. Once Imported, your part will be shown like below. Notice in the bottom right corner of MeshMixer the number of vertices and triangles of the part is shown. This is important to keep in mind, for SolidWorks can generally handle up to 10,000-11,500 triangles (or faces).

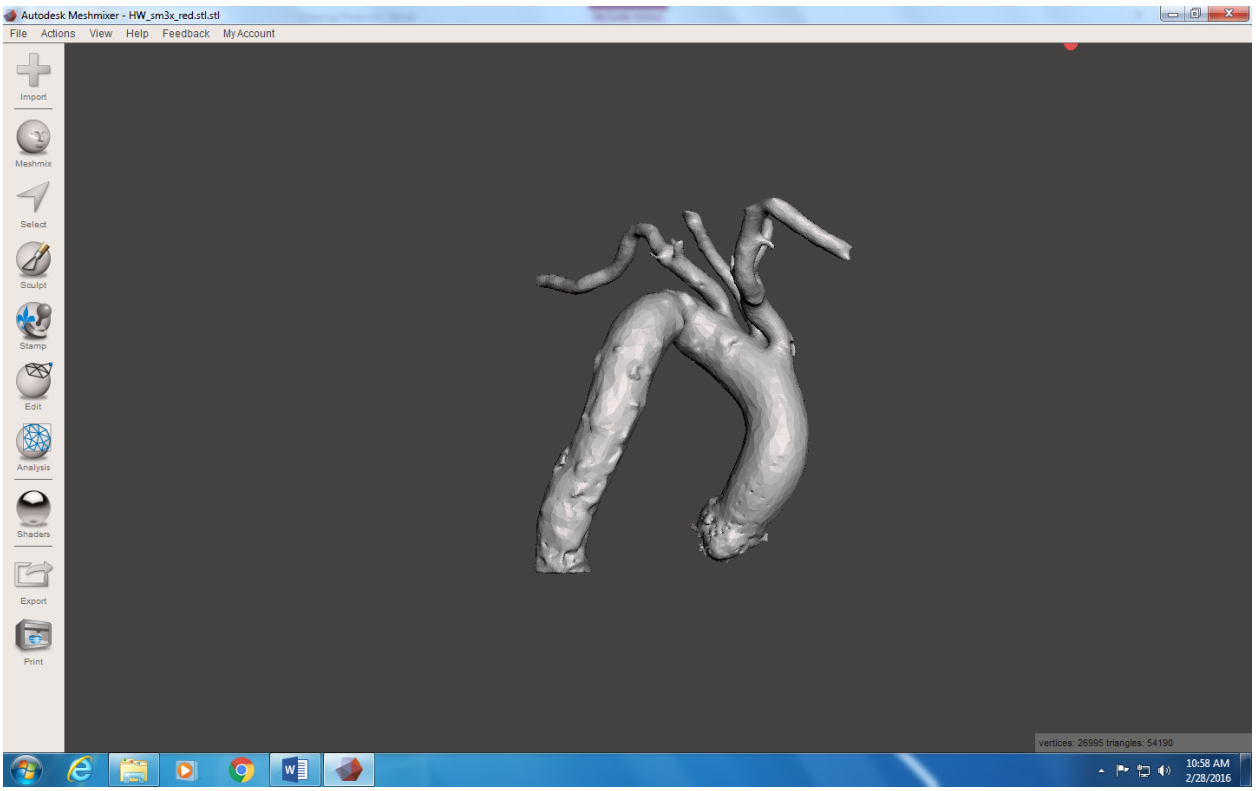

Smooth the Part as a Whole:

1. Choose **Select** (on left panel) → double-click part to select entire part (notice it changes color, in this case orange)
2. Deform → **Smooth**

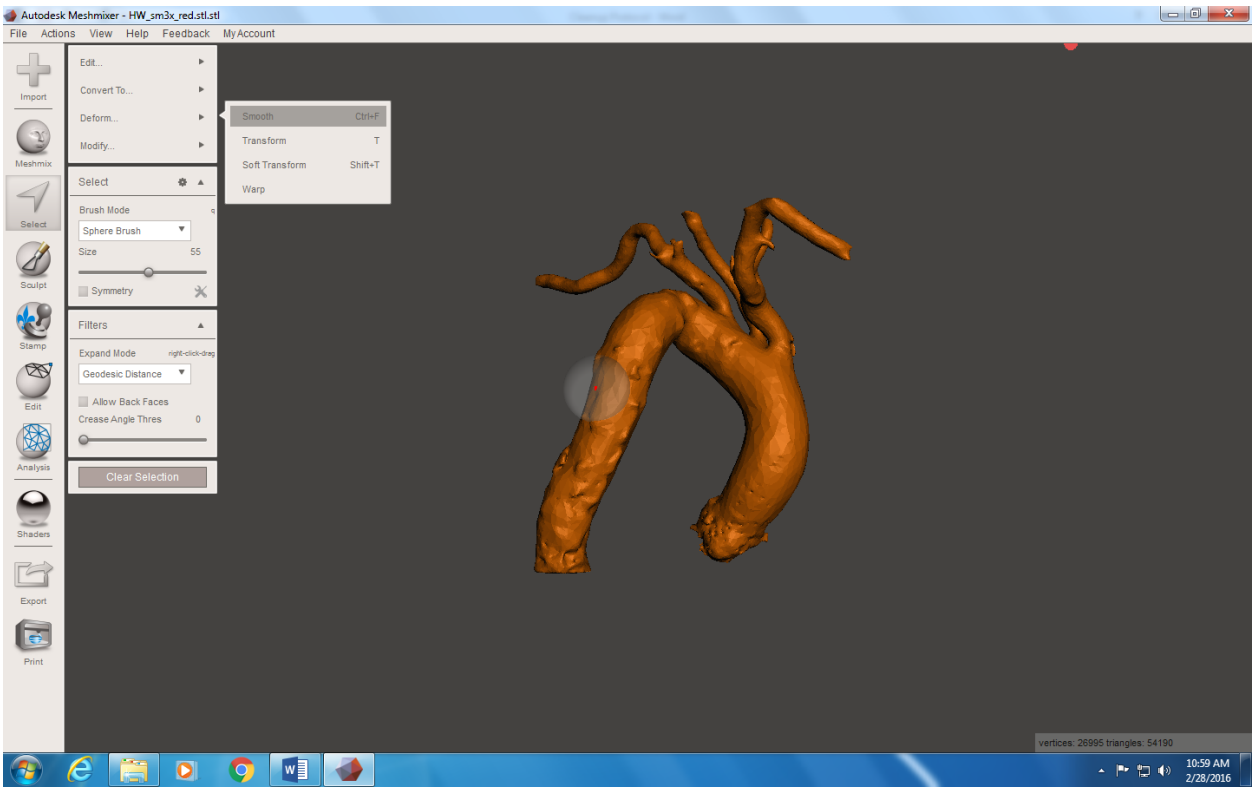

3. Keep Smooth settings as shown (notice the part is now shown as a preview of what it will look like if these settings are accepted)
4. Accept

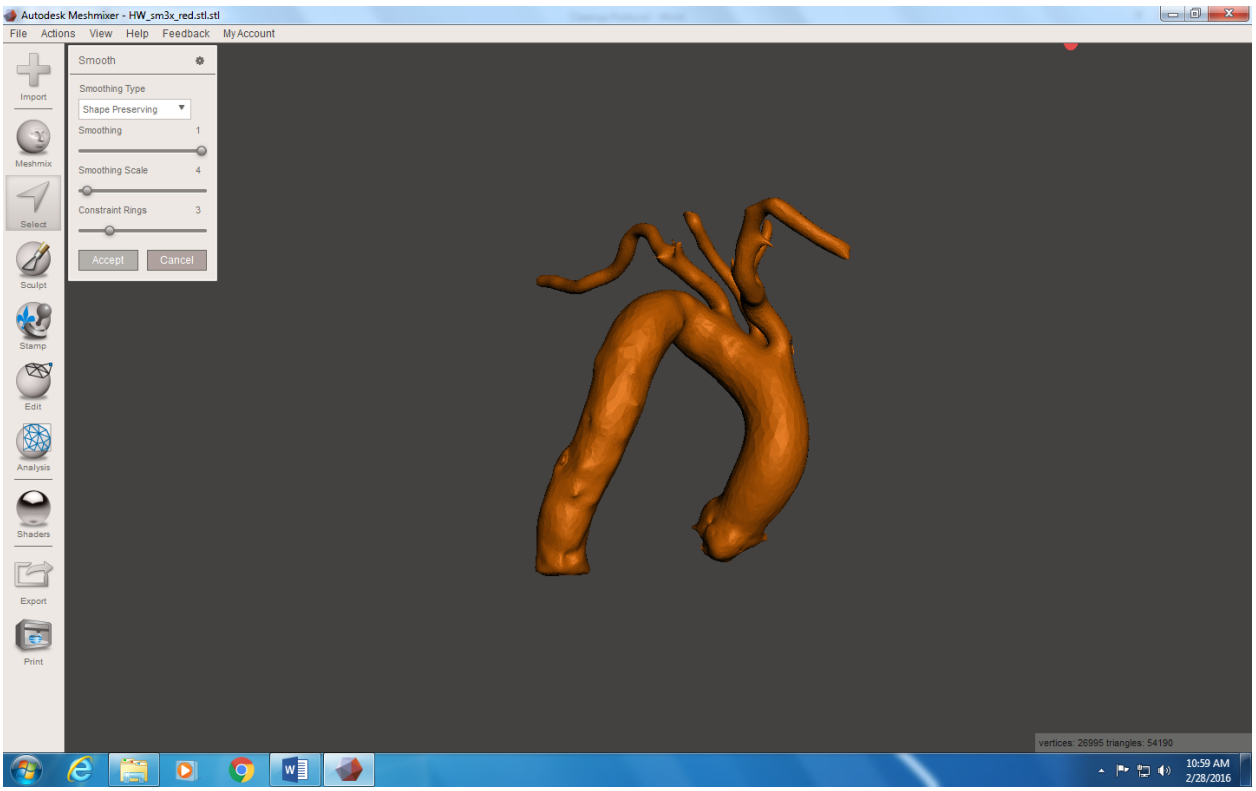

Reduce the Mesh Size (decrease triangle count)

1. **Select** → double-click part to select entire part
2. Edit → **Reduce**

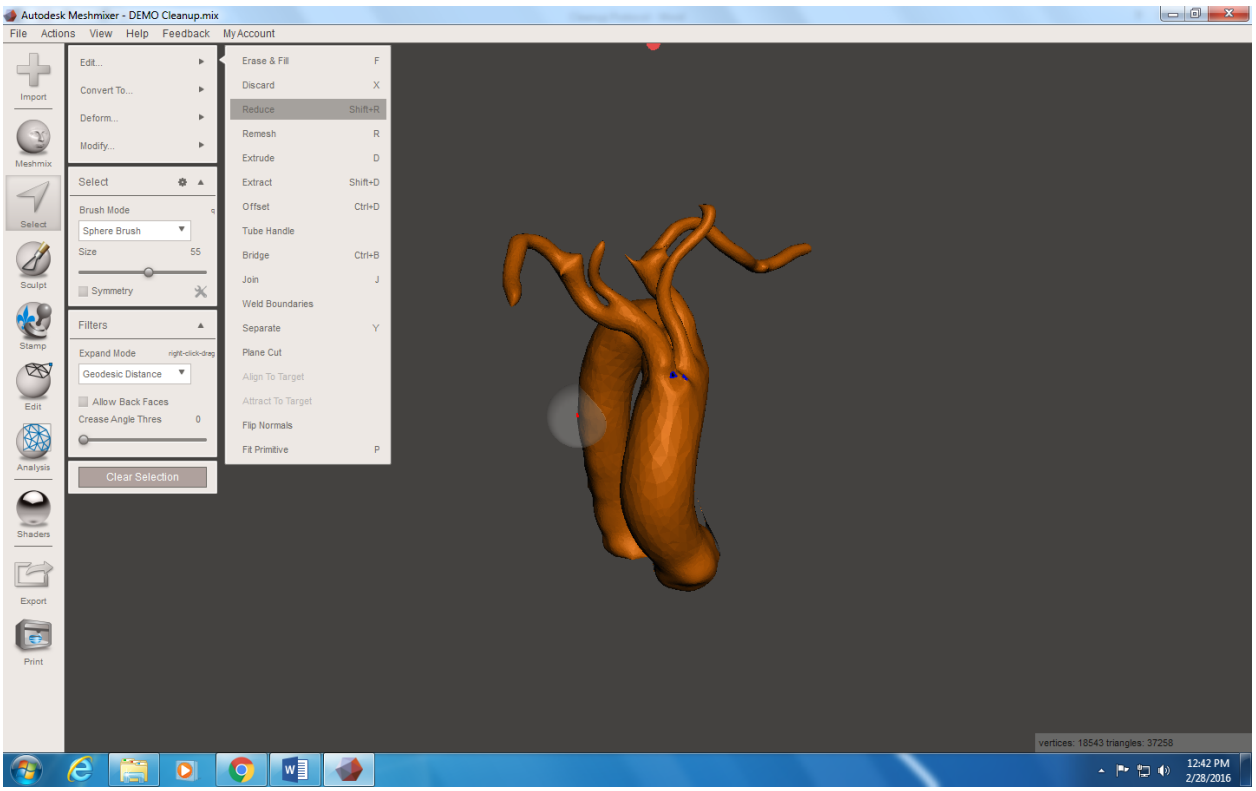

3. Select how you want to reduce the mesh size (‘Reduce Target’). This can be done in three ways: Percentage, Triangle Budget, and Max Deviation. It is recommended to use Percentage or Triangle Budget. Once an option is chosen, ensure that ‘Reduce Type’ is set to ‘Shape Preserving’.
4. Use the appropriate slider (slider associated with ‘Reduce Target’ that has been chosen) to adjust the part mesh size. Again, the part will change and show a preview of what it will look like prior to accepting the change.
5. Recommended to use **Percentage** reduce target initially, and change the Percentage slider to **70%**.
6. Accept
    a. Notice that the Triangle Count of the part decreases (lower right corner).

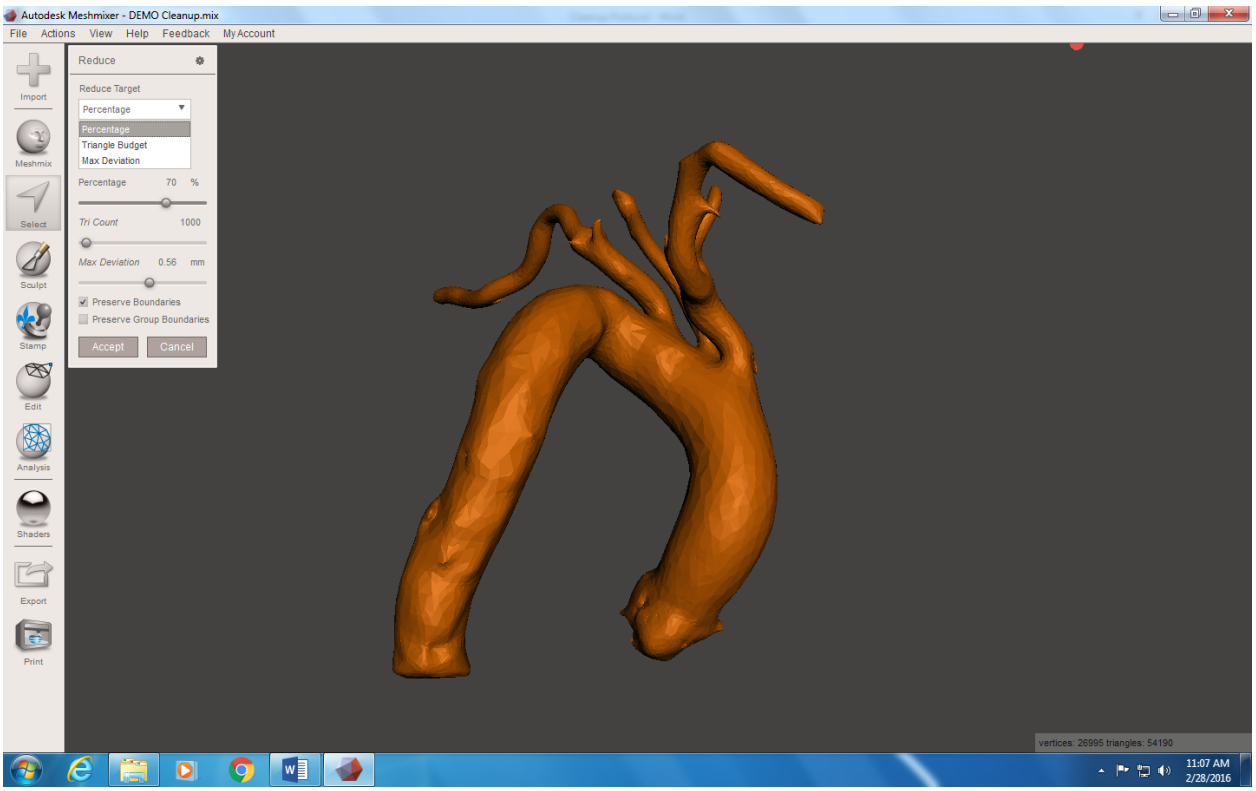

Cleaning up/Smoothing out Specific Sections:

1. **Select** → click on area of interest (this can be done by clicking on a specific area, or click and hold to paint a certain area). The selection brush size can be changed, by adjusting the 'Size' slider under 'Select' tab. The area that has been selected and will be modified is now a different color (orange).

2. Edit → Erase & Fill

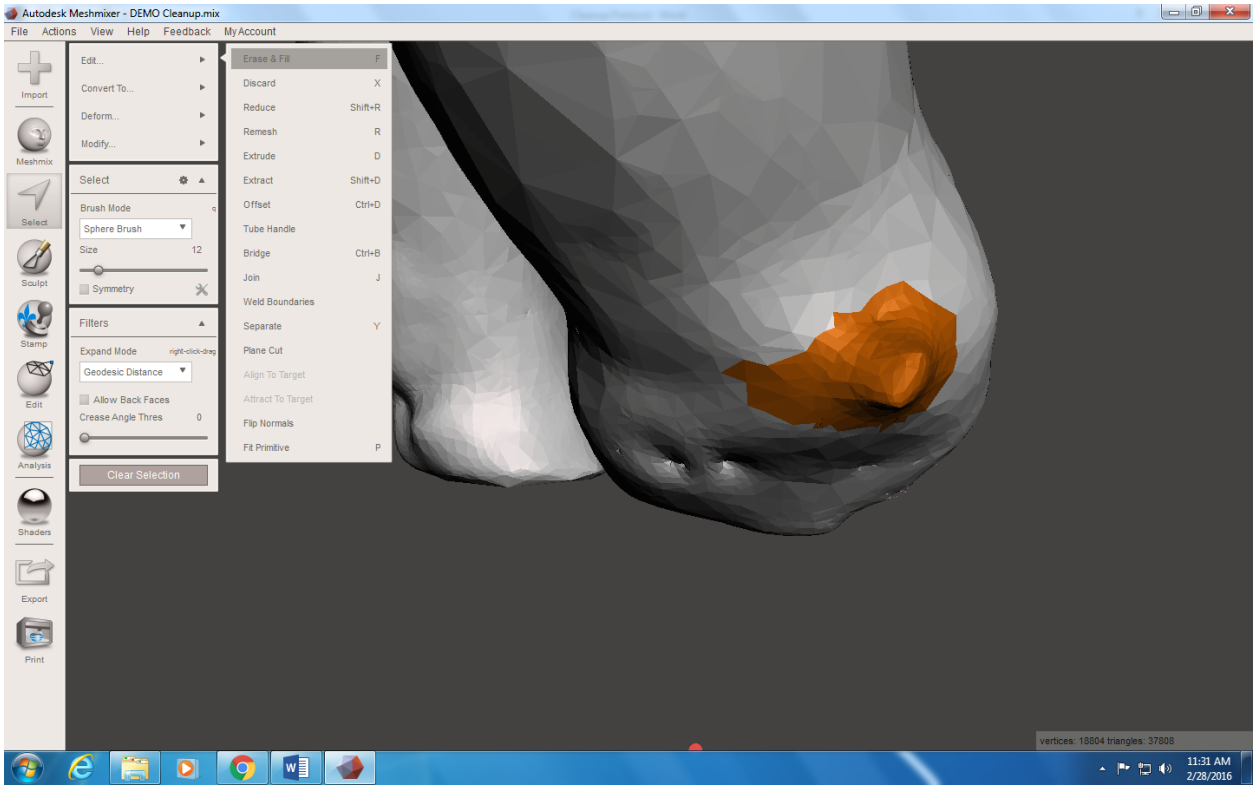

3. Leave default settings. Again, a preview of the change is shown prior to accepting the change.
4. Accept
5. **Clear Selection** to deselect the area of the part that was just altered
6. Repeat for all areas of interest that need to be smoothed out

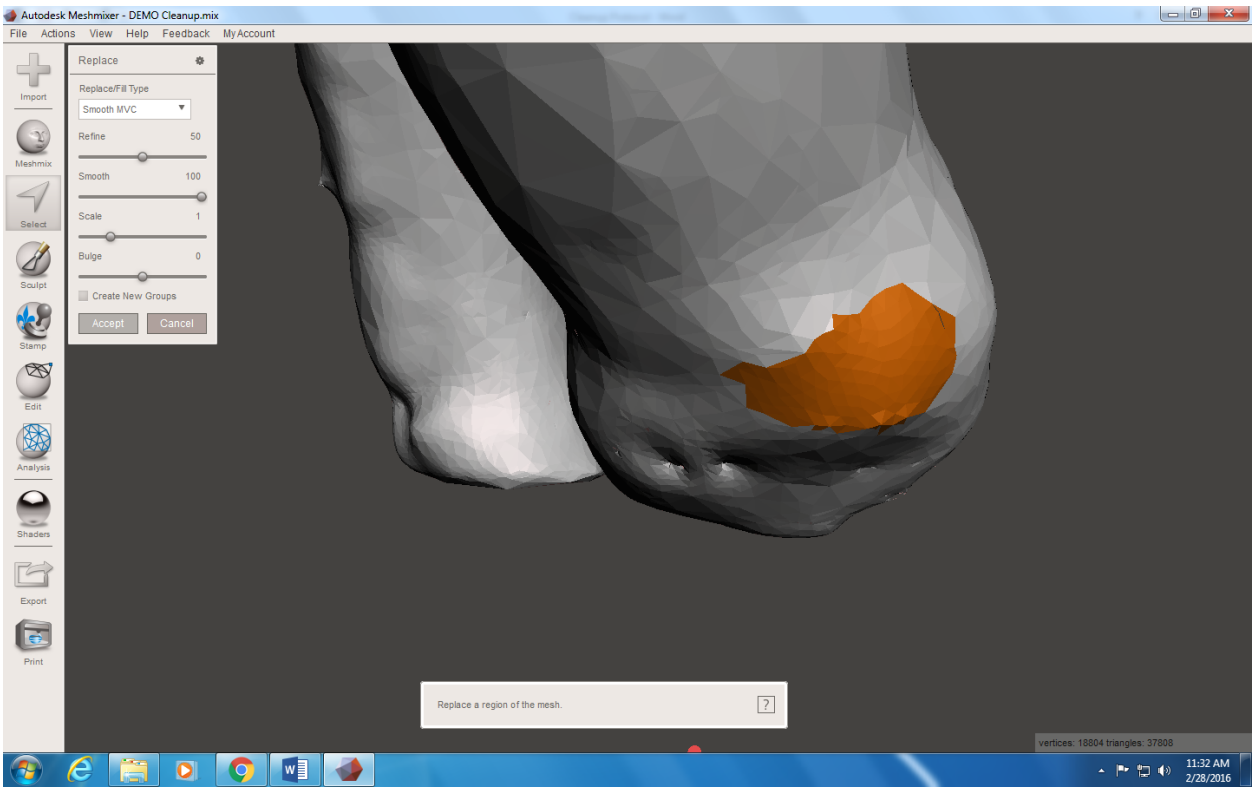

Removing Sections of the Part:

1. **Select** → select area of interest (notices it changes color)

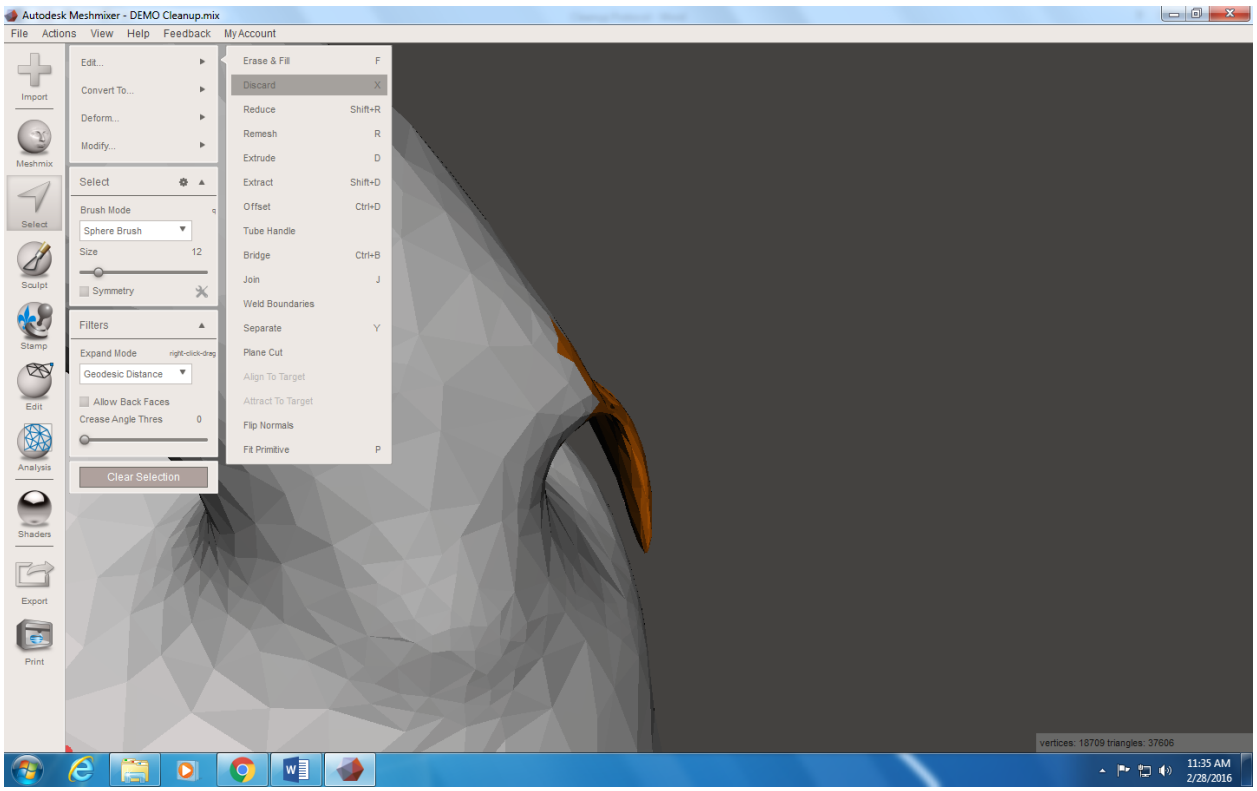

2. Edit → **Discard**

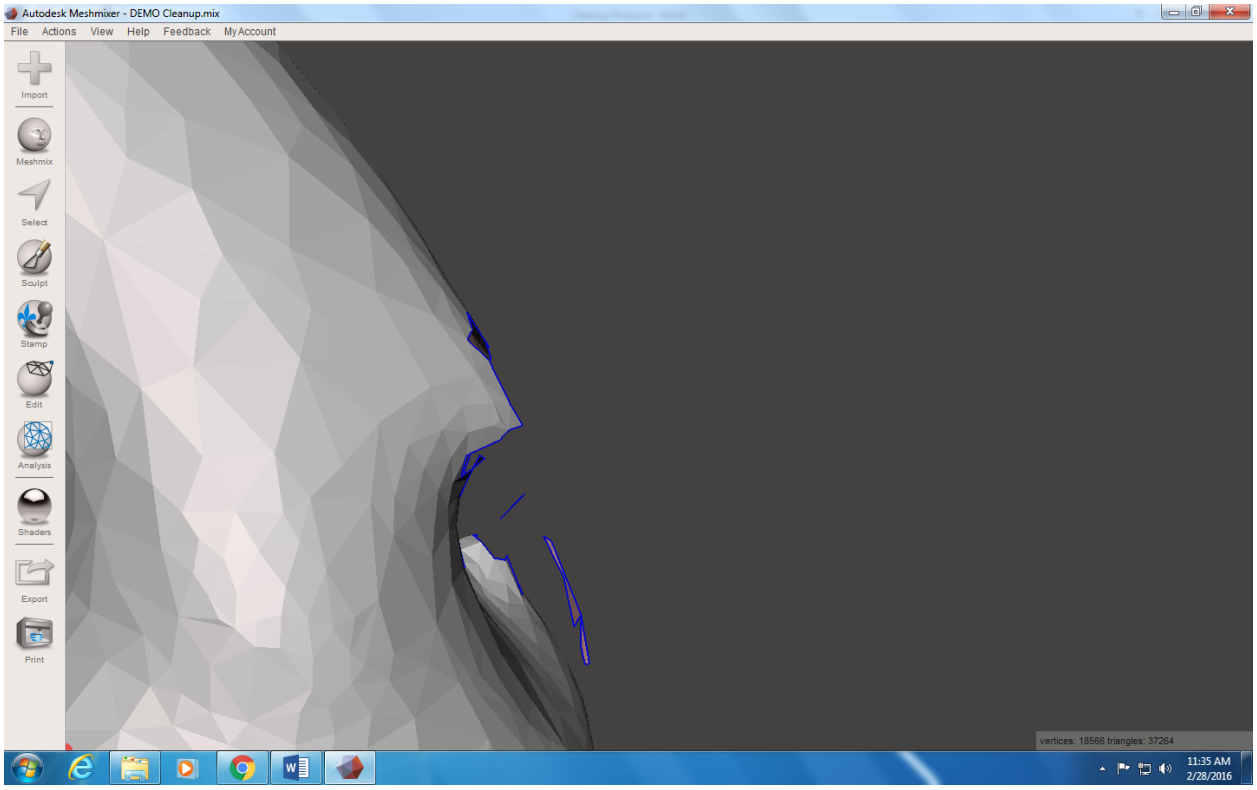

Removing Sections of the Part: Troubleshooting

1. If there are “floating meshes” still present after removing the section of interest, they can be removed by performing the same steps as above (clicking on individual triangles) or by this method (selecting by drawing around the floating triangles).

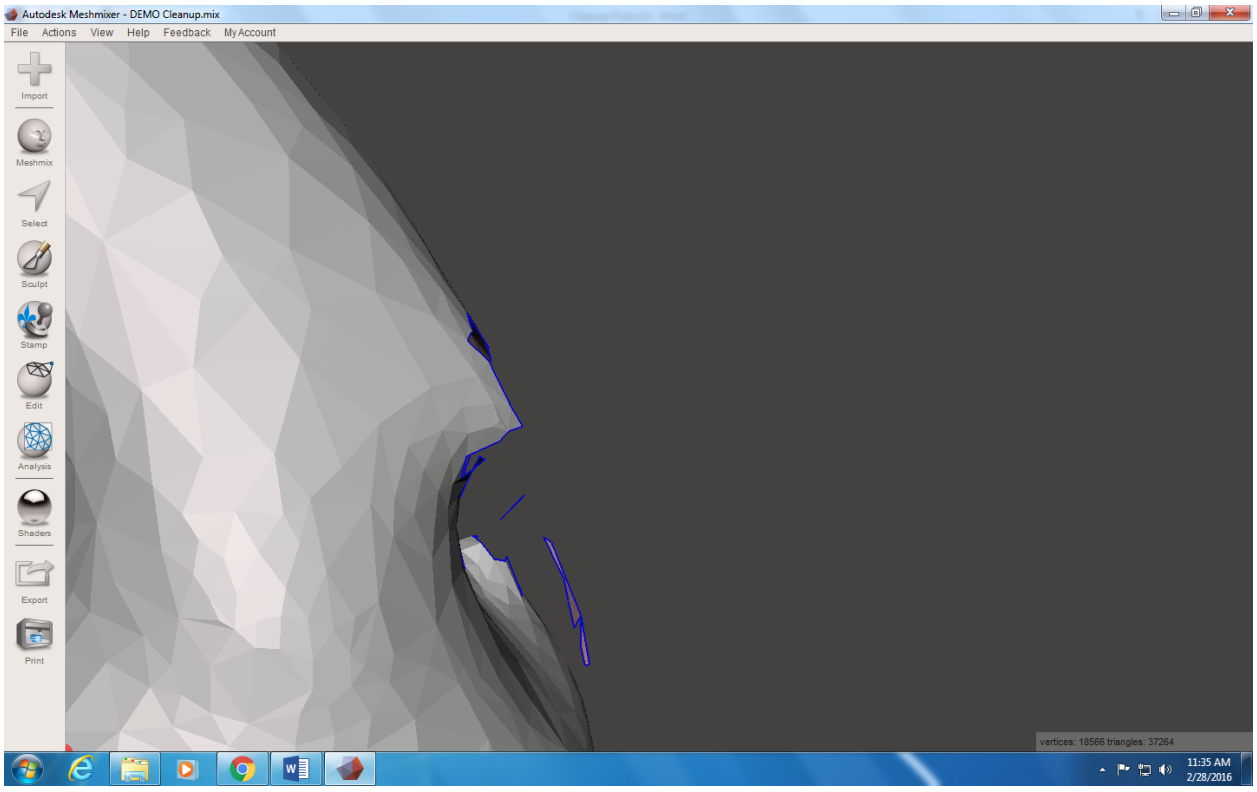

2. **Select** → instead of clicking on individual triangles, draw a circle around the floating triangles by clicking and holding down the mouse. You will see where you are drawing with the red line left from your cursor. Ensure that you close up your loop around the floating triangles. NOTE: Before moving to the next step,

make sure you did not accidentally select any other areas of the part (zoom out and examine the part for a change in color, indicating part selection).

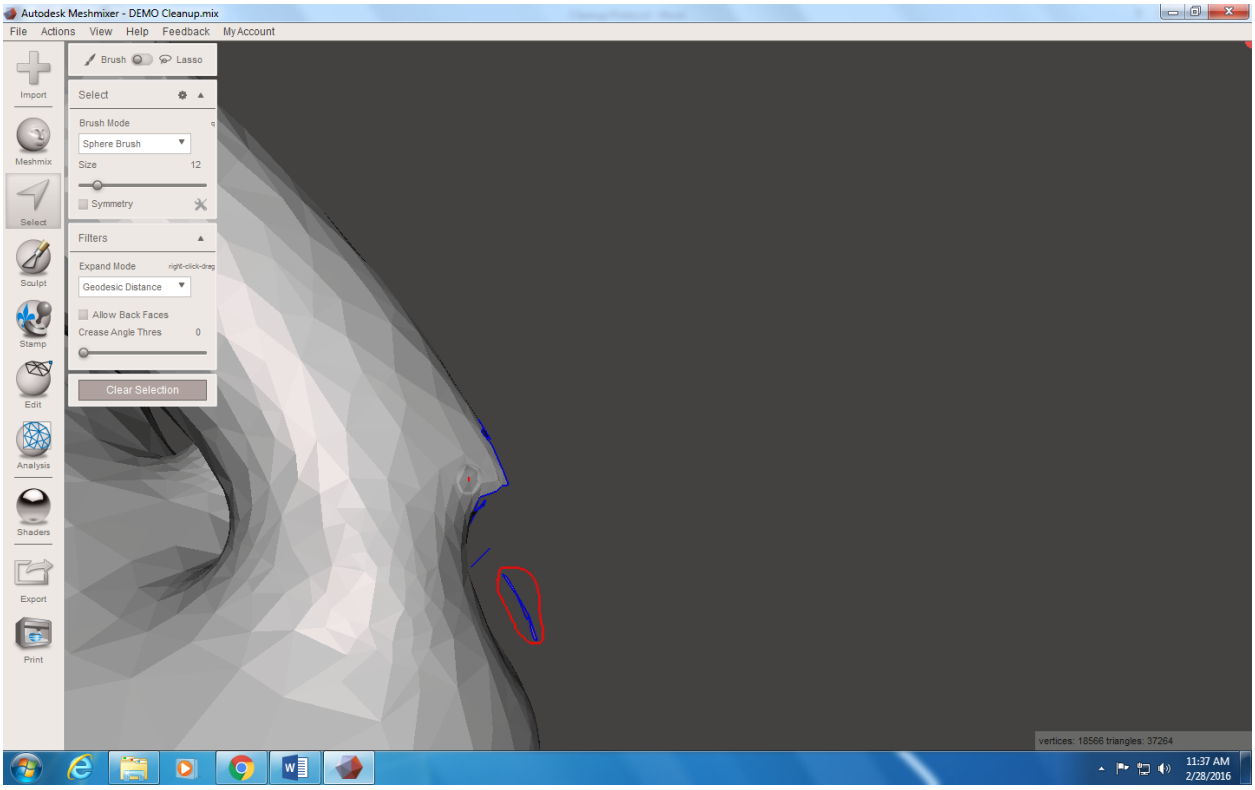

3. Edit → **Discard**

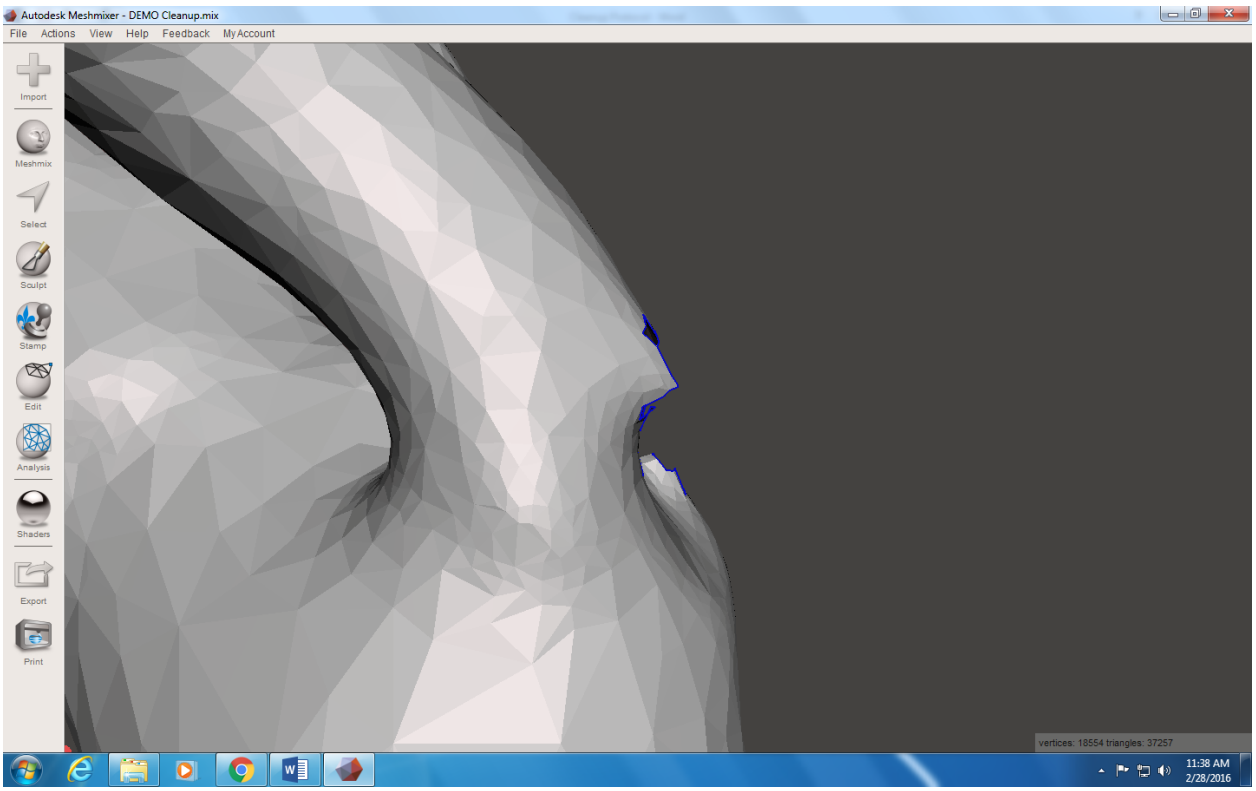

NOTE: If you have accidentally removed more than you wanted, you can undo the last action by going to **Action → Undo|Back** (or Ctrl+z).

Filling a Hole using MeshMixer:

1. **Select** → Select area around the hole you desire to fill
2. Edit → Erase & Fill

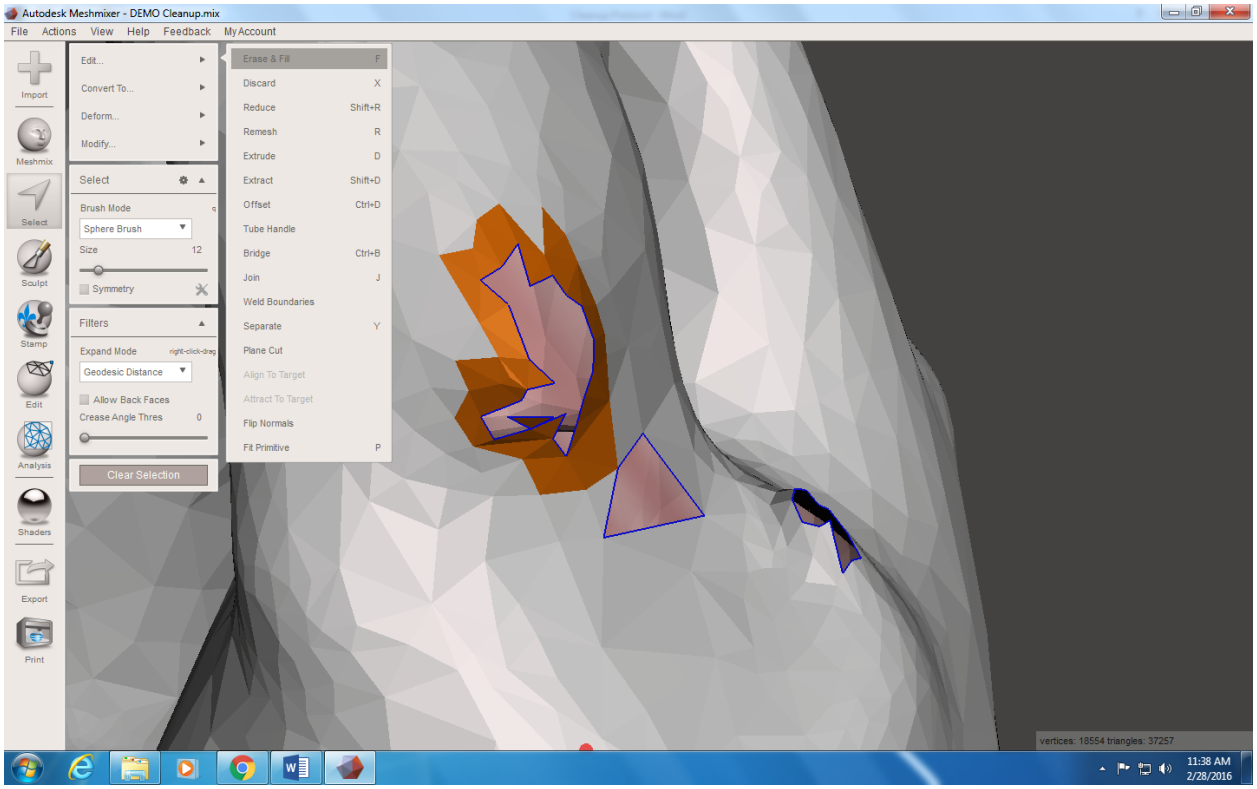

3. Check the preview of how MeshMixer will fix the section. If you like the preview, click **Accept**

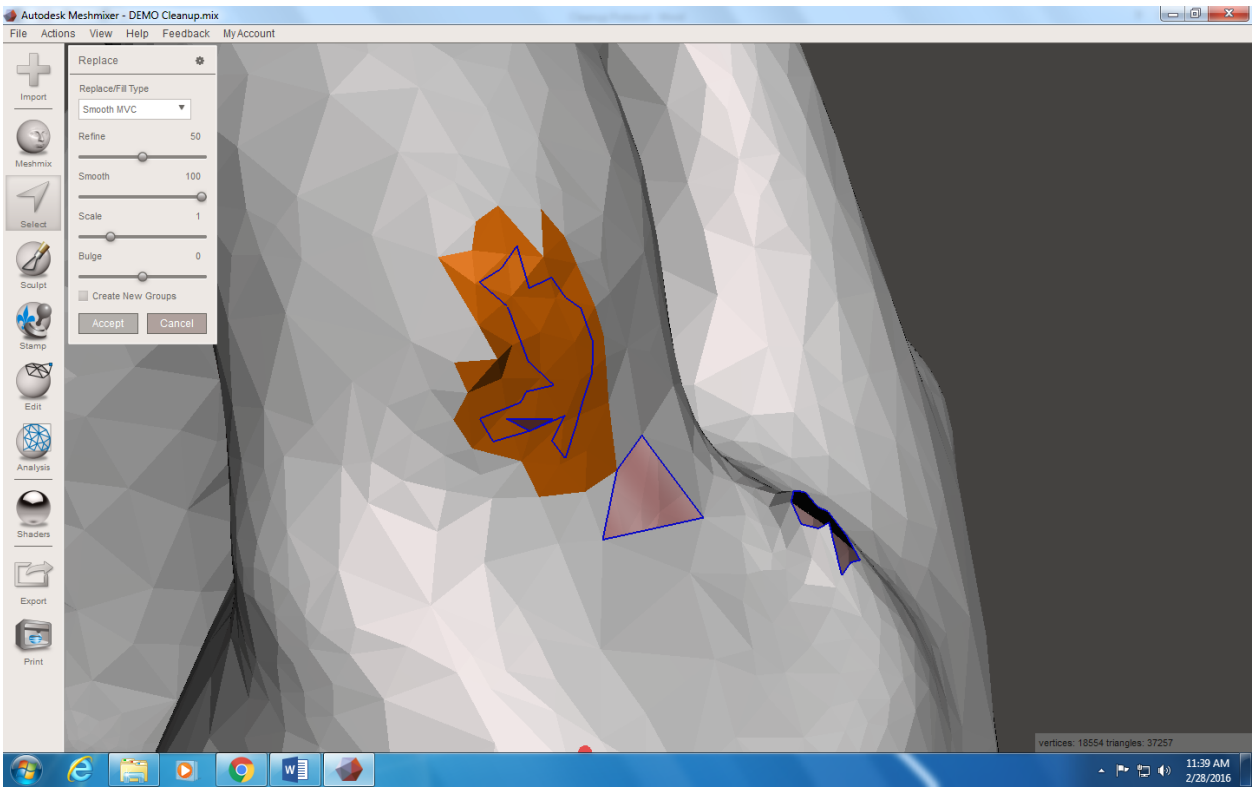

NOTE: It can be challenging to fill holes exactly how you would like them to be filled in MeshMixer. Later on in the process, NetFab Basic is used to again check for holes, and will repair the part (fill all holes). However, NetFab Basic does not allow for any control on how the holes are filled, so it is recommended to attempt to fill holes using MeshMixer for it allows more control on the shape the part will take.

Separating Sections in MeshMixer:

1. To separate sections in MeshMixer, **Select→** highlight section you wish to remove

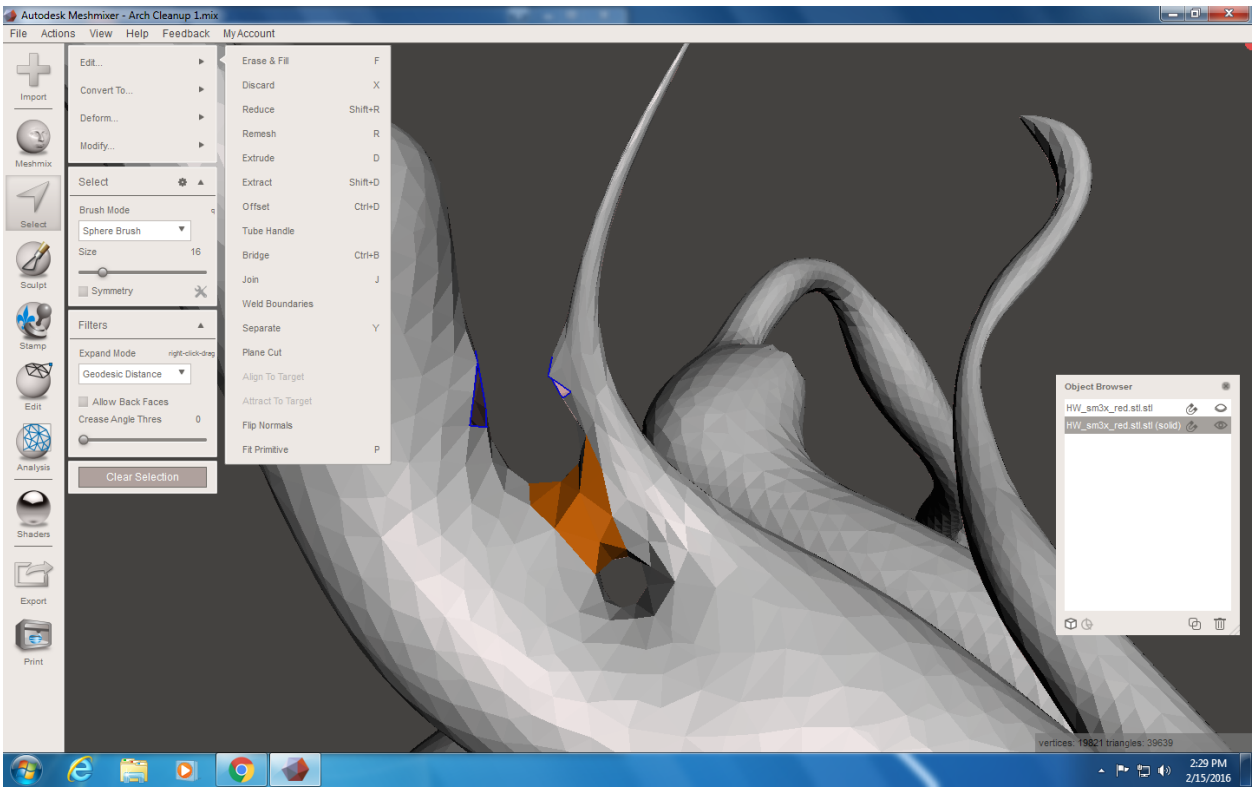

2. Edit → Separate.

NOTE: Once you click Separate, the highlighted region will become its own section (own piece in the object browser window). There is no preview or accept button associated with Separate, so if you made an error in the section you wanted to separate, use **Action → Undo|Back** (or Ctrl+z) to remove the change.

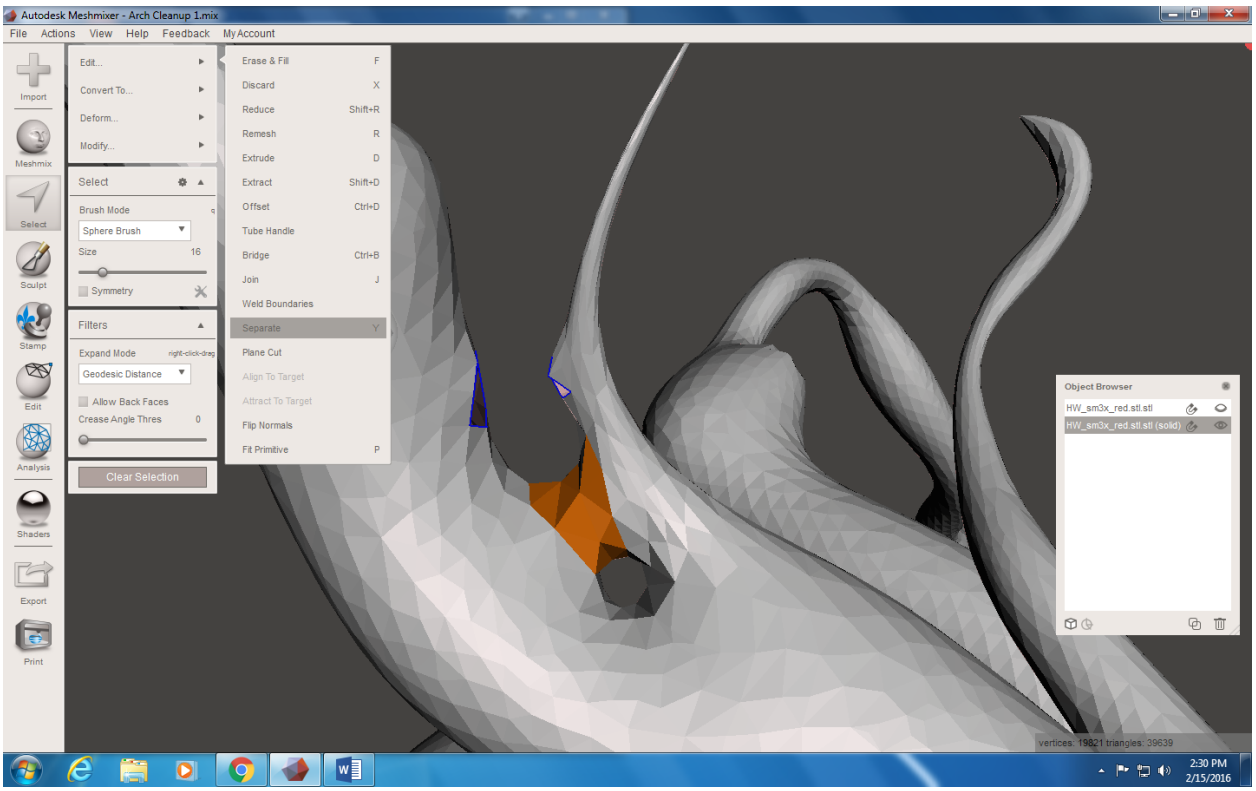

3. The section is now its own object in the object browser. To delete this section, ensure that you have just this section selected (rest of the part is dimmed when only one object is selected), and click the trash can ‘Delete’ button in the bottom right of the Object Browser.

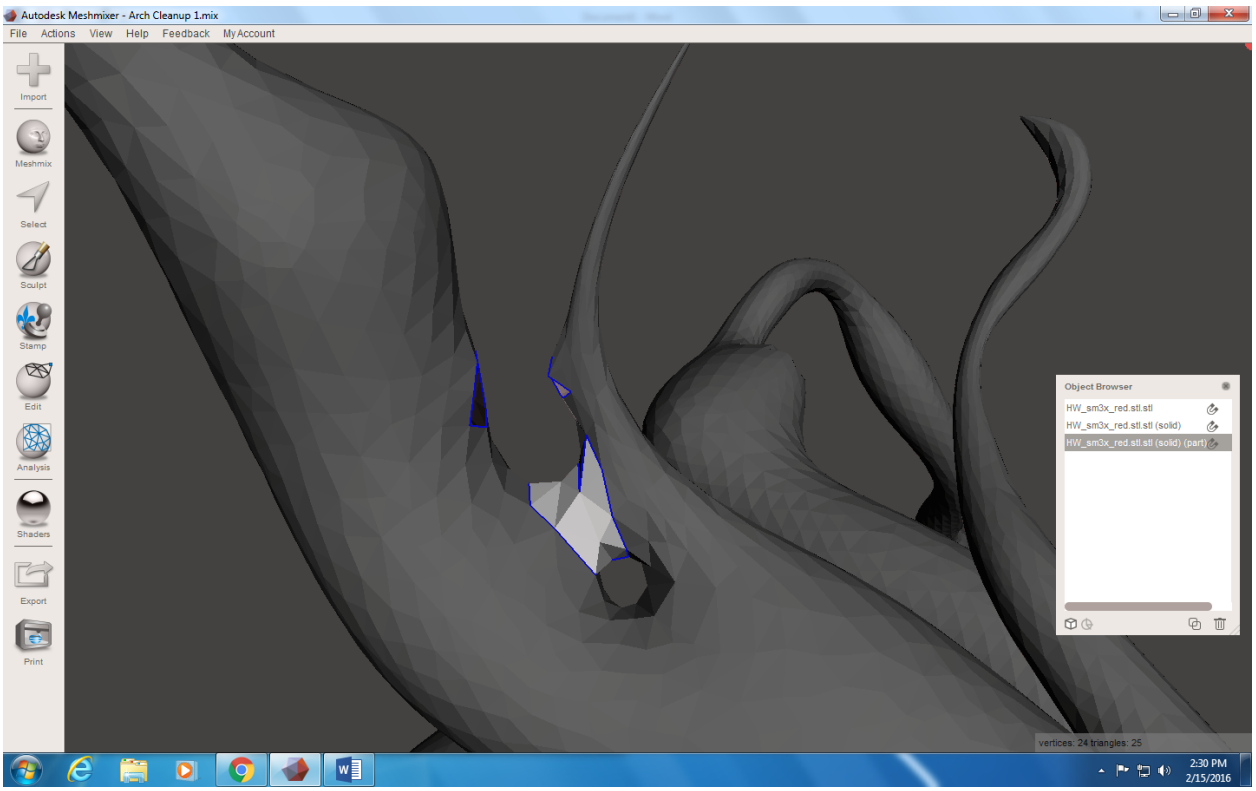
Autodesk Meshmixer - Arch Cleanup 1.mix
File Actions View Help Feedback My Account
Import
Meshmix
Select
Sculpt
Stamp
Edit
Analysis
Shaders
Export
Print
Object Browser
HW_sm3x_red.stl.stl
HW_sm3x_red.stl.stl (solid)
HW_sm3x_red.stl.stl (solid) (part)
vertices: 24 triangles: 25
2:30 PM
2/15/2016

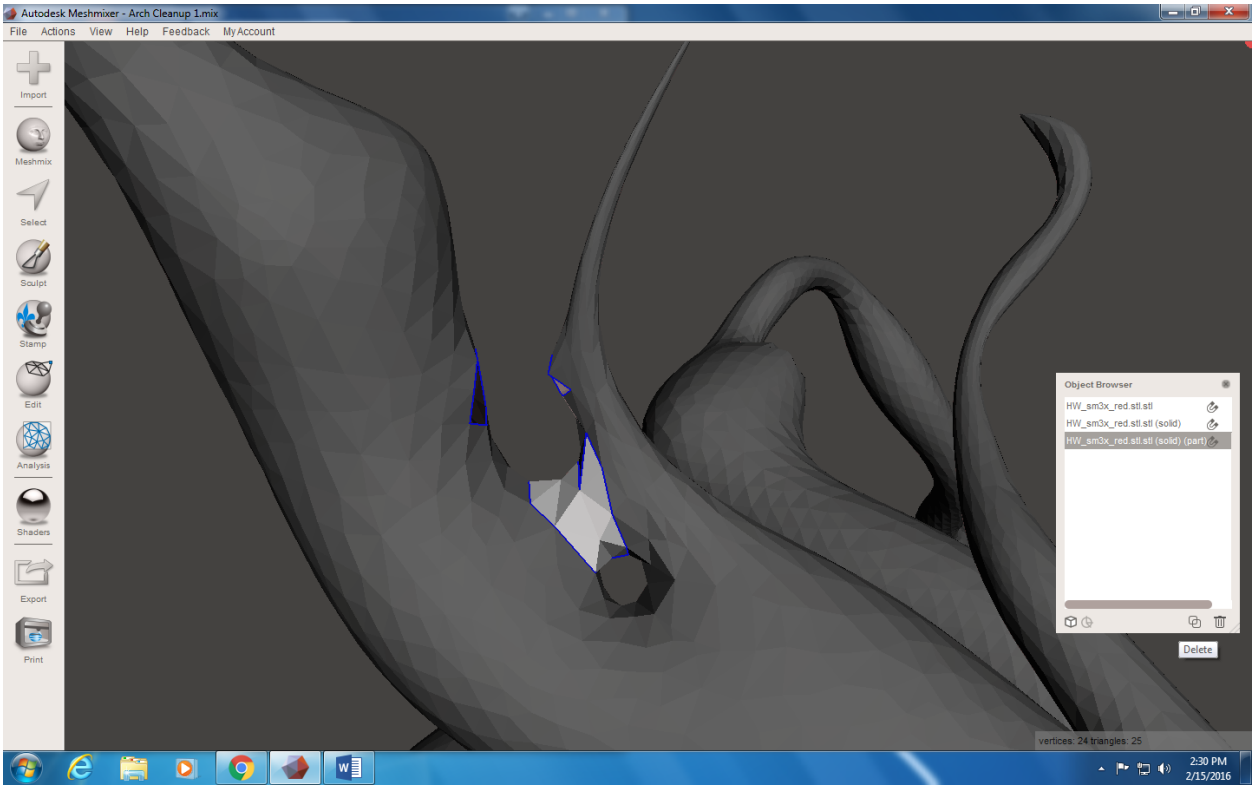
Autodesk Meshmixer - Arch Cleanup 1.mix
File Actions View Help Feedback My Account
Import
Meshmix
Select
Sculpt
Stamp
Edit
Analysis
Shaders
Export
Print
Object Browser
HW_sm3x_red.stl.stl
HW_sm3x_red.stl.stl (solid)
HW_sm3x_red.stl.stl (solid) (part)
Delete
vertices: 24 triangles: 25
2:30 PM
2/15/2016

Final Triangle Size Check:

1. Prior to exporting the part, double check the number of triangles in the mesh (bottom right corner of MeshMixer window). SolidWorks can generally handle 10,000-11,500 triangles. If you are not in this range, you can reduce the mesh size by using a 'Triangle Budget' reduction. This is better to do once your part is near the range required (10,000-11,500), for it will not drastically alter the shape and "cleanliness" of the part.
2. To reduce the mesh size further, **Select** → select entire part (double click part)
3. Edit → **Reduce**
4. Change "Reduce Target" to "Triangle Budget". The "Tri Count" slider is now able to be changed.
5. Side to desired mesh triangle count. A preview of the part is shown. Click **Accept** if the changes are desired.

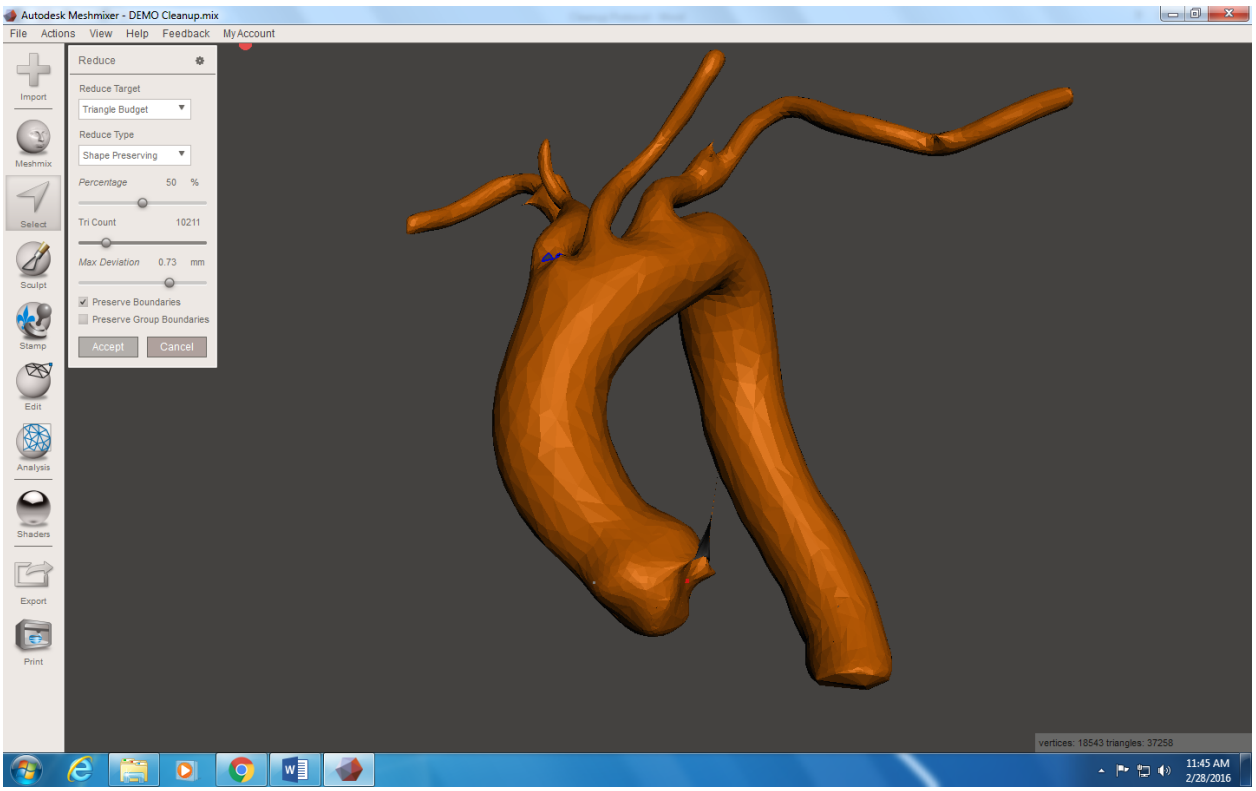

Exporting Part for Mesh Count Check:

1. File → **Export**
2. Save it as a ".PLY" file type. Save it in the location of your choice. Remember where the file is saved for ease of locating it for further use.

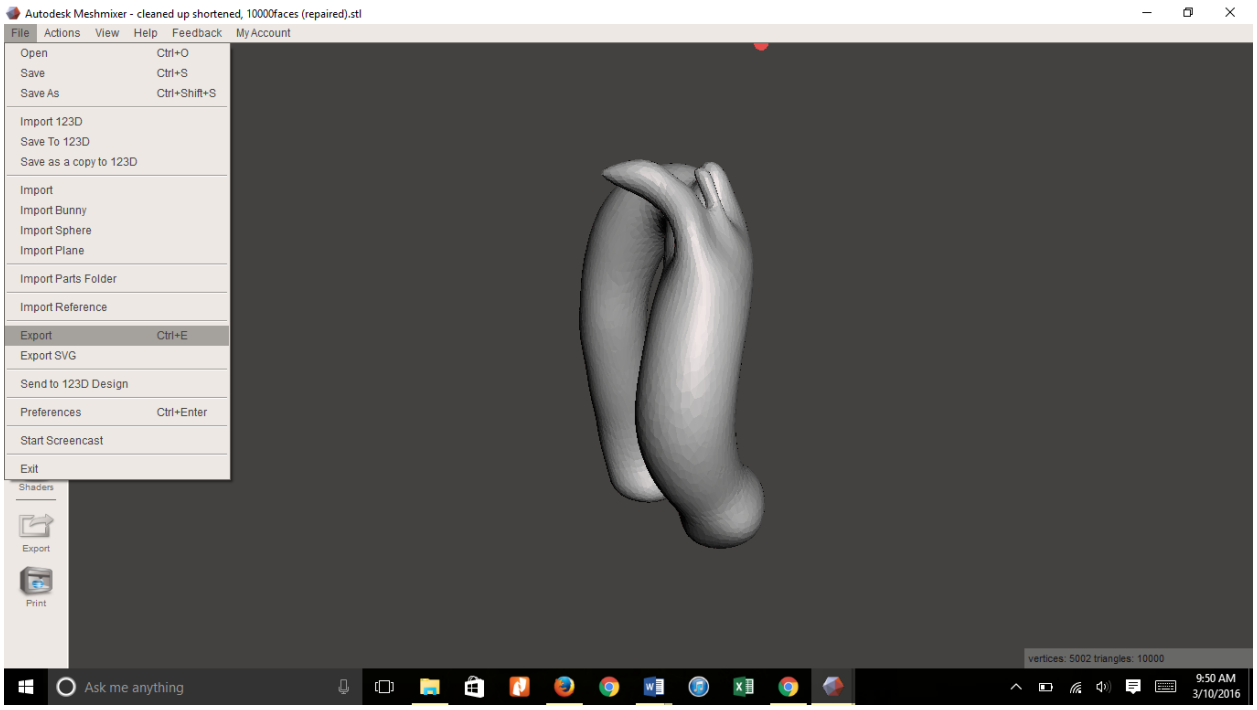

SourceForge Meshlab

Meshlab is another free software that can be used to manipulate parts for 3D printing. Download Meshlab at http://meshlab.sourceforge.net/

Exact Mesh Count in Meshlab:

1. File → Import Mesh

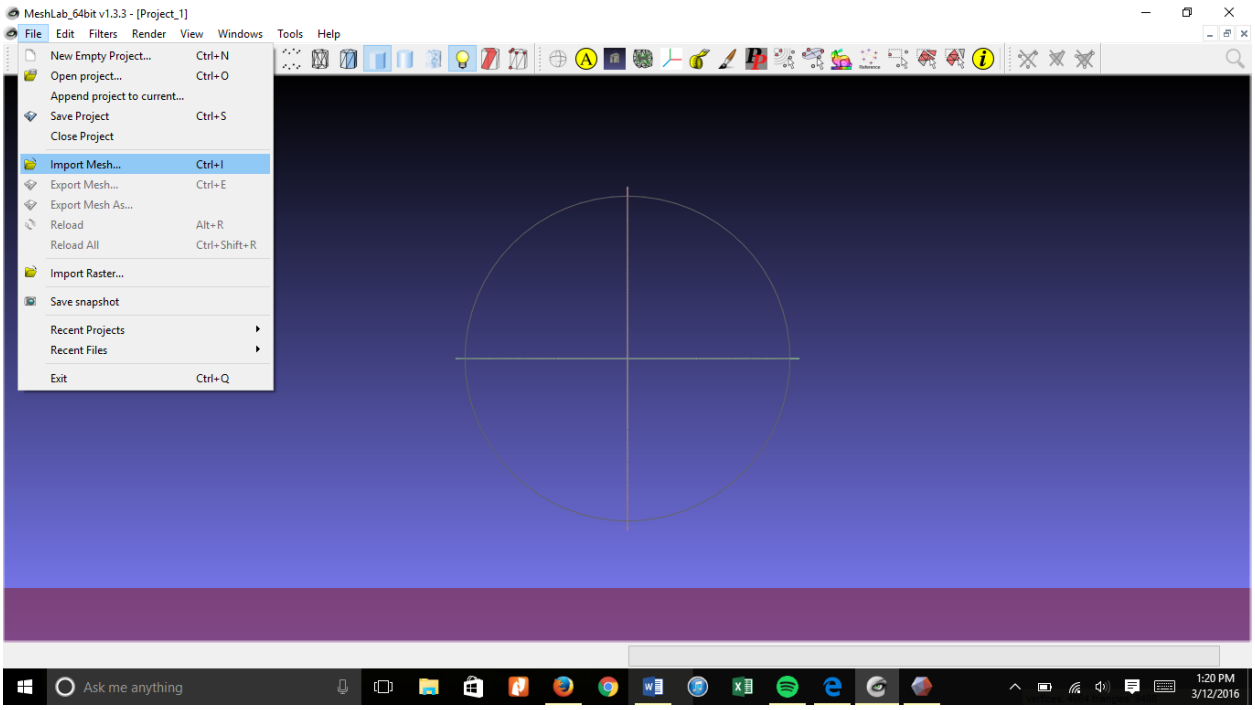

2. Locate and select the part file of interest.
3. Filters → Remeshing, Simplification, and Reconstruction → **Quadratic Edge Collapse Decimation**

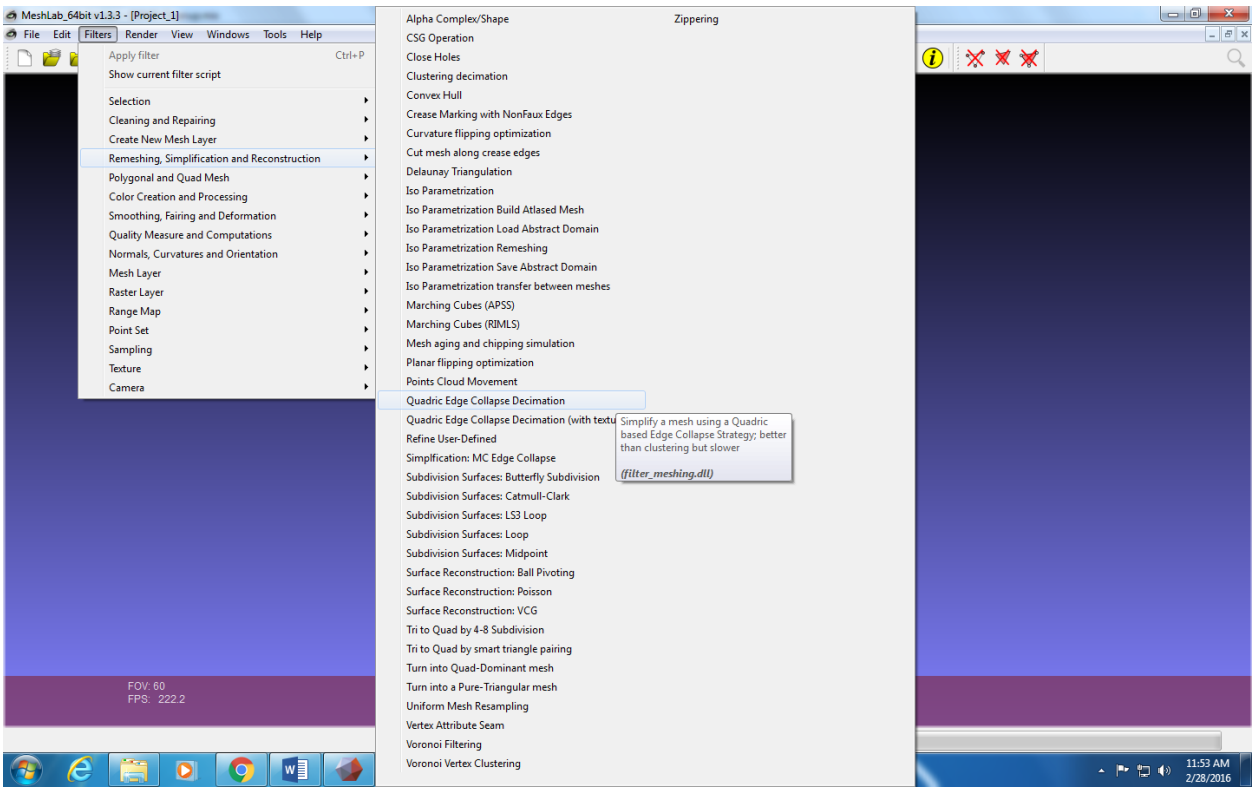

4. Enter your Target Number of Faces (10,000 in this example). Keep the other number options as the defaults (shown in following image). Check the following boxes: **Preserve Normal, Preserve Topology, Optimal position of simplified vertices, and Post-simplification cleaning.**

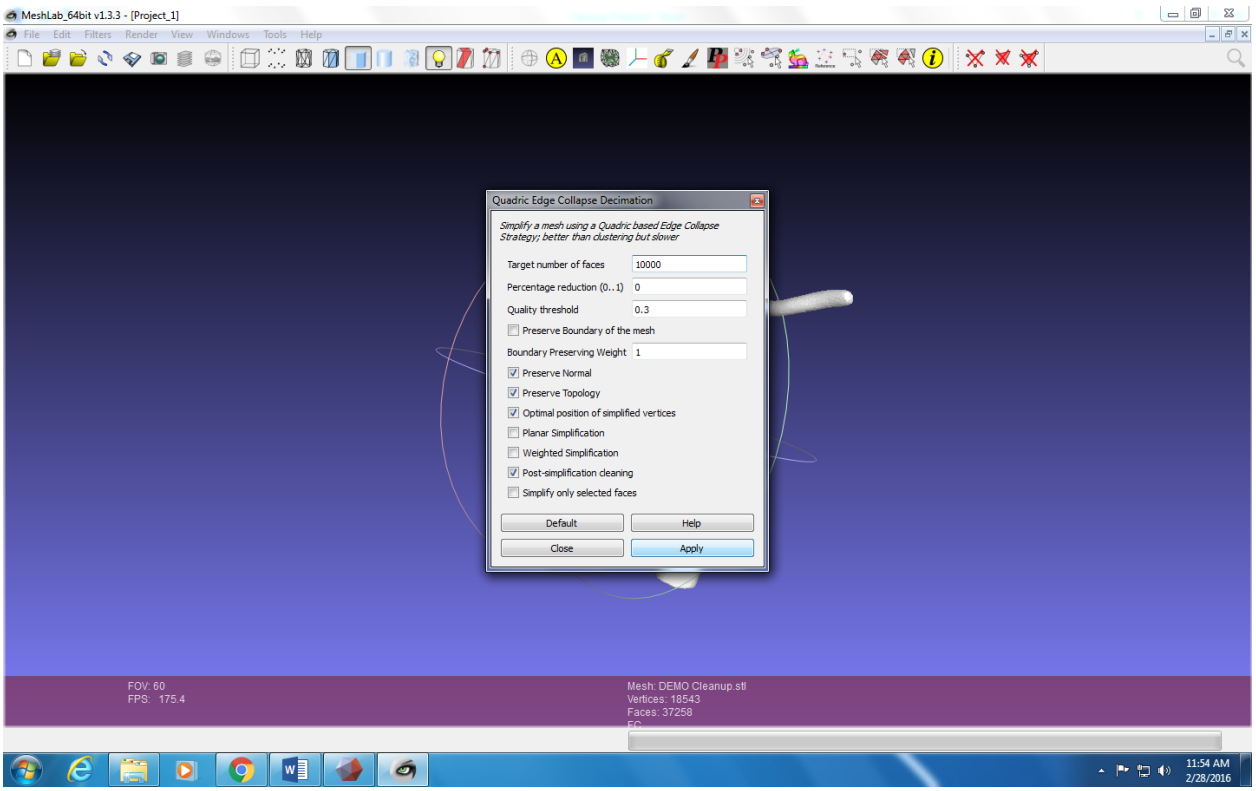

5. **Apply.** Notice that in the bottom purple bar, the number of faces now reflects the target number you entered previously.
6. File → **Export Mesh As…** export the mesh as a ".PLY" in order to be imported into Netfabb Basic for repair/hole checking. Be sure to remember where you saved the exported file.

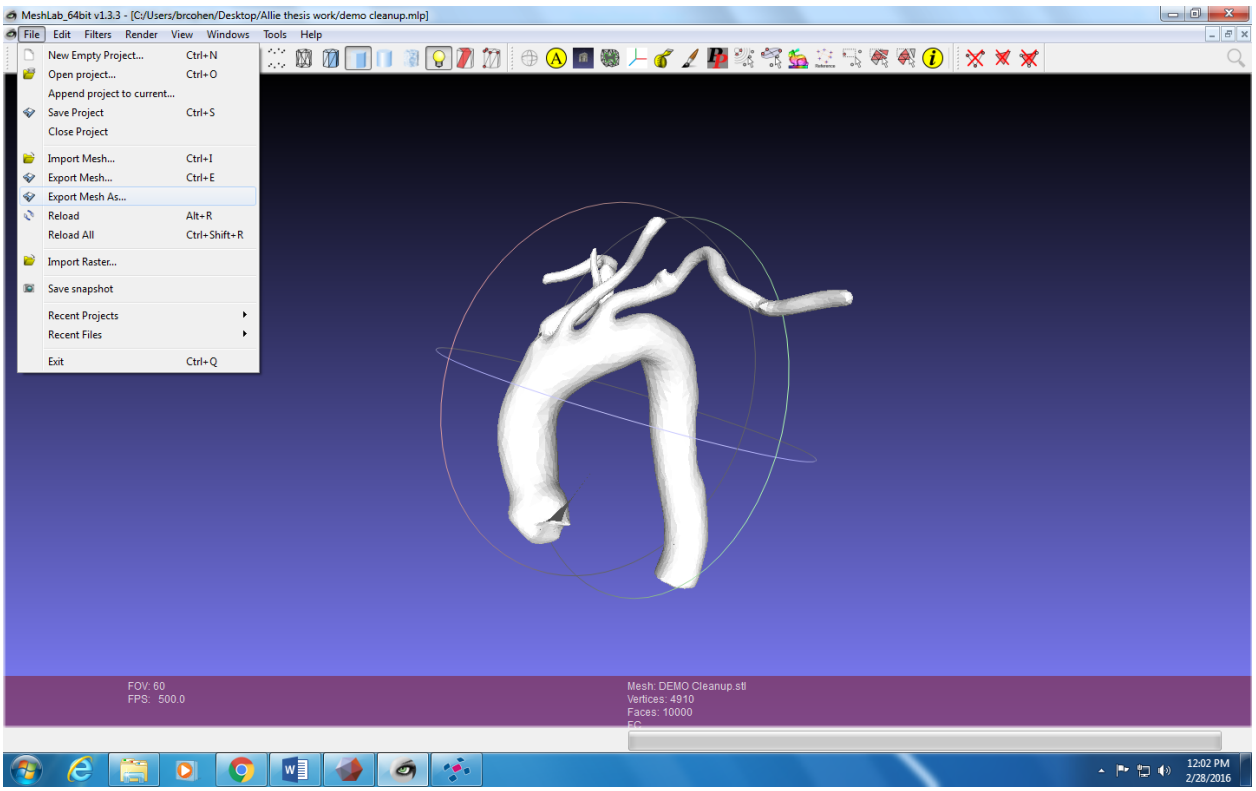

Netfabb Basic

Netfabb Basic is free software used for cleanup of STL files. Download at

http://www.netfabb.com/downloadcenter.php?basic=1

Repairing the Part:

1. Open Netfabb Basic. This registration popup screen will appear. Select “I accept the terms of usage” and click **Later.**

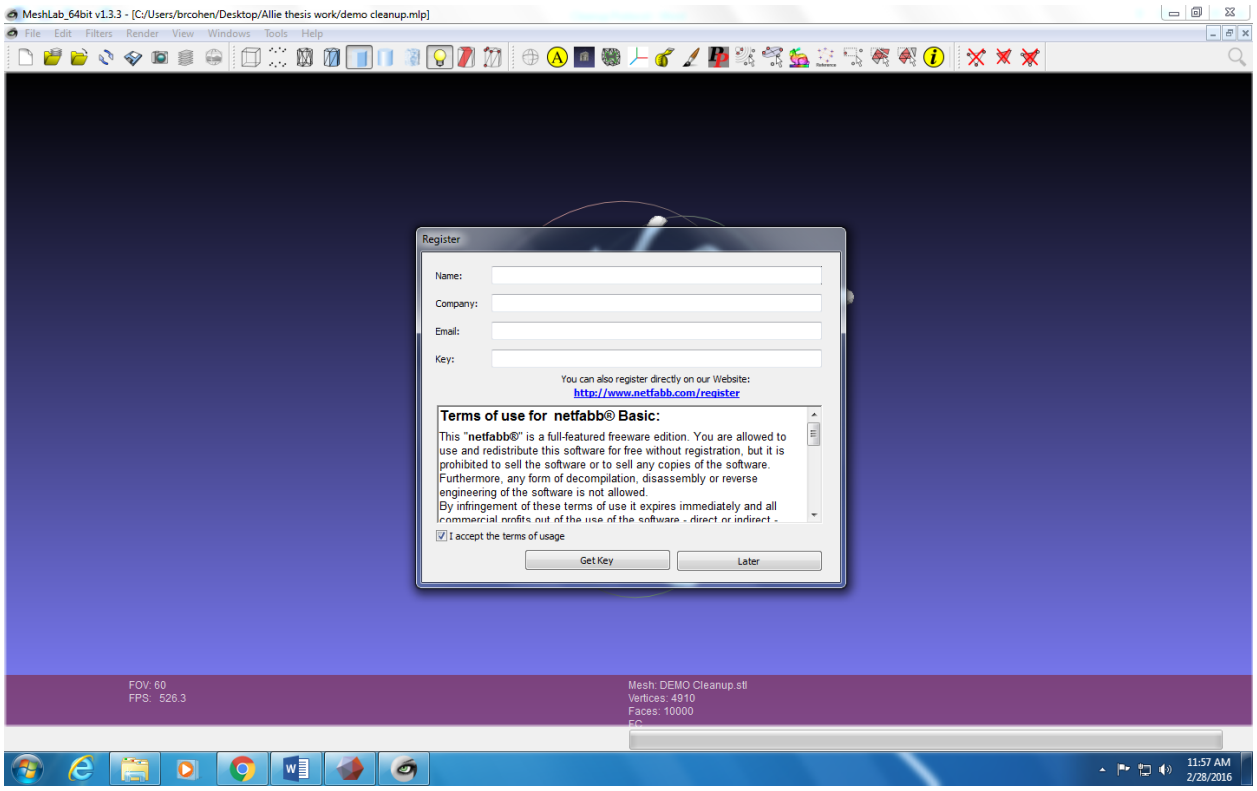

2. Project → **Add Part.** Locate and select your part.

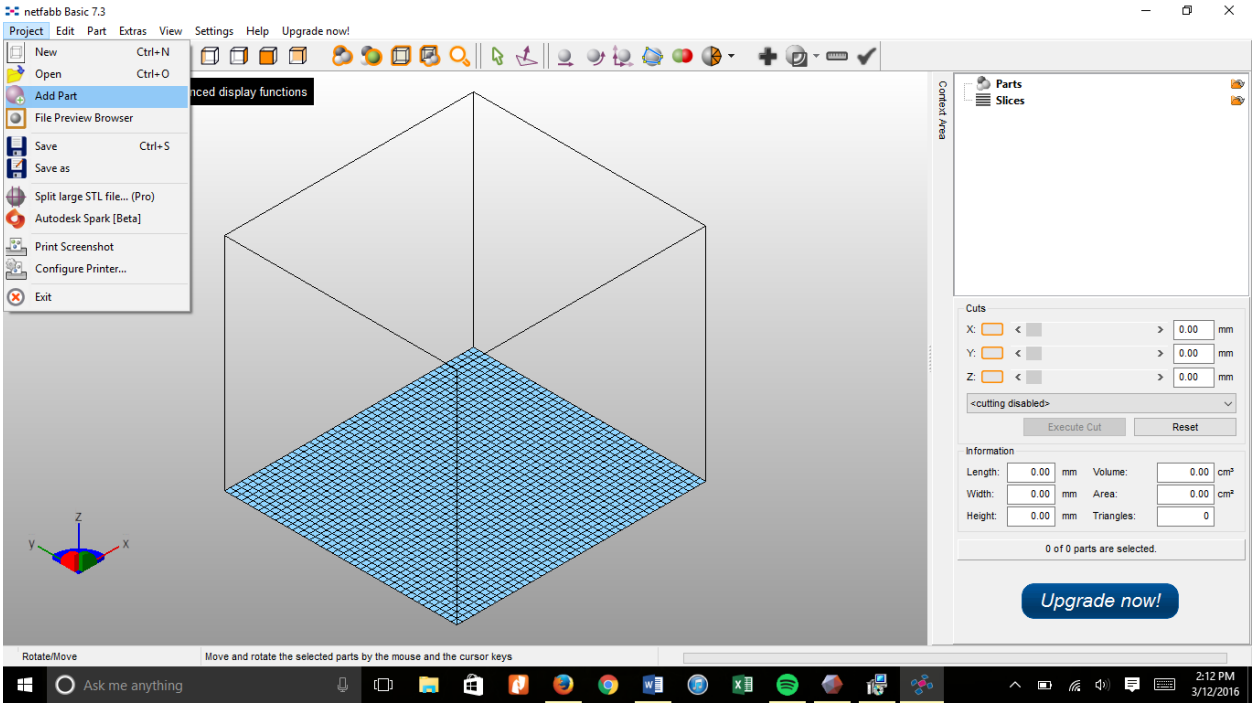

3. When your part is loaded into Netfabb Basic, it checks it for any holes in the part. If there are holes present, there will be a warning triangle in the lower right corner of the window. Additionally, the holes will be shown in red on the part. **NOTE**: Even if you load your part, and there are no red locations on it and no warning in the bottom right corner, you should still follow the rest of this repair step to ensure your part loads properly in SolidWorks.

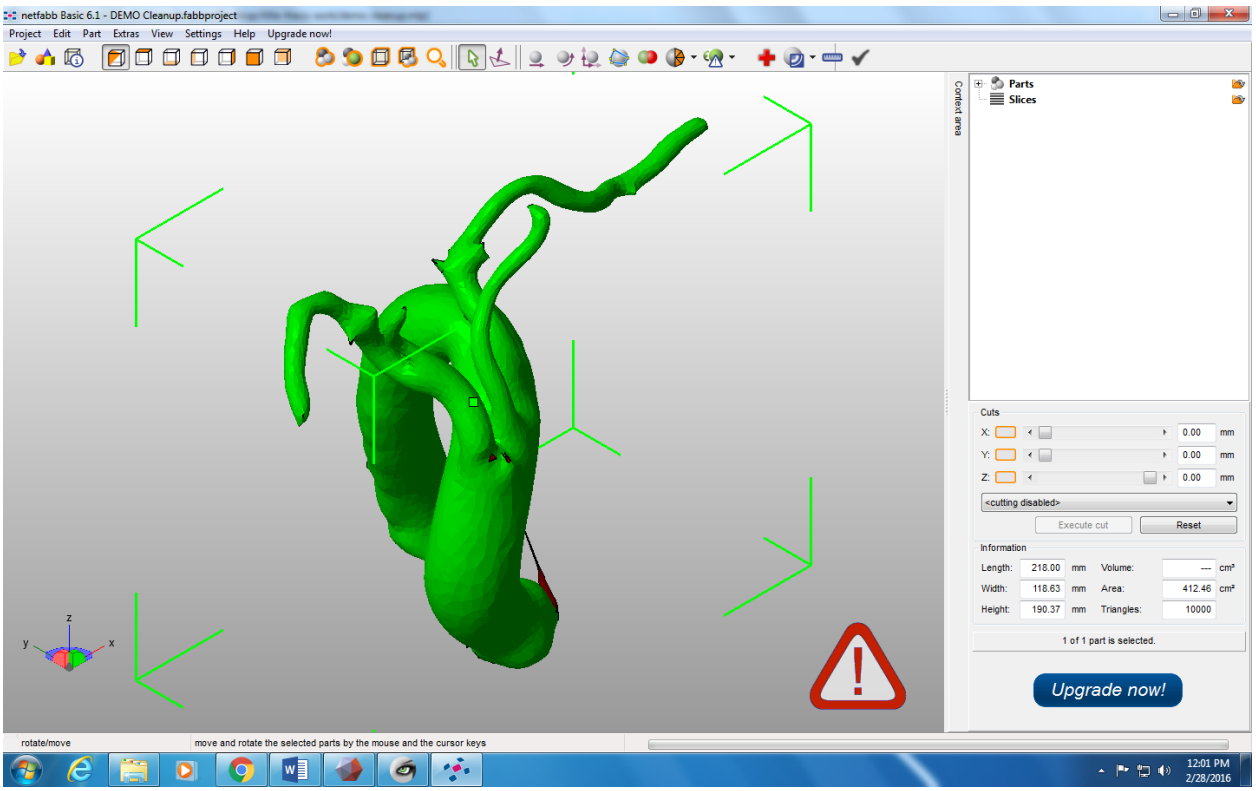
netfabb Basic 6.1 - DEMO Cleanup.fabbproject
Project Edit Part Extras View Settings Help Upgrade now!
Parts
Slices
Context area
Cuts
X: 0.00 mm
Y: 0.00 mm
Z: 0.00 mm
<cutting disabled>
Execute cut
Reset
Information
Length: 218.00 mm
Volume: --- cm³
Width: 118.63 mm
Area: 412.46 cm²
Height: 190.37 mm
Triangles: 10000
1 of 1 part is selected.
Upgrade now!
rotate/move
move and rotate the selected parts by the mouse and the cursor keys
12:01 PM
2/28/2016

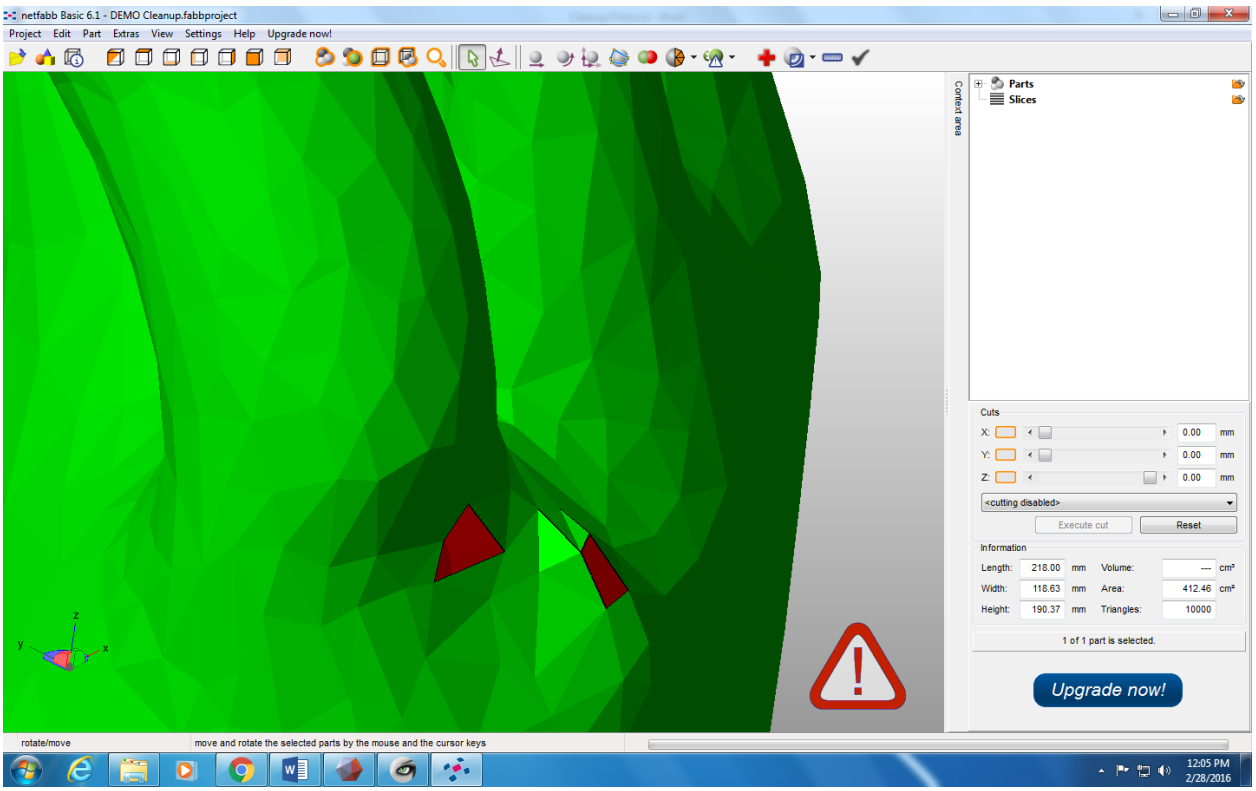

4. Click on the **Red Cross** in the top toolbar (**Repair** button).

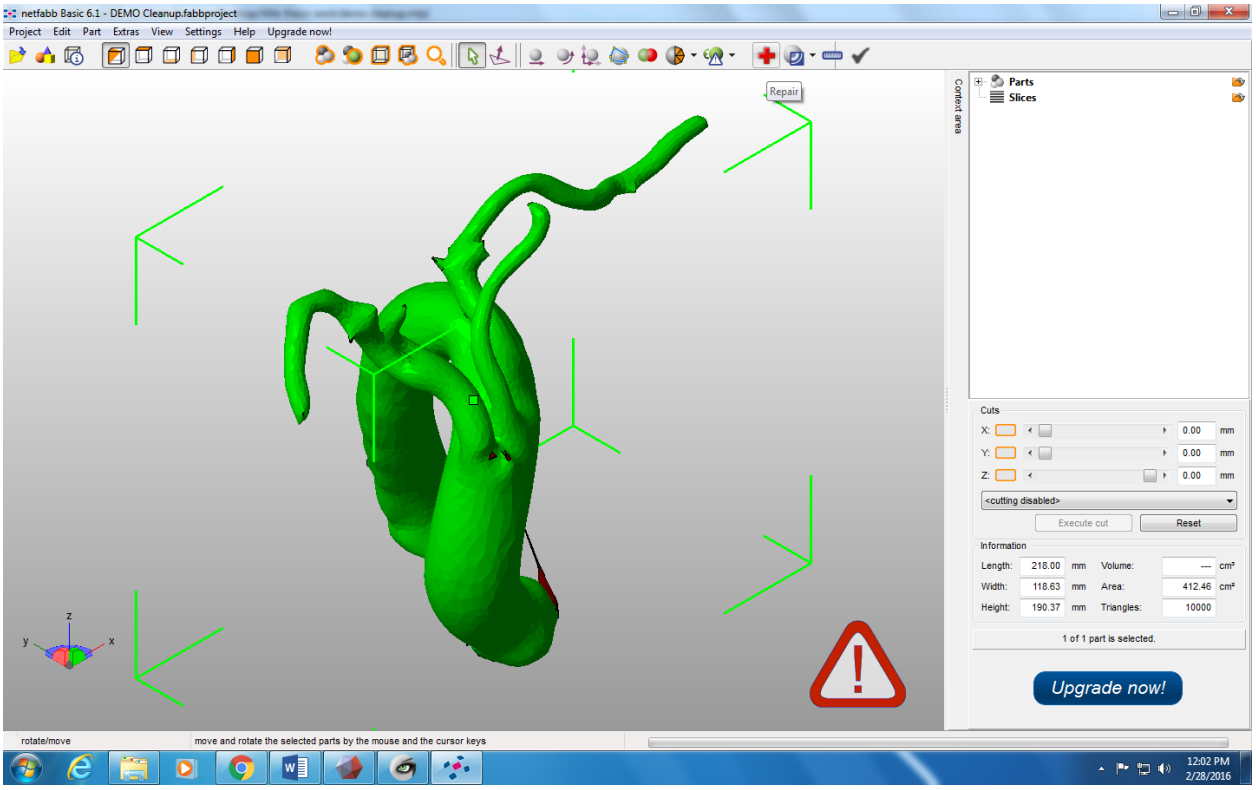

5. The part now changes color, and shows all of the individual triangles. On the right toolbar, leave all of the repair settings at the defaults. Click **Automatic Repair** in the bottom of the right toolbar.

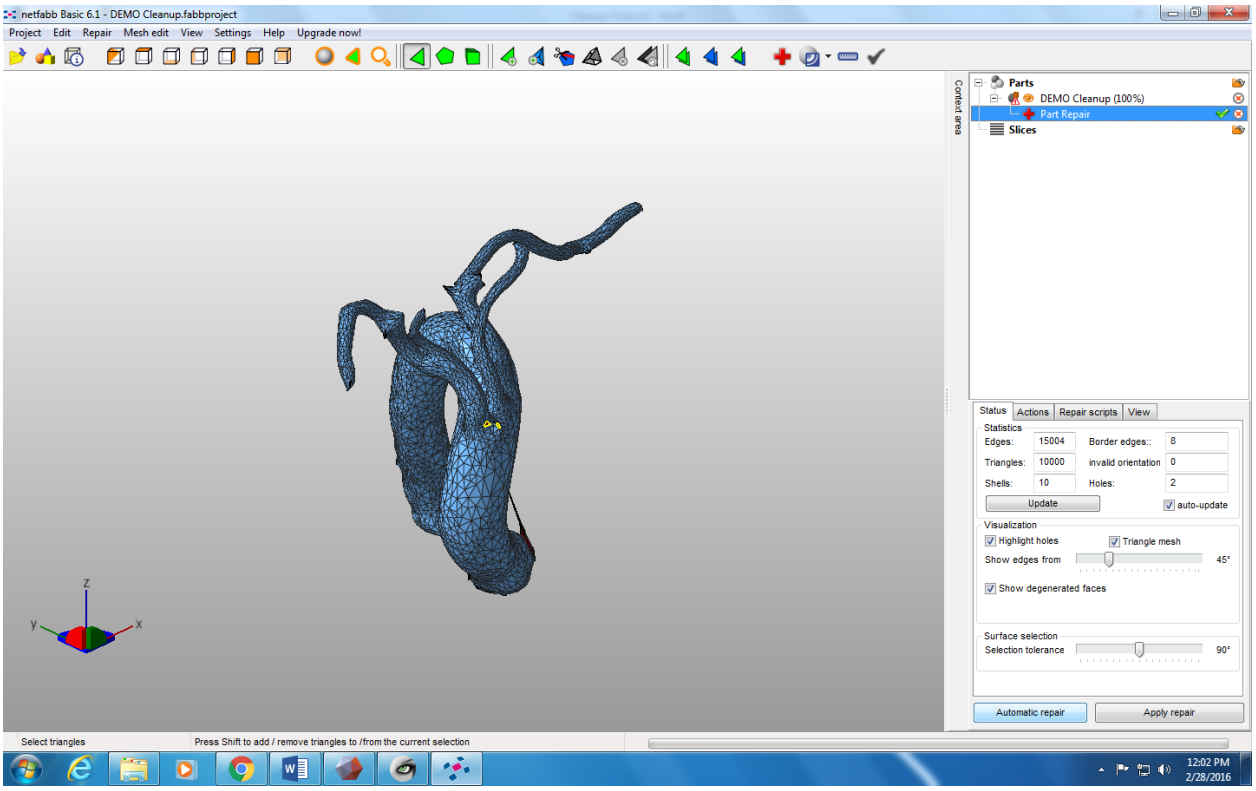

6. Select **Default Repair** in the popup window. Click **Execute.** Then click **Apply Repair** on the right toolbar.

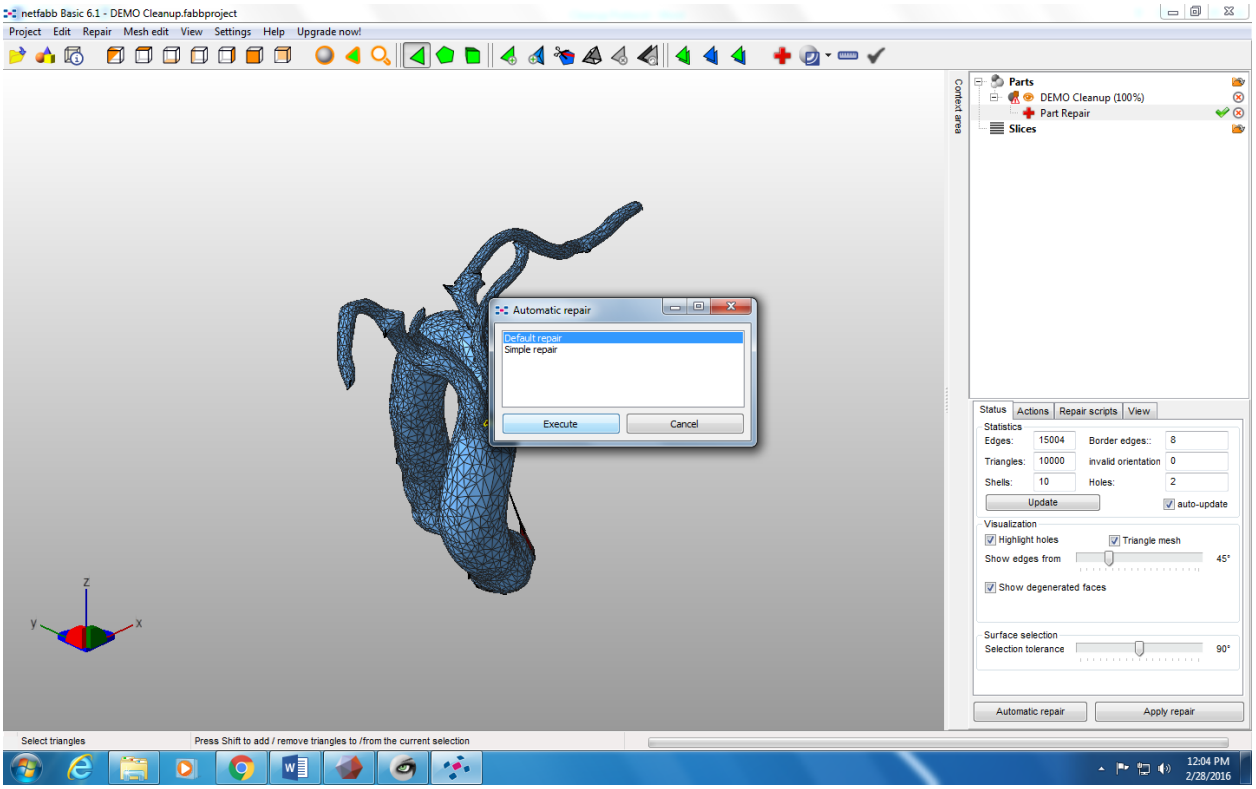
netfabb Basic 6.1 - DEMO Cleanup.fabbproject
Project Edit Repair Mesh edit View Settings Help Upgrade now!
Automatic repair
Default repair
Simple repair
Execute
Cancel
Parts
DEMO Cleanup (100%)
Part Repair
Slices
Status Actions Repair scripts View
Statistics
Edges: 15004
Border edges:: 8
Triangles: 10000
invalid orientation 0
Shells: 10
Holes: 2
Update
auto-update
Visualization
Highlight holes
Triangle mesh
Show edges from 45°
Show degenerated faces
Surface selection
Selection tolerance 90°
Automatic repair
Apply repair
Select triangles
Press Shift to add / remove triangles to /from the current selection
12:04 PM
2/28/2016

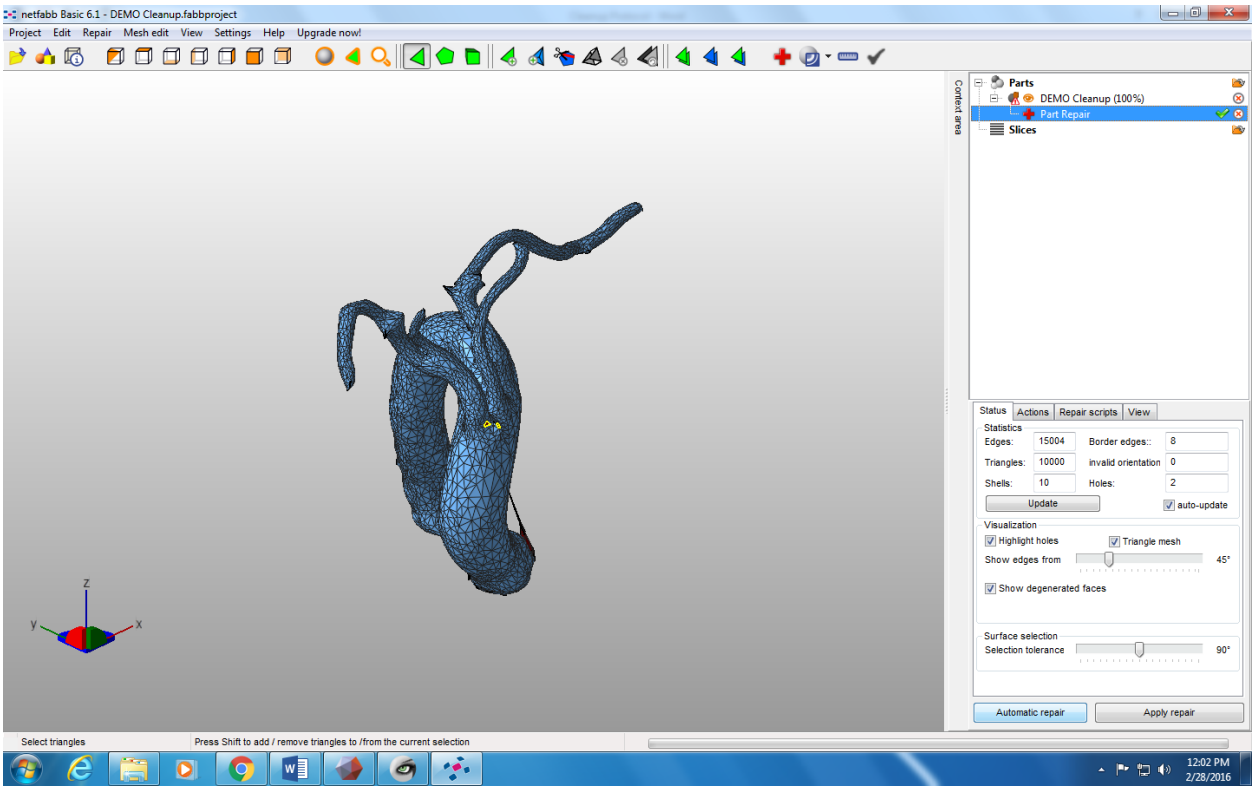
netfabb Basic 6.1 - DEMO Cleanup.fabbproject
Project Edit Repair Mesh edit View Settings Help Upgrade now!
Parts
DEMO Cleanup (100%)
Part Repair
Slices
Status Actions Repair scripts View
Statistics
Edges: 15004
Border edges:: 8
Triangles: 10000
invalid orientation 0
Shells: 10
Holes: 2
Update
auto-update
Visualization
Highlight holes
Triangle mesh
Show edges from 45°
Show degenerated faces
Surface selection
Selection tolerance 90°
Automatic repair
Apply repair
Select triangles
Press Shift to add / remove triangles to /from the current selection
12:02 PM
2/28/2016

7. Click **Remove Old Part** in the next popup window. The part is now shown green again, and there is no warning triangle in the bottom right of the window. Your part is now ready for exporting.

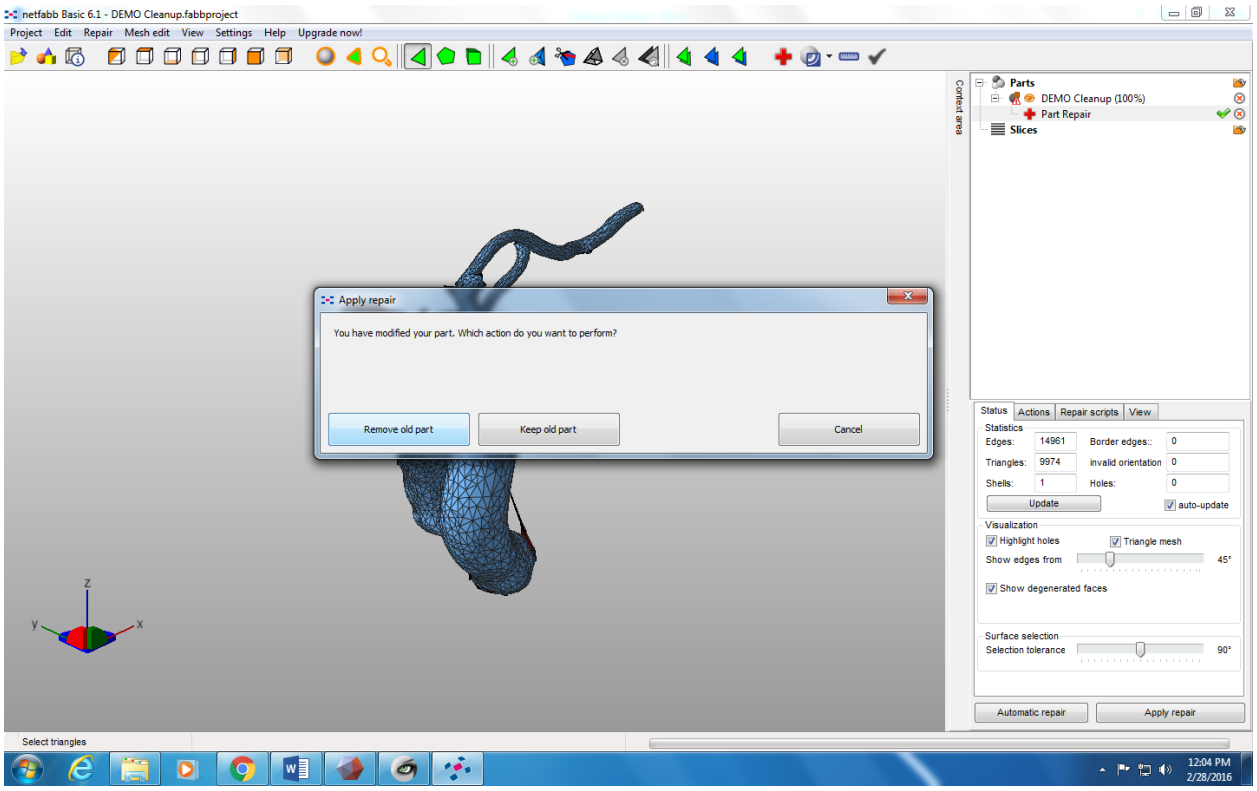

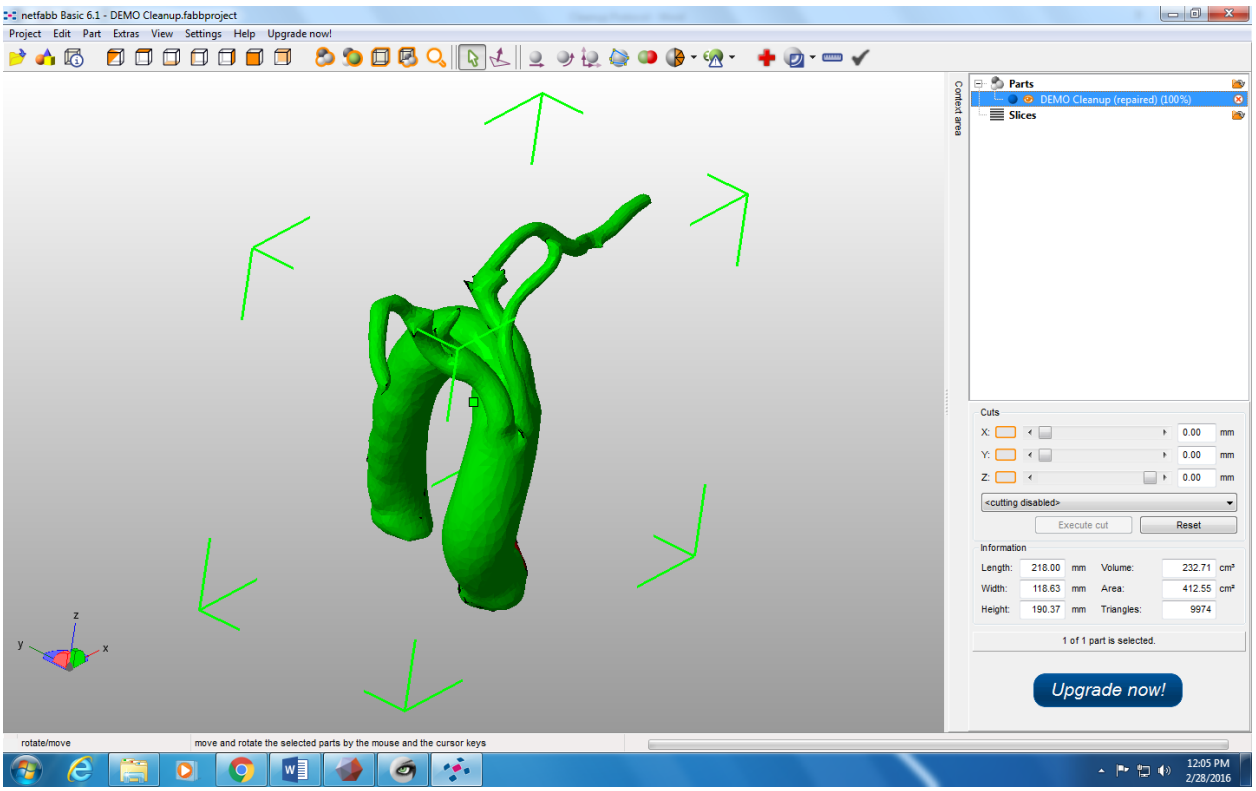

8. Part → Export Part → **as STL**

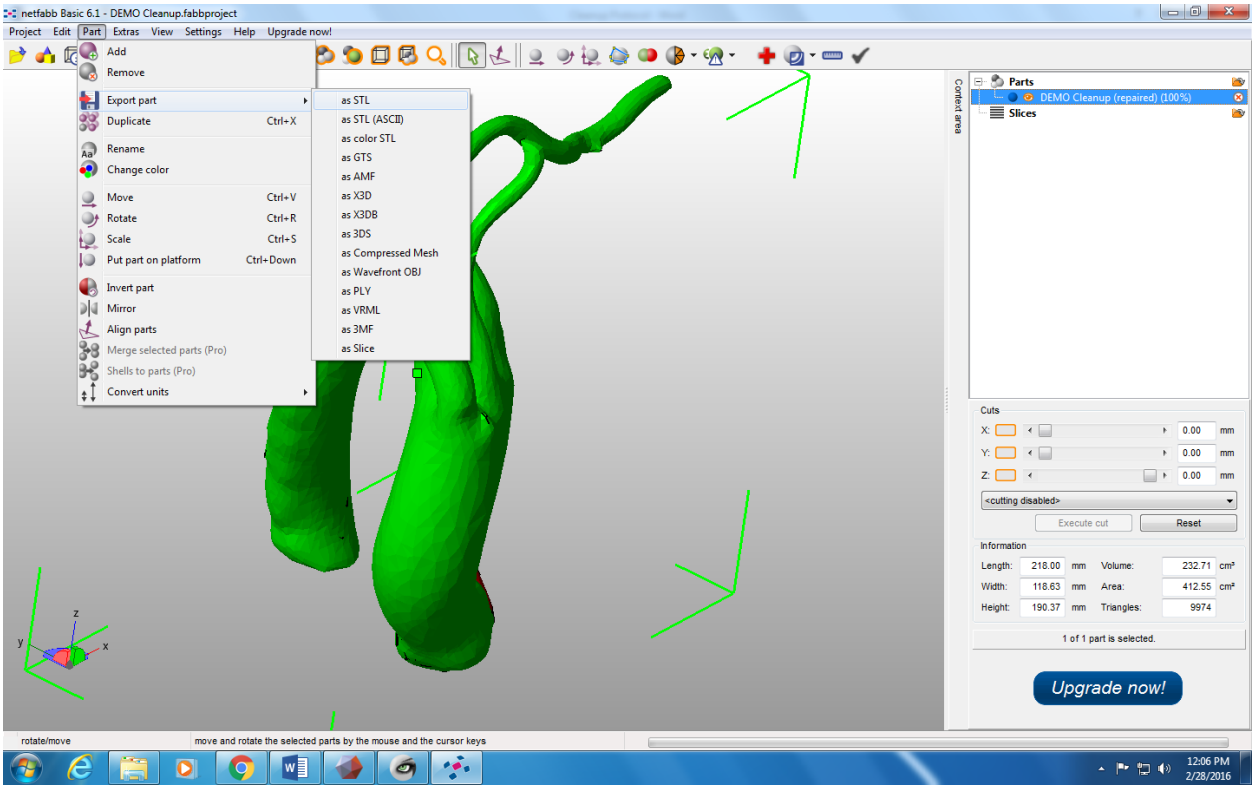

9. Your part is now saved as a repaired STL, and can be opened in SolidWorks. If after selecting export this warning popup appears, click **Optimize**. The warning triangle now becomes a green checkmark. Click **Export.**

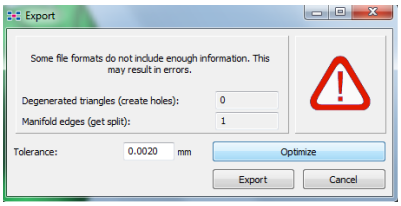

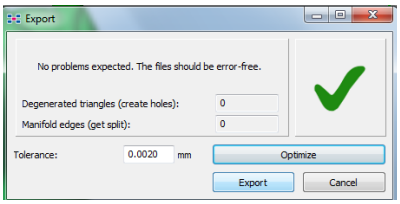

Opening Part in SolidWorks:

1. Open SolidWorks
2. Open your part (filter to .STL files)

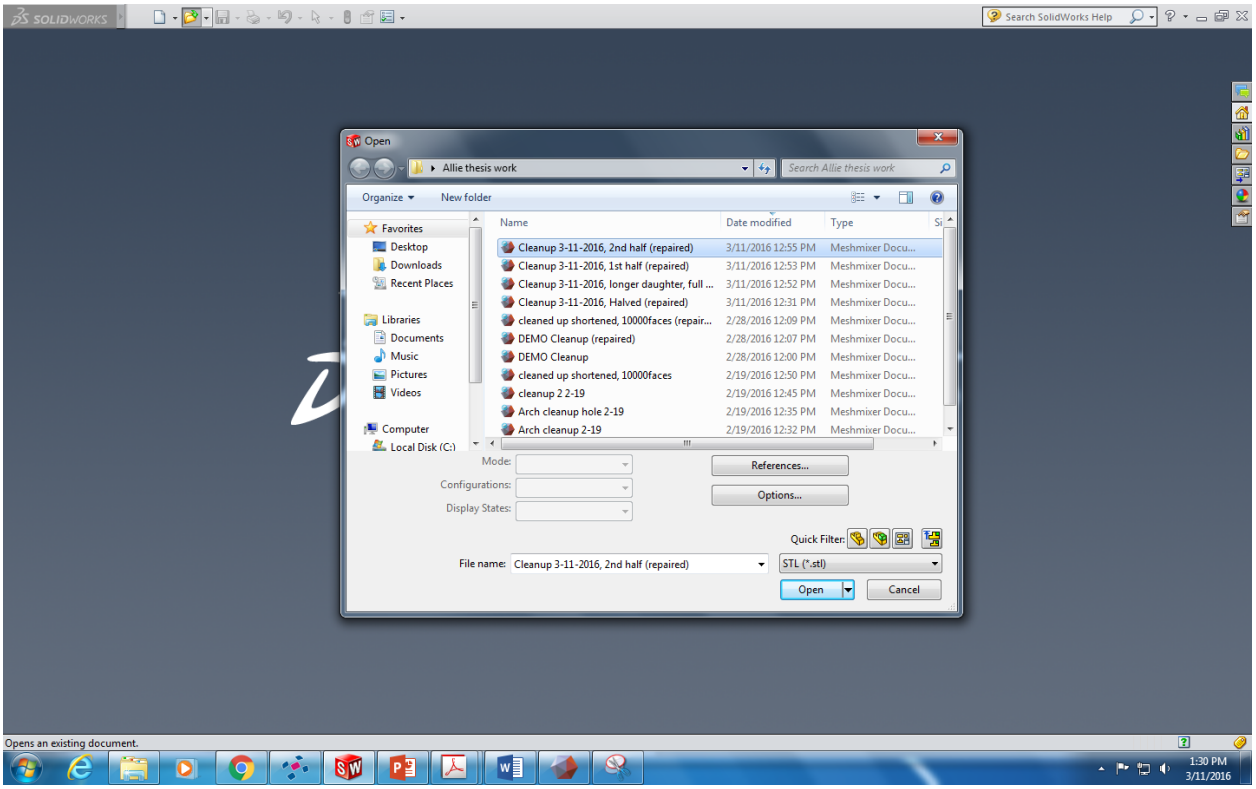

3. Accept the Import Diagnostics (click **Yes)**

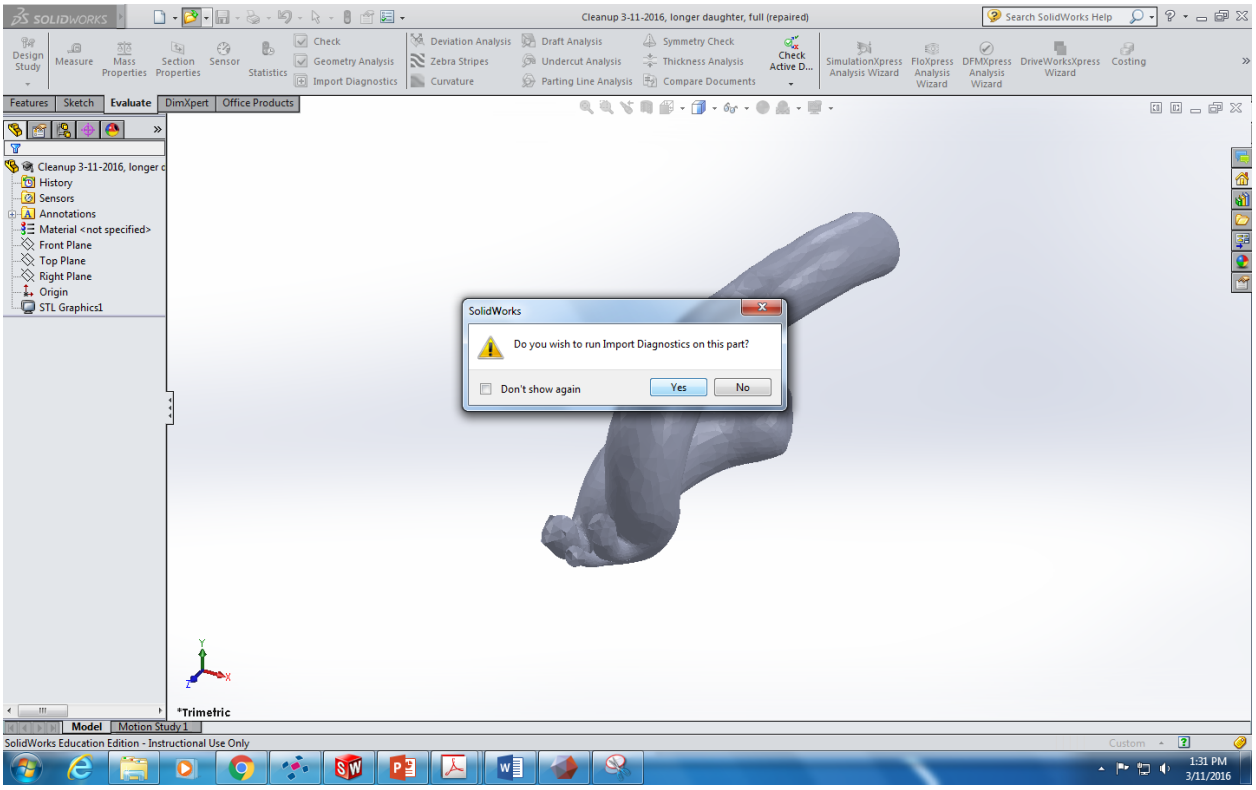

4. The part should now be imported into SolidWorks as a solid part. The message box on the left of the import diagnostics window should be green and read “No faulty faces or gaps remain in the geometry.”

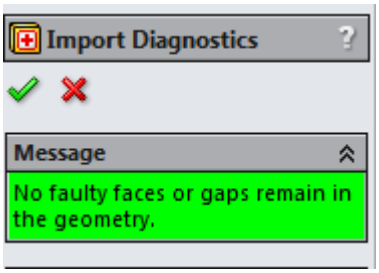

Click the Green Checkmark. Your part is now a solid part and can be modified using SolidWorks.

Appendix B: 3D Printer Basic and Advanced Settings

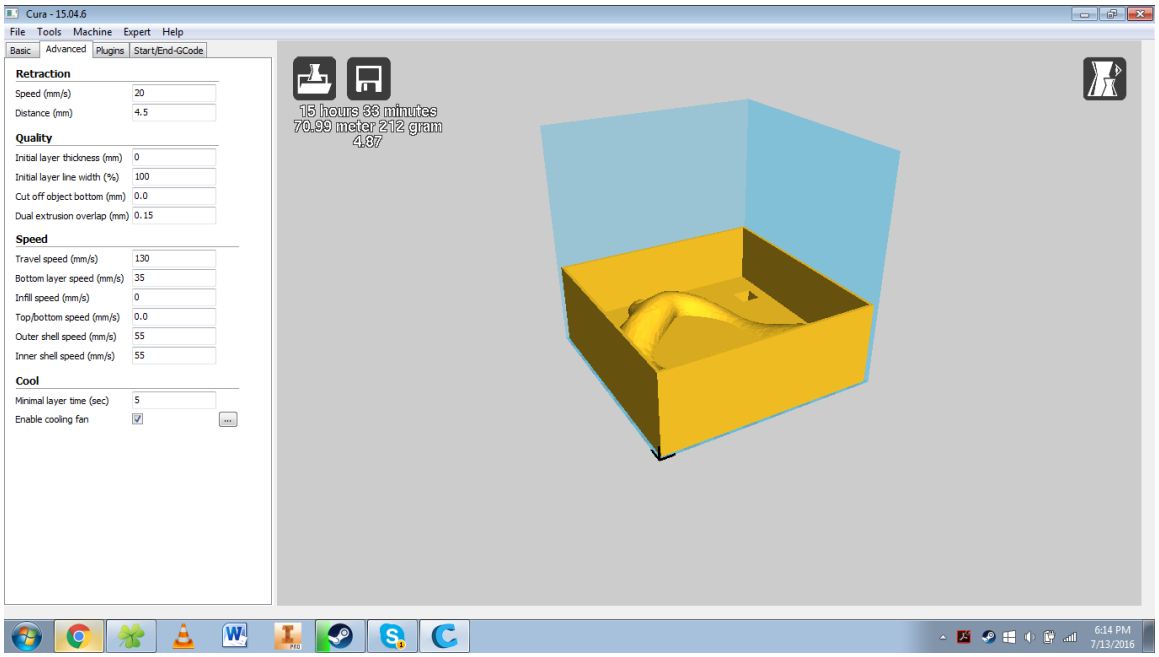

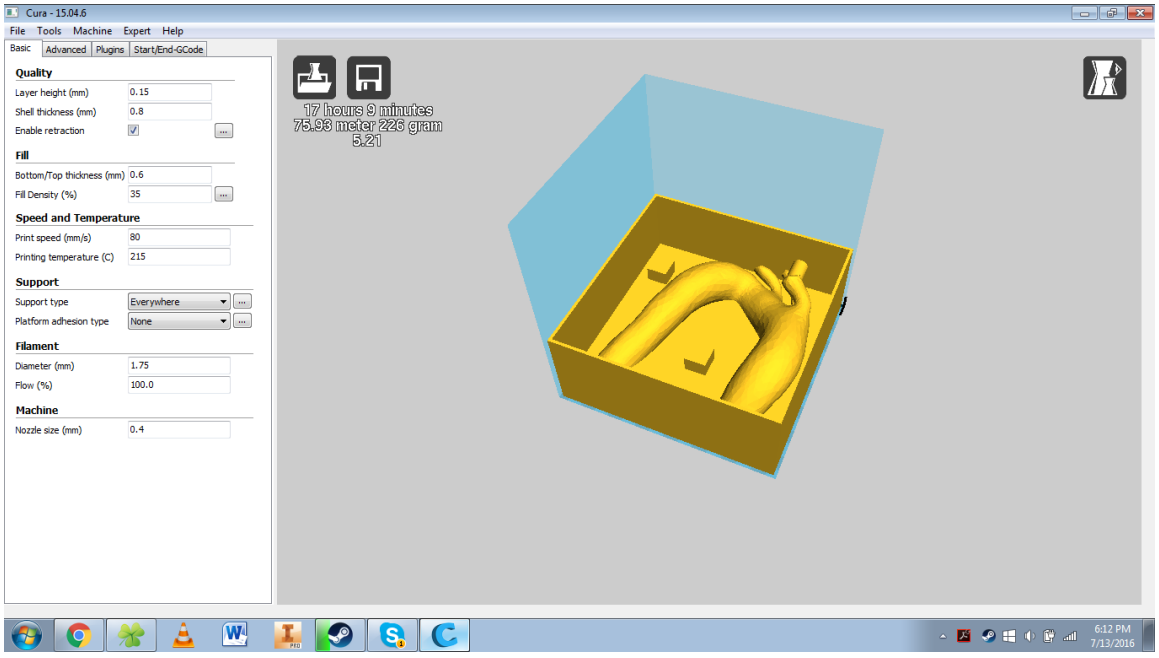

Appendix C: Inlet Velocity Calculations

Average measured inlet flow rate: 13.737 seconds per liter

$$\frac{1\ Liter}{13.737\ seconds} * \frac{60\ seconds}{1\ minute} = 4.367\ Liters/minute$$

$$Q = V * A$$

$$(\frac{4.367\ Liters}{60\ Seconds} * \frac{1\ meter^3}{10000\ Liters}) = V * (\pi * (0.0127\ meters)^2)$$

$$V = 0.1436\ meters\ per\ second$$

Appendix D: ImageJ Processing Methods

1) Setting the image scale:

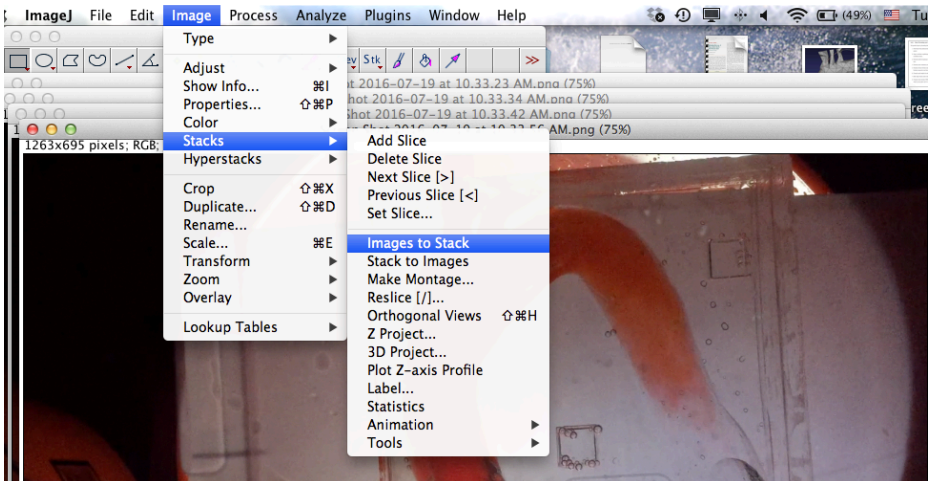

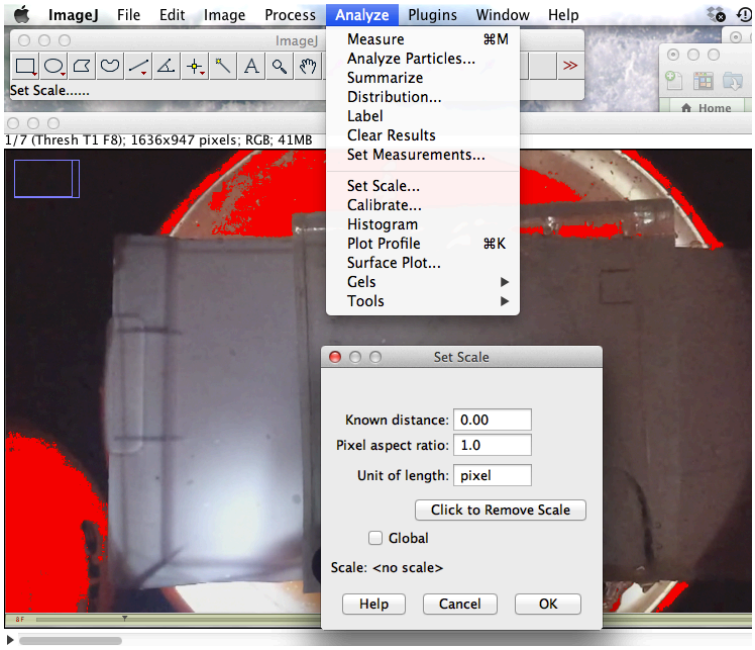

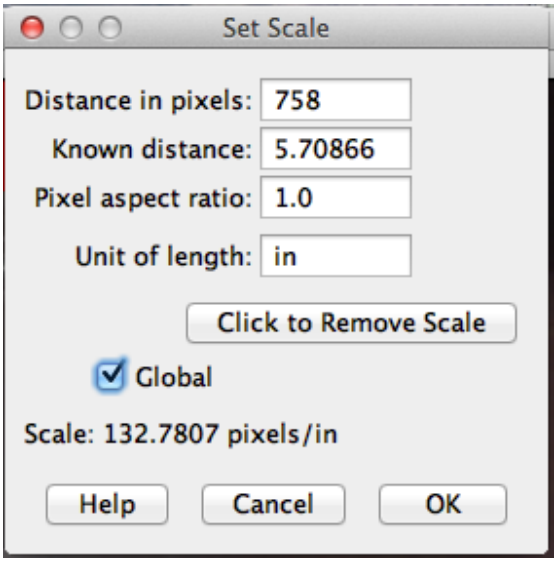

2) Adjusting image threshold and measure pixel path length from the origin:

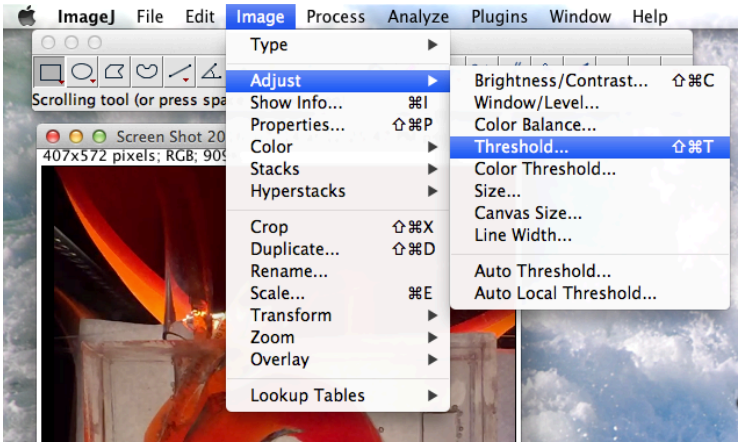

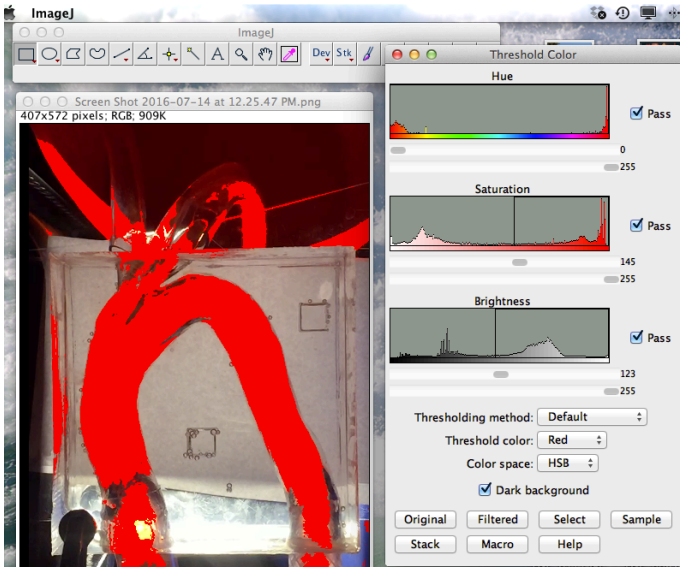

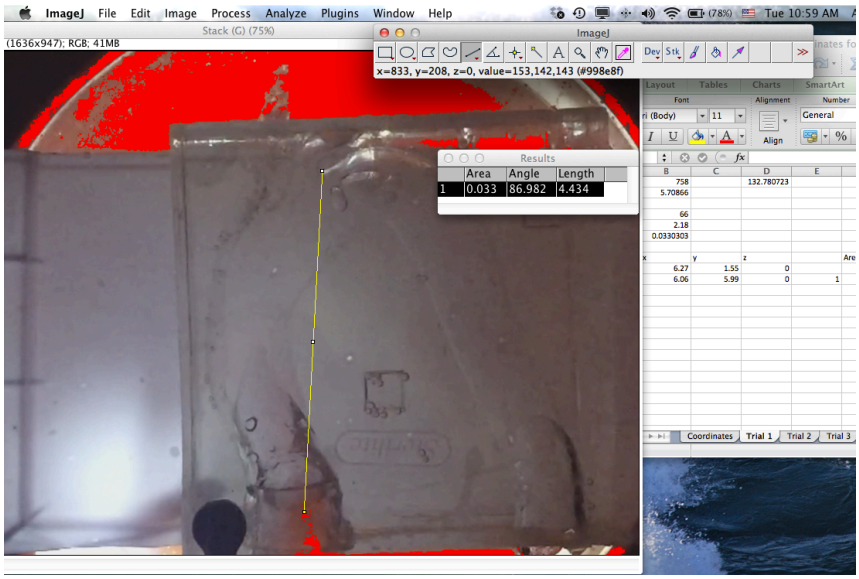

3) Measuring the model's angle of rotation:

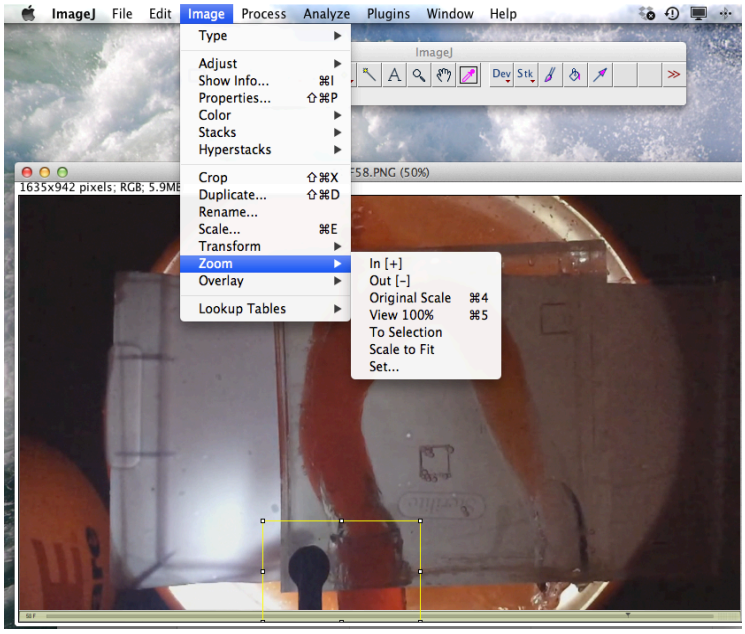

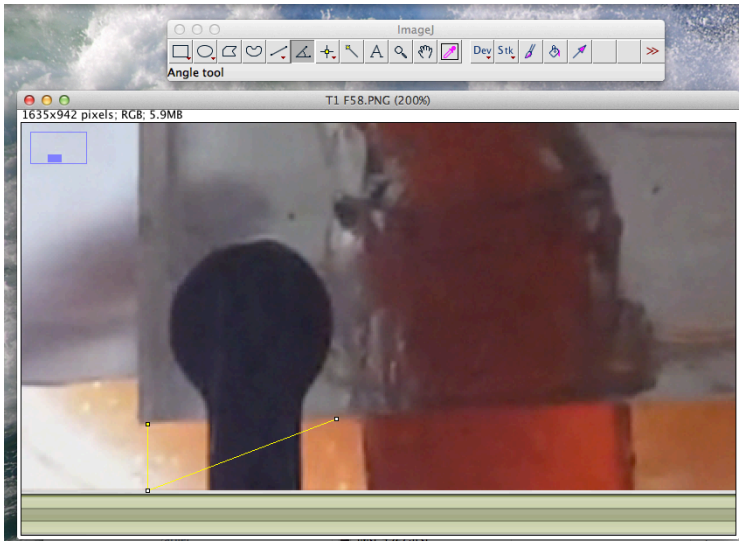

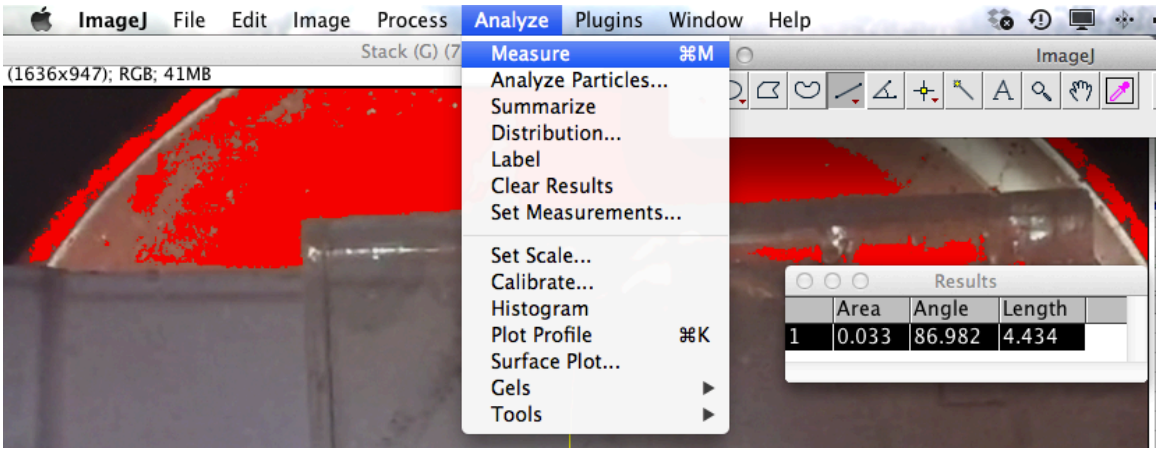

Appendix E: Example Images of Dye Trial 1

Raw Images:

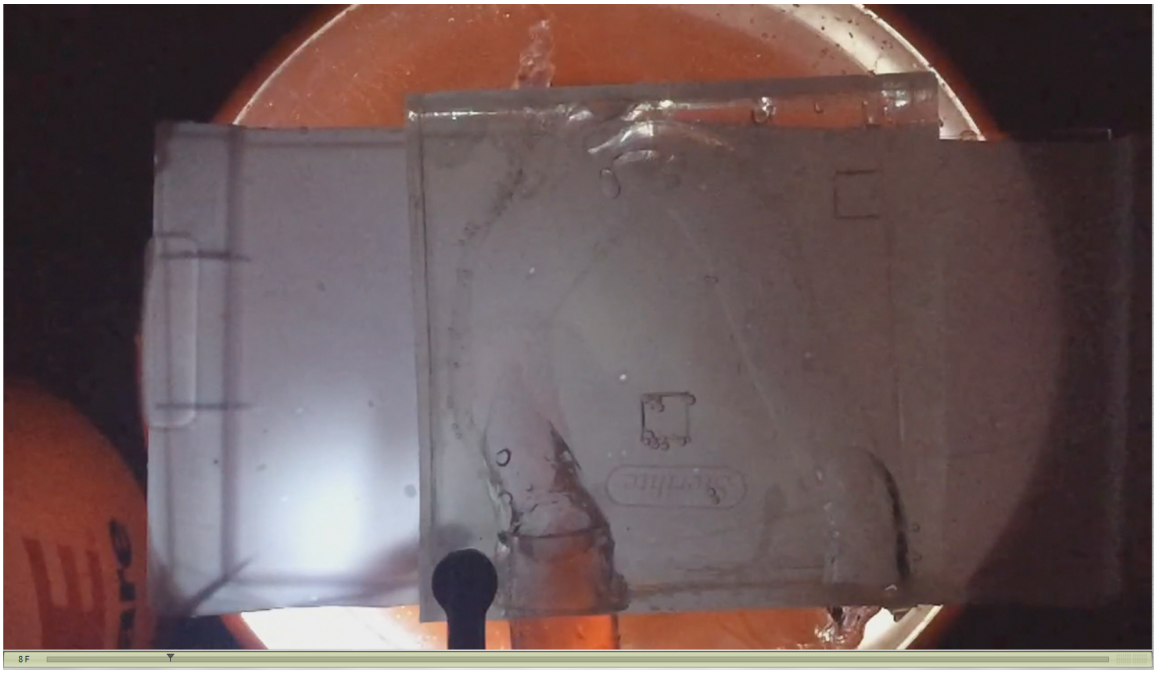

Trial 1, Frame 8

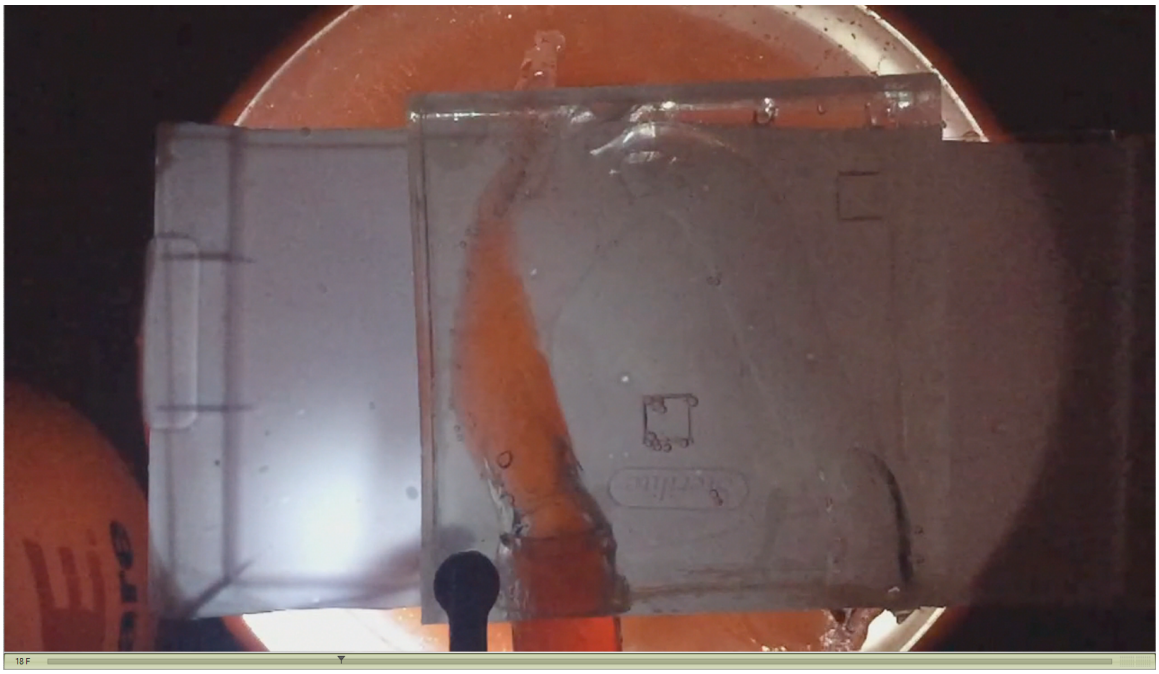

Trial 1, Frame 18

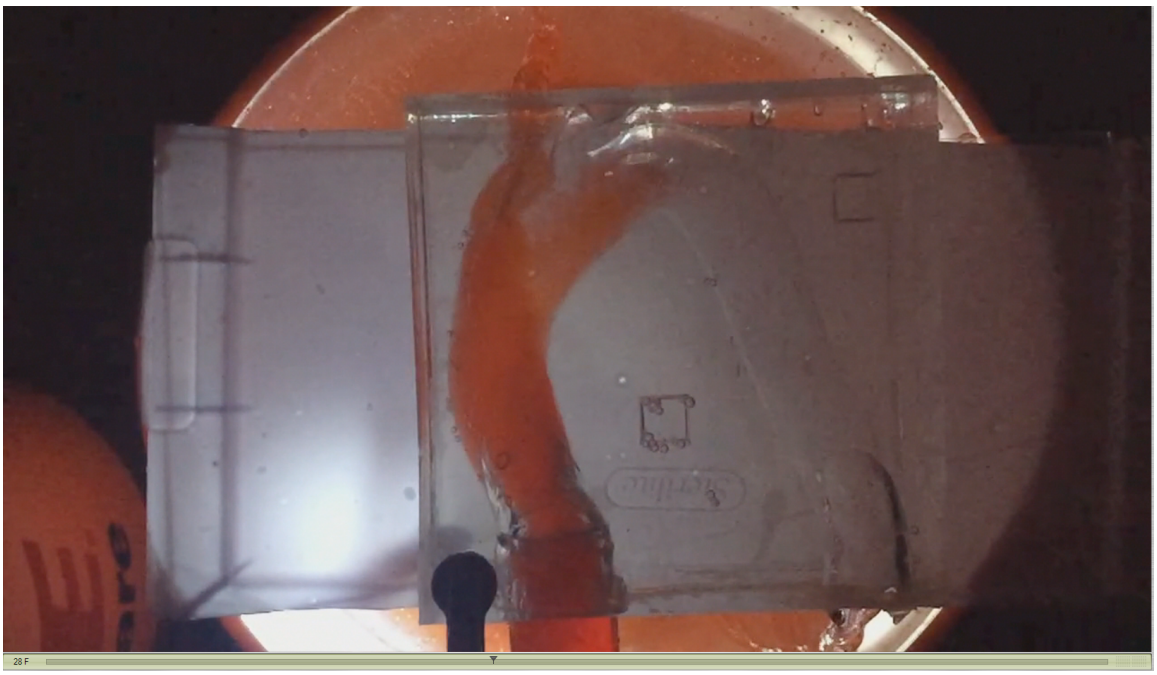

Trial 1, Frame 28

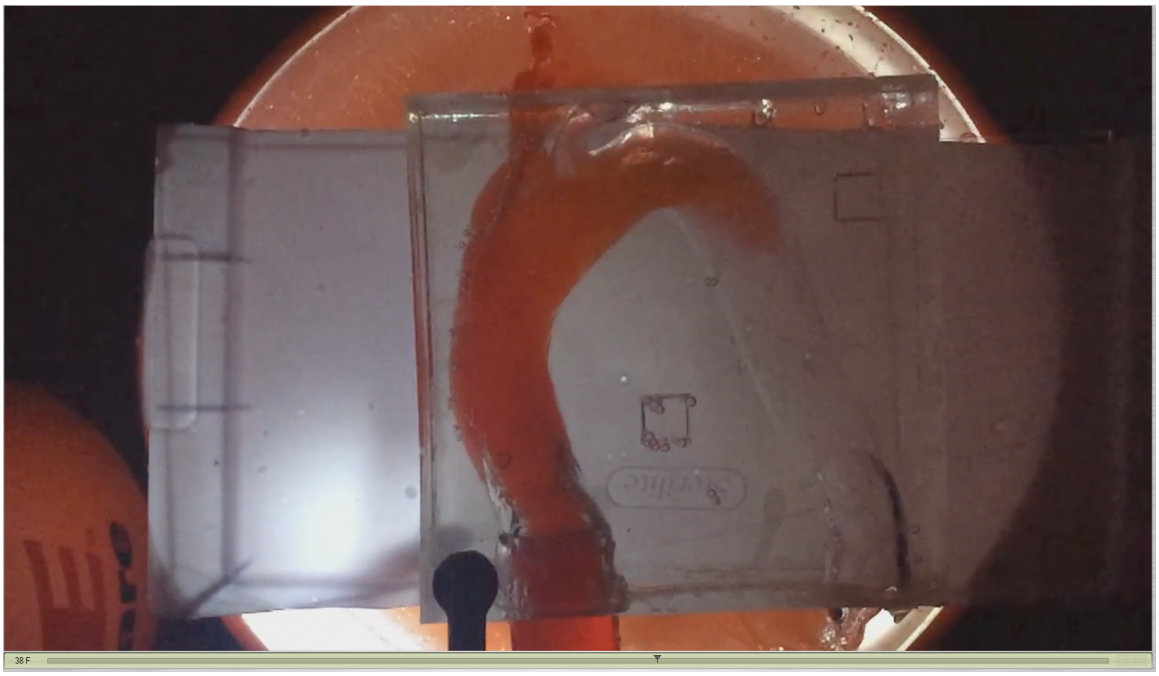

Trial 1, Frame 38

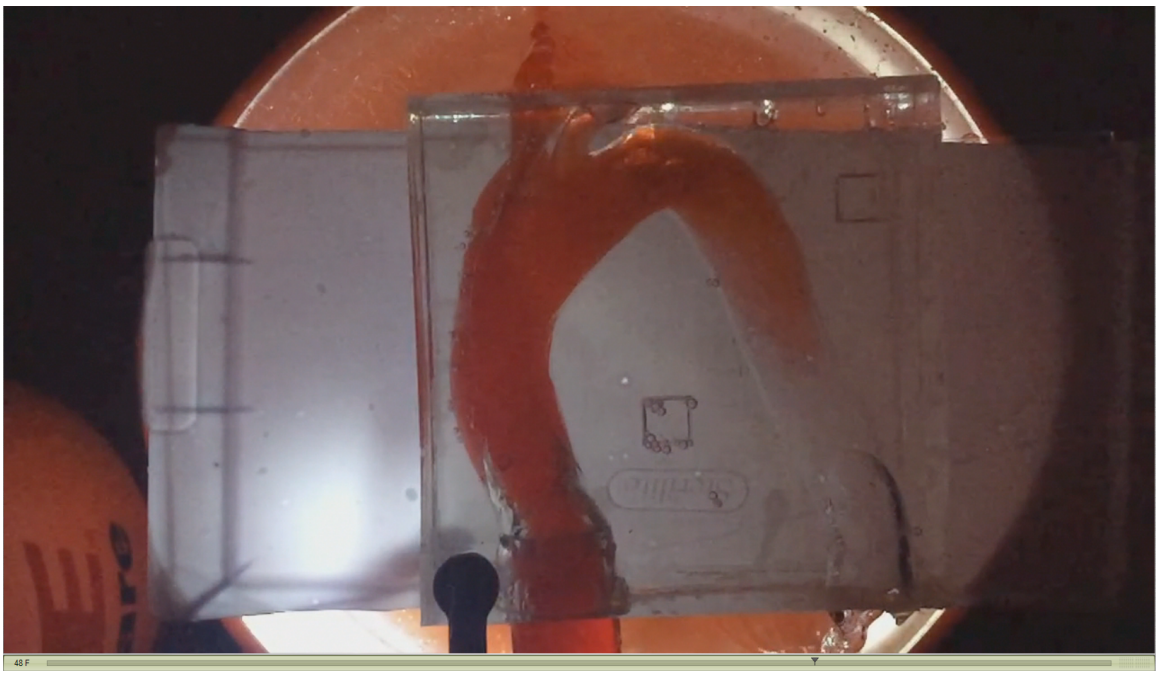

Trial 1, Frame 48

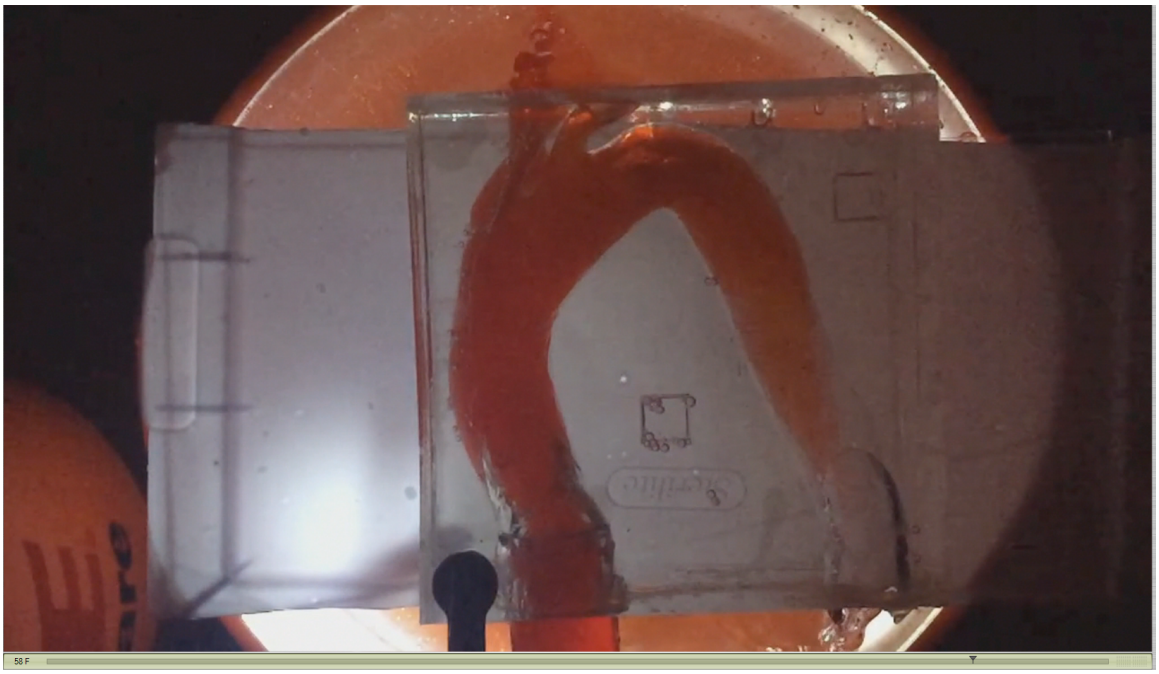

Trial 1, Frame 58

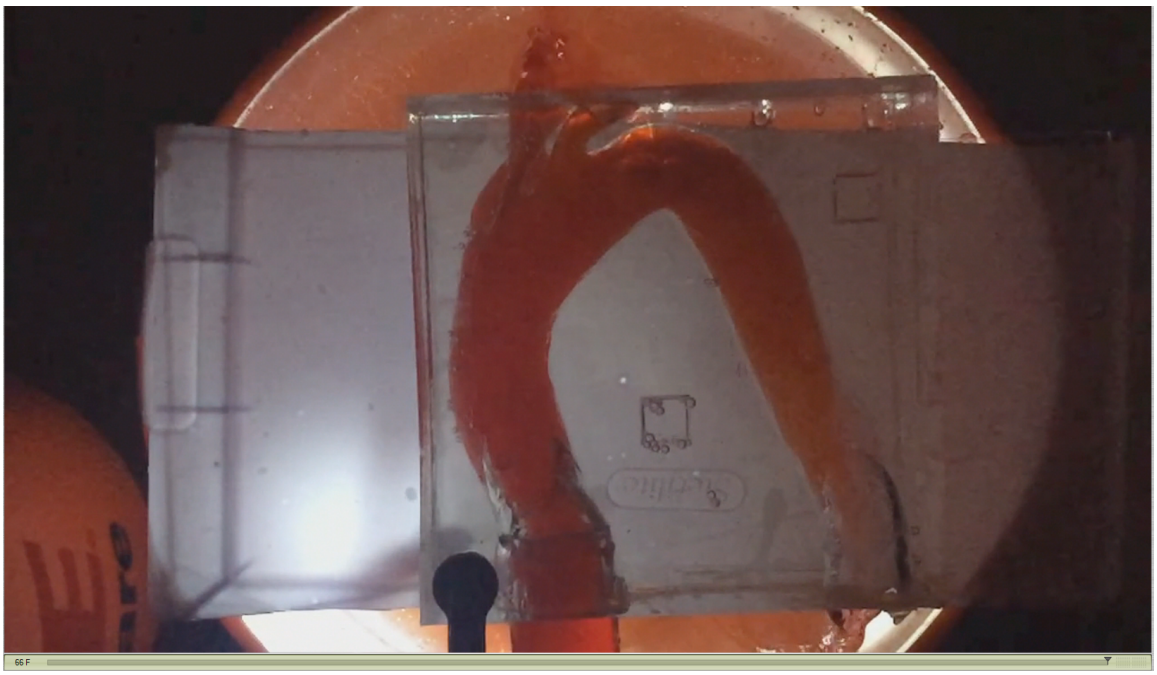

Trial 1, Frame 68

Images with threshold from ImageJ:

Trial 1, Frame 8, Threshold

Trial 1, Frame 18, Threshold

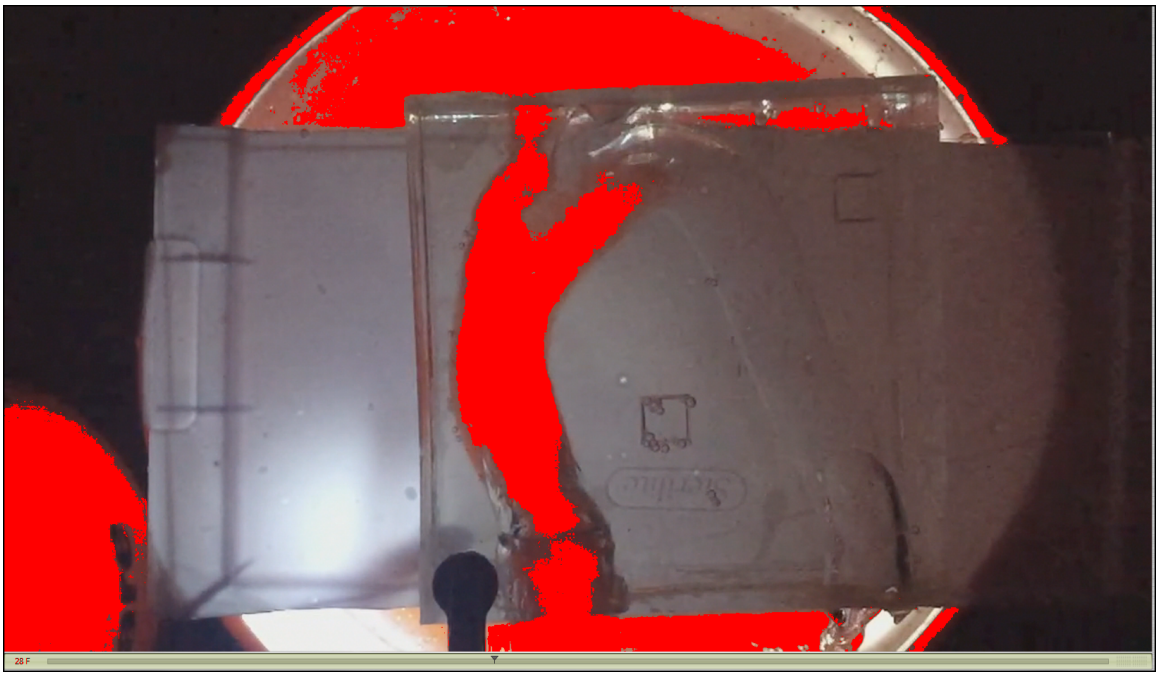

Trial 1, Frame 28, Threshold

Trial 1, Frame 38, Threshold

Trial 1, Frame 48, Threshold

Trial 1, Frame 58, Threshold

Trial 1, Frame 68, Threshold